Small Earthquakes in Southwestern British Columbia (1975-1991)

by

Taimi Lynn Mulder
B.Sc., University of British Columbia, 1987

A Thesis Submitted in Partial Fulfillment of the
Requirements for the Degree of

MASTER OF SCIENCE

in the School of Earth and Ocean Sciences

We accept this thesis as conforming
to the required standard

[redacted]

Dr. G.C. Rogers, Supervisor (Pacific Geoscience Centre, Geological Survey of Canada and School of Earth and Ocean Sciences)

[redacted]

Dr. G. Spence, Supervisor (School of Earth and Ocean Sciences)

[redacted]

Dr. H. Dosso, Outside Member (Department of Physics)

[redacted]

Dr. R.M. Ellis, External Examiner (Department of Geophysics and Astronomy, University of British Columbia)

University of Victoria

Supervisor: Dr. Garry C. Rogers

ABSTRACT

Digital seismographs were first installed on the west coast of Canada in 1975. From 1981 to 1984 the seismic network expanded from the initial four stations to twenty-two stations. This provided a large database of digital data and well located earthquakes in southwestern British Columbia. In this thesis, the character of the seismicity in the North America plate was examined by calculating b-values (recurrence relationships) and Poisson's ratios for sub-regions of southwestern British Columbia and by investigating correlations of seismicity with geology, and with gravity and magnetic data. A rheological profile for the middle of the Strait of Georgia was calculated. One hundred and eleven focal mechanism solutions were computed from earthquakes in southwestern British Columbia from which the regional stress directions were determined (from P and T-axes). The following are the main conclusions from this study:

1. There is a bimodal earthquake distribution: a group of shallow events (< 10 km) and a group of deeper events (> 10 km), peaking around 20 km. In the Coast Plutonic Complex the majority of events are shallow, and beneath Vancouver Island the majority of events are deep (> 10 km).

2. The maximum regional compressive stress direction in southwestern British Columbia is north-northwest. The P-axes (maximum compressive stress) lie horizontally and dominate the focal mechanism solutions. The T-axes (minimum compressive stress) are oriented south-southwest and have no preferential angle of inclination, which implies they are close to the same magnitude as the intermediate compressive stress. Together the P and T-axes suggest right-lateral shear or north-northwest compression.

3. Victoria area seismicity is not correlated with subsurface extensions of the Leech River, Survey Mountain, or Hurricane Ridge faults.

Examiners:

[redacted]

Dr. G.C. Rogers, Supervisor (Pacific Geoscience Centre, Geological Survey of Canada and School of Earth and Ocean Sciences)

[redacted]

Dr. G. Spence, Co-Supervisor, Departmental Member (School of Earth and Ocean Sciences)

[redacted]

Dr. H. Dosso, Outside Member (Department of Physics)

[redacted]

Dr. R.M. Ellis, External Examiner (Department of Geophysics and Astronomy, University of British Columbia)

TABLE OF CONTENTS

LIST OF TABLES

LIST OF FIGURES

ACKNOWLEDGMENTS

I wish to thank Dr. Garry Rogers, who suggested and supervised this project, for his guidance, patience, and support in addition to his thorough editorial review. I also wish to thank Dr. George Spence for his discussions, patience, support. I am indebted to Bob Horner, Garry Rogers, and Chris Spindler, among other Pacific Geoscience Centre Staff, for routine locations of local seismicity from the Western Canadian Telemetered Network, University of British Columbia, and the University of Washington seismic array data, without which this project would not have been possible. I wish to thank Dr. Carmel Lowe for her guidance with the gravity and magnetic data processing, and rheological calculations; Dr. Randy Enkin for his assistance and use of his statistical analysis program and to Judith Baker for the initial plots; and Dr. Dieter Weichert for his assistance and use of his program in calculating b-values. Many thanks to the staff of the Pacific Geoscience Centre, in particular to Drs. Ted Irving and John Cassidy and to Richard Baldwin, Chris Spindler, Dan McDonald, Dave Seeman, Jane Wynne, Gail Jewsbury, and Alison Bird for insightful discussions, assistance, and support. To Drs. Paul Hoffman, George Spence, Chris Rees, and to Karyn Drysdale, all of the University of Victoria, I also thank for insightful discussions, assistance, and support. This thesis benefitted from editorial review by Drs. Garry Rogers, George Spence, Bob Ellis, and Carmel Lowe. Finally, I am forever indebted to Shane Vahey, the Patron Saint of Thesis Writers, for his much needed assistance during the final stages of creating and submitting this thesis.

Funding for this research was provided, in part, by COSEP and term employment at the Pacific Geoscience Centre, and by graduate teaching assistantships and Fellowships from the University of Victoria. Travel grants to conferences were from the Faculty of Graduate Studies, the Physics department, the Pacific Geoscience Centre, and Lithoprobe.

CHAPTER 1

INTRODUCTION

1.1 INTRODUCTION

The first digital seismographs were installed on the west coast of Canada in 1975. Between late 1981 and 1984 the seismic network expanded from the initial four stations to twenty-two stations. This provided coverage of southern Vancouver Island and the adjacent mainland with precise earthquake locations and, for the first time, precise focal depth determinations. There are now approximately 10 years worth of digital data and well located earthquakes in southwestern British Columbia. These data form a large database for examining characteristics of the seismicity and to explore any correlation between seismicity and other geophysical data.

1.2 TECTONIC SETTING

In southwestern B.C. the continental North America lithospheric plate borders the

subducting, oceanic Juan de Fuca plate system (figure 1.1). The Juan de Fuca ridge separates the Pacific plate from the young, hot Juan de Fuca oceanic plate. The Juan de Fuca plate system can be divided into four smaller plates; from north to south these are the Winona block, the Explorer plate, the Juan de Fuca plate, and the Gorda plate.

1.2.1 Past Motions

Reconstructions of past plate motions from sea floor magnetic anomalies [*Vine*, 1966; *Morgan*, 1968; *Isacks et al.*, 1968; *McKenzie and Morgan*, 1969; *Atwater*, 1970; *Riddihough*, 1977] has demonstrated that the Juan de Fuca plate system and the Rivera and Cocos plates (south of the San Andreas fault) are remnants of the Farallon plate which covered a good portion of the Pacific floor in the Late Cretaceous and Cenozoic (the past 150 Ma) as it converged with the western margin of North America. Fragmentation of the Farallon plate began at 37 Ma resulting in subduction boundaries where it remained in contact with the North America plate and strike-slip boundaries where the Pacific plate abutted directly against the North America plate (the San Andreas and Queen Charlotte faults are examples of this boundary) [*Atwater*, 1970]. The Farallon plate has been progressively diminishing over time as it continues to subduct beneath the North America plate leaving the Juan de Fuca plate system as the northern remaining fragment.

This northern remnant of the Farallon plate also fragmented into the Winona, Explorer, Juan de Fuca, and Gorda plates, further complicating the relative motions of the Juan de Fuca system. Cox and Engebretson [1985] and Engebretson *et al.* [1985] provide evidence for a change in Pacific plate hotspot motion at 5 mya from a west-northwesterly direction to a northwesterly direction, perhaps contributing to changes of plate motion in the Juan de Fuca plate system. At 6.5 Ma the relative motion of the entire Juan de Fuca plate system was to the

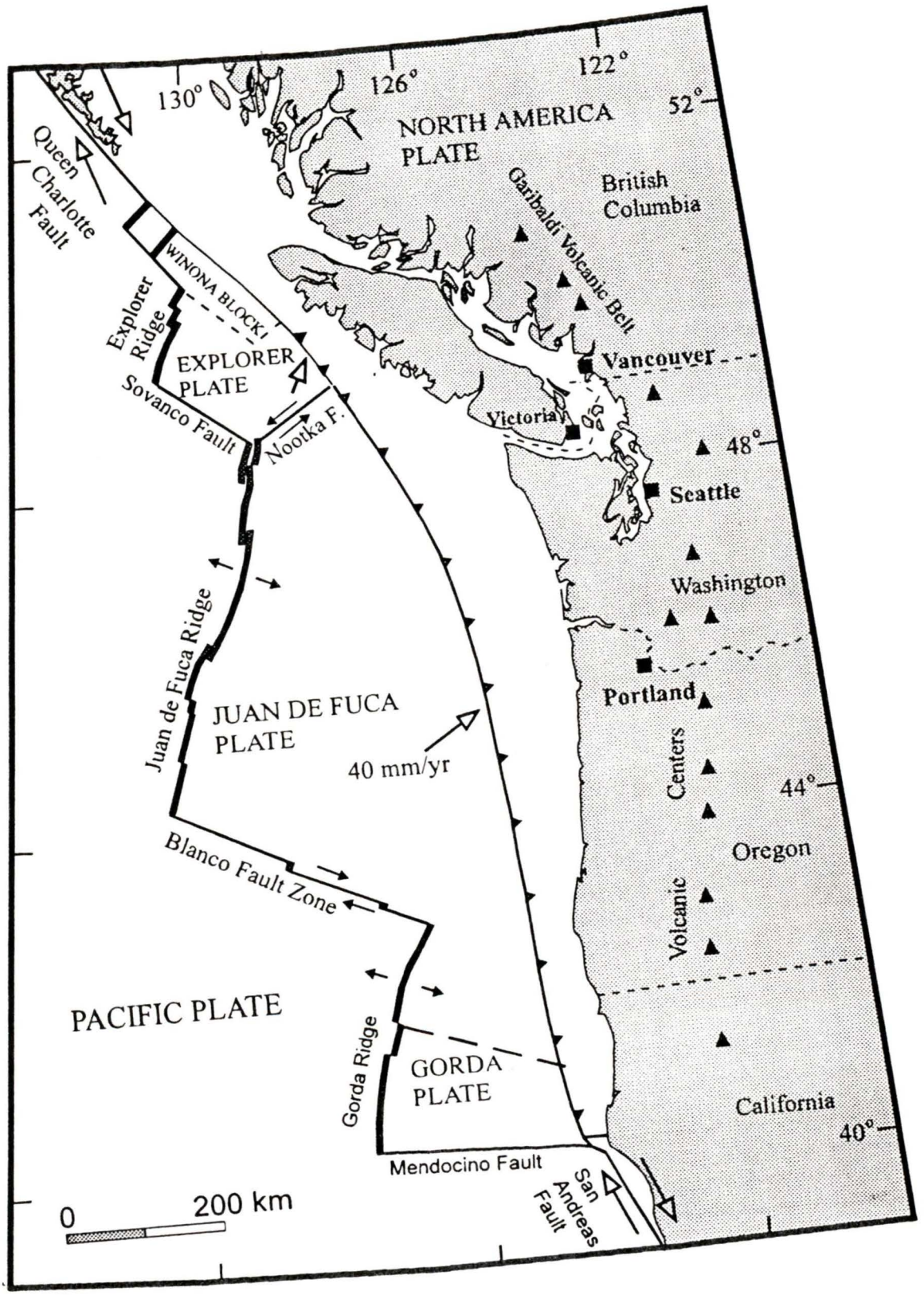

Figure 1.1 Tectonic plate map of the Pacific Northwest.

northeast at 6.0 to 7.0 cm/yr with respect to the North America plate. At 3.5 Ma the Explorer plate started to move independently at a reduced convergence rate [*Riddihough*, 1984], at which time the Juan de Fuca/North America convergence rates also dropped substantially to 4.6 cm/yr. The Juan de Fuca/North America pole remained stable after breakaway of the Explorer plate at 3.5 Ma. However, the Explorer/North America pole, which is to the southeast of the Explorer plate and indicates clockwise motion of the Explorer plate about the pole, has apparently migrated northwards [*Riddihough*, 1984].

1.2.2 Present Motions

Contemporary plate geometry and motions are defined by recent magnetic anomaly patterns and present-day seismicity. The major ridges and fault zones depicted in figure 1.1 are outlined by current seismicity patterns. The Explorer ridge, Sovanco fault, Juan de Fuca ridge, Blanco fault zone, Gorda ridge, and Mendocino fault mark the boundary between the Pacific plate and the Juan de Fuca plate system. The Nootka fault separates the Juan de Fuca plate and Explorer plate. It has left-lateral motion at a rate of 2 cm/yr [*Riddihough*, 1984]. The Explorer plate diverges from the Pacific plate at 4 cm/yr and the Juan de Fuca diverges from the Pacific at 6 cm/yr [*Riddihough*, 1984].

With respect to the North America plate the relative motions of the Juan de Fuca plate system decrease as the northern edge of the plate system is approached. Relative to the North America plate, the Winona block converges at about 1 cm/yr [*Davis and Riddihough*, 1982], the Explorer converges at 2.5 cm/yr (northeast), and the Juan de Fuca converges at 4.5 cm/yr [*Riddihough*, 1984]. Riddihough [1984] suggested that the Explorer plate has decoupled from the North America plate and may be no longer actively subducting. Because the Explorer plate is relatively young, hot and therefore buoyant, it supports and thus underplates the North America

plate. Seismic evidence and magnetic anomalies indicate the Juan de Fuca plate is still actively subducting, but slower than it was at 4 Ma. The absolute pole of motion (the point at which the plate rotates with respect to the hot spot frame of reference) for the Juan de Fuca plate may be almost within the subducted portion of the plate and therefore suggests it is rapidly slowing and will soon be controlled by its larger neighbours, the Pacific and North America plates [*Riddihough*, 1984]. However this does not mean coupling to the Pacific or North America plates has necessarily increased.

1.3 REGIONAL GEOLOGICAL STRUCTURE

British Columbia is a region of complex geological structure. From east to west it is composed of five major geological/morphological belts (figure 1.2): the Foreland, Omineca, Intermontane, Coast, and Insular belts [*Monger et al.*, 1982]. These belts are morphological features separated by major faults. Each is composed of several terranes which joined together and subsequently docked onto North America. In latest Triassic - earliest Jurassic time, the small terranes which make up the Intermontane belt and parts of the Omineca and Coast belts had amalgamated. By the early Jurassic (approximately 175 Ma) this large composite terrane accreted onto the edge of the ancient continental margin, forming the Omineca Crystalline belt between the Foreland and Intermontane belts [*Monger et al.*, 1982]. By late Jurassic the small terranes which make up the Insular belt had amalgamated. The Insular superterrane collided with the Intermontane superterrane by Cretaceous time (around 100 Ma), forming the Coast Plutonic Complex (Coast belt) between these two amalgamated terranes [*Monger et al.*, 1982].

In southwestern British Columbia (figure 1.3) the Insular belt is composed primarily of

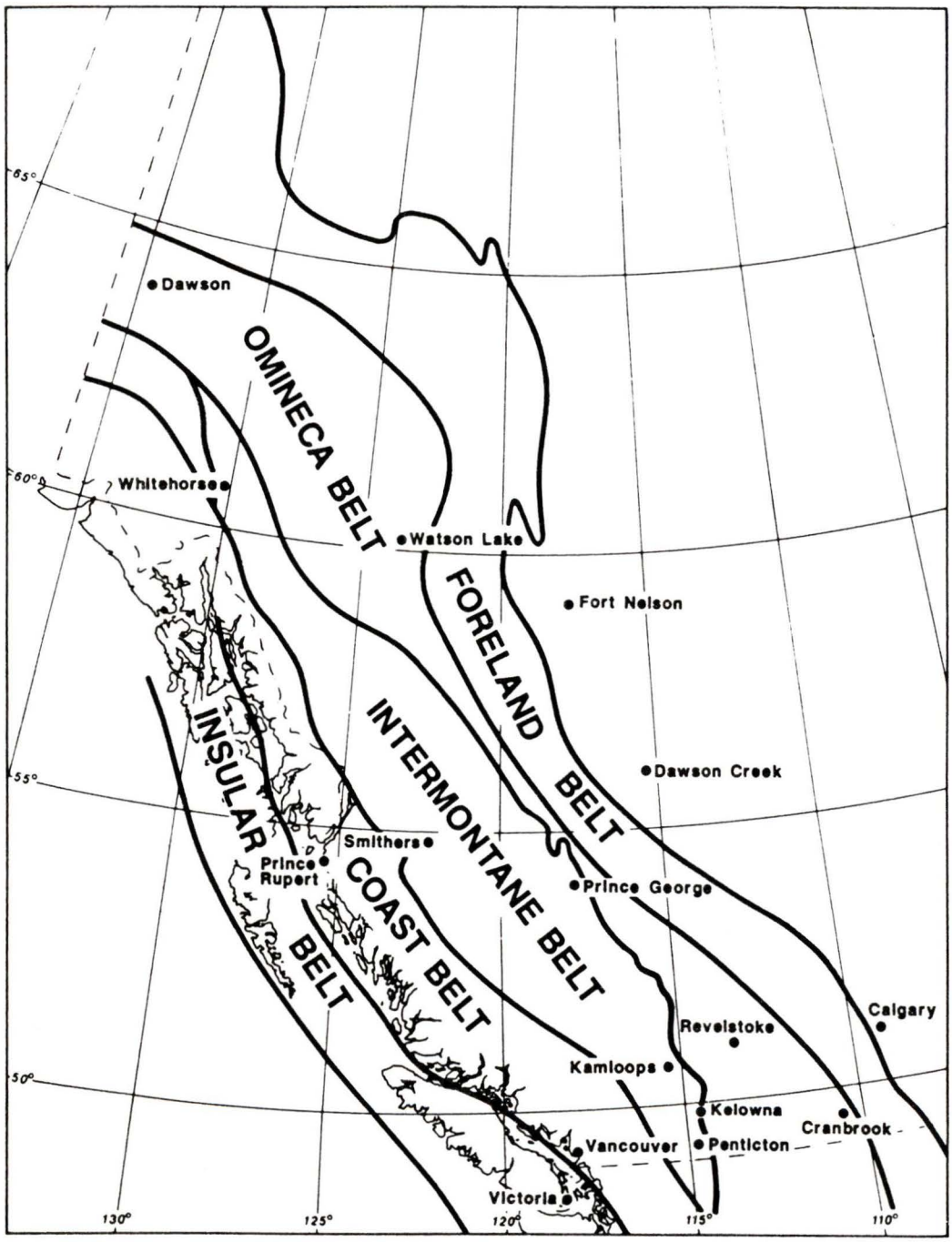

Figure 1.2 The five geologic and physiographic belts which make up the Canadian Cordillera. The Intermontane and Insular belts are primarily composed of allocthonous terranes and the Foreland, Omineca, and Coast belts are regions resulting from the docking of the allocthonous terranes onto North America [after *Yorath*, 1990].

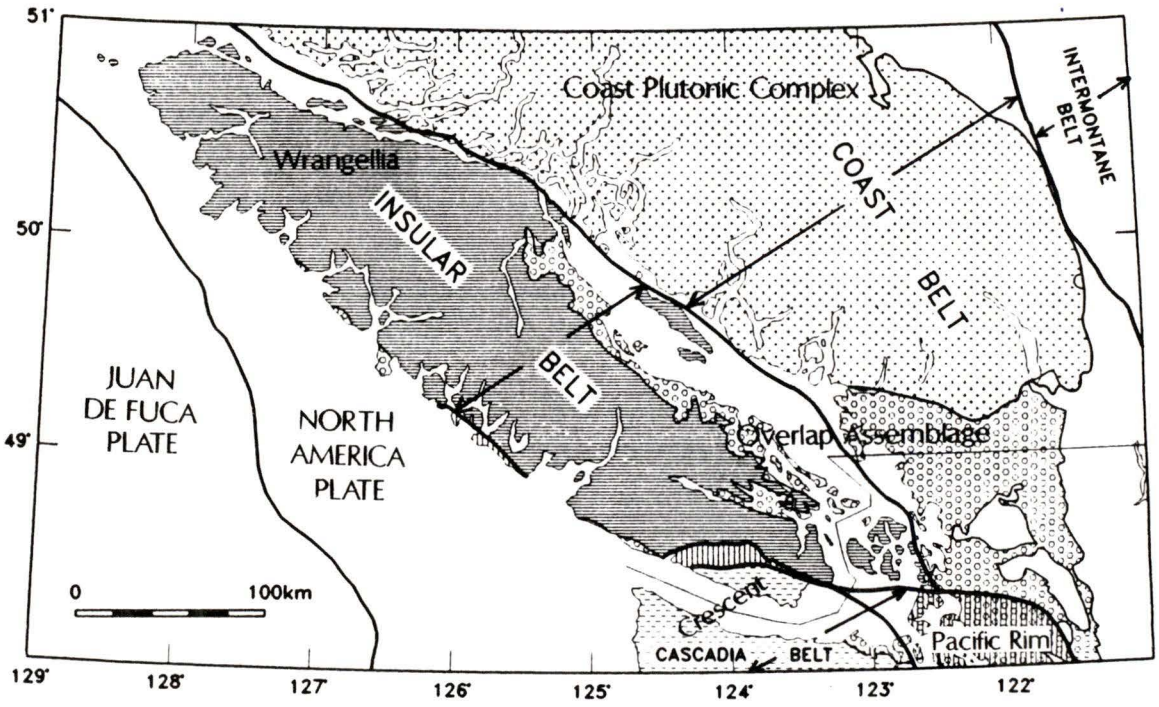

Figure 1.3 Tectonic map of southwestern British Columbia. The broad physiographic/geologic belts are outlined and the boundaries for the small geologic terranes (which make up these belts) are also marked.

Wrangellia terrane which comprises late Palaeozoic volcanic rocks (the Sicker Group) overlain by Triassic basalts [*Muller*, 1977]. The southern tip of Vancouver Island consists of two small terranes which were emplaced beneath Wrangellia during Eocene (38-54 Ma) time: the Pacific Rim terrane, upper Mesozoic (Jurassic and Cretaceous) sedimentary and metamorphic melange, and the Crescent terrane, Eocene oceanic crust of pillow basalts and breccia, deposited in a marginal basin [*Massey*, 1986].

1.4 GENERAL SEISMICITY

Figure 1.4 shows a ten year sample of the seismicity distribution in southwestern British Columbia. The offshore earthquakes occur in the oceanic Juan de Fuca and Explorer plates. The band of seismicity offshore and two-thirds of the way up Vancouver Island, running in a southwesterly direction, outlines the Nootka fault zone (see figure 1.1 for a diagrammatic view of the plate boundaries), the left-lateral, strike-slip transform fault which marks the boundary between the northern edge of the Juan de Fuca plate and the southern edge of the Explorer plate [*Riddihough*, 1984]. Farther inland, there is a concentration of seismicity located where the North America plate margin changes direction from north-south in Washington state to northwest-southeast in British Columbia. The earthquakes in southwestern B.C. occur in three distinct source regions as has been pointed out by Rogers [1994]: earthquakes within the overlying, continental North America plate; earthquakes within the subducting, oceanic plate; and earthquakes occurring on the interface between these two plates (figure 1.5). Seismicity within the North America plate, which will be the subject of this thesis, extends to approximately 30 km depth in most of southwestern B.C.. Eastward, from the Garibaldi Volcanic Belt (figure 1.1),

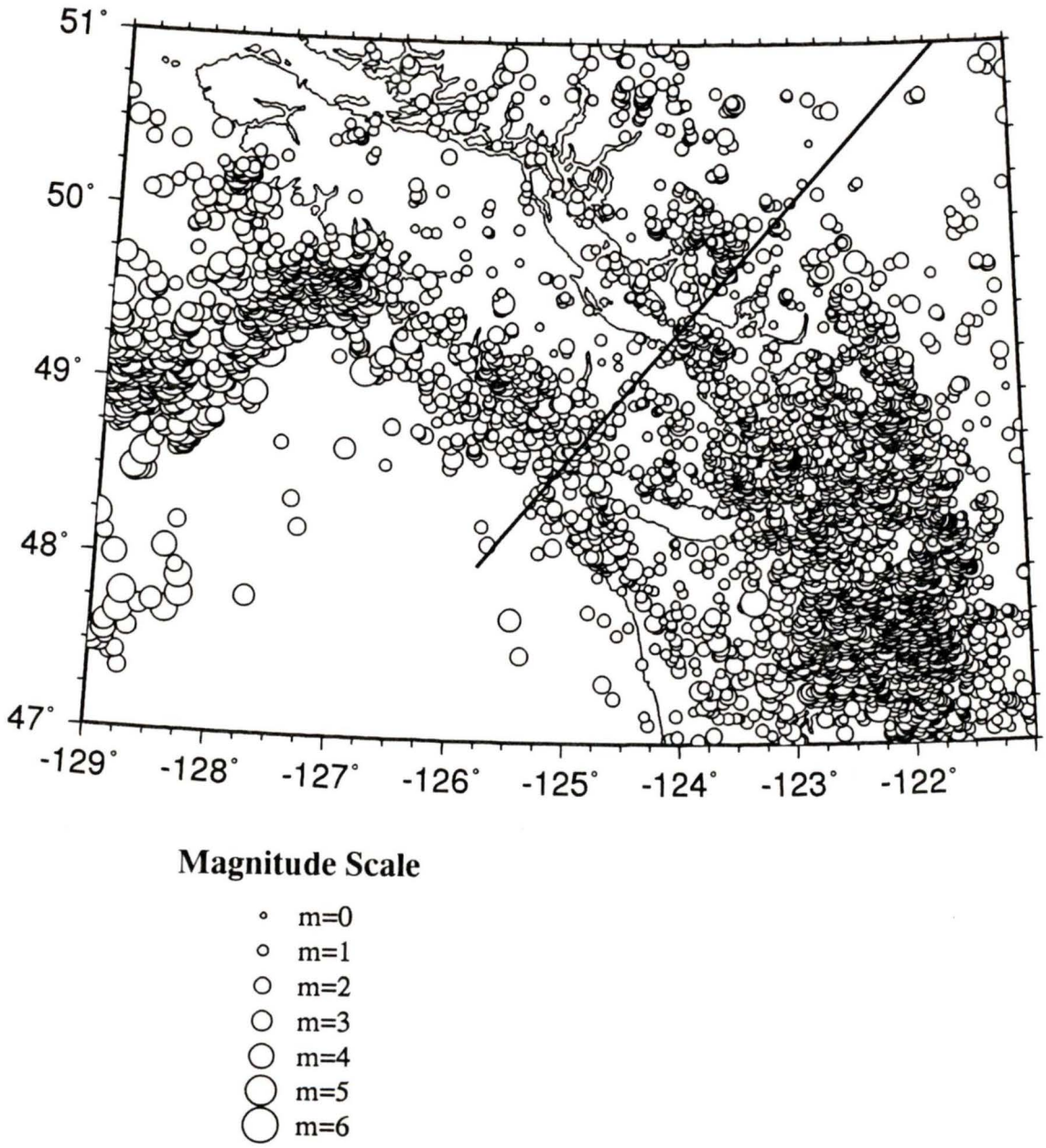

Figure 1.4 Seismicity of southwestern British Columbia ($M \geq 2$). Most of the offshore events, and those beneath the west coast of Vancouver Island, lie in oceanic crust. The band of earthquakes running southwest off the northern end of Vancouver Island (from 49°N, 129°W to 49.6°N, 127°W) marks the Nootka fault zone, the boundary between the Juan de Fuca and Explorer plates (see figure 1.1 for plate boundaries). Most of the onshore events lie in the continental crust of the North America plate. Note the inland concentration of seismicity which occurs inland from the bend in the coastline (from 49.25°N, 122°W to 47°N, 121°W to 47°N, 123°W to 49°N, 123.5°W).

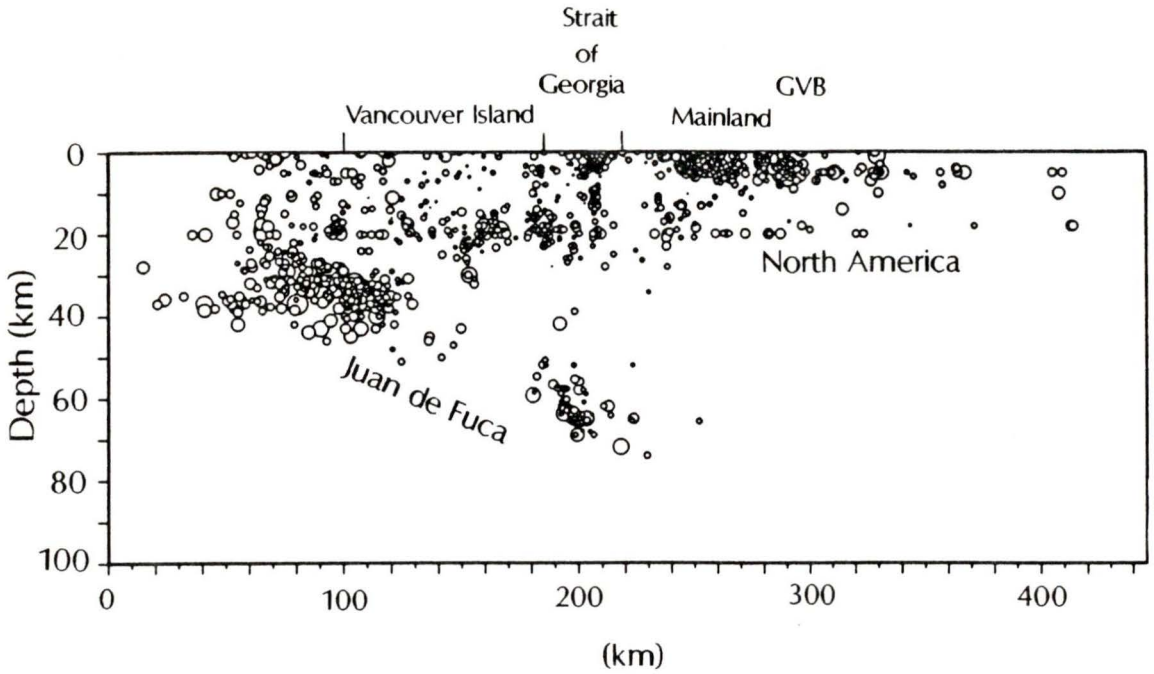

Figure 1.5 Cross-section of Cascadia margin seismicity as indicated in figure 1.4. The data are from 1981-1991 and of magnitude $0 \leq m < 5$; the width of the cross-section is 80 km. Earthquakes occur within the subducting Juan de Fuca plate, between the Juan de Fuca and North America plates (interplate earthquakes), and within the overlying North America plate (intraplate earthquakes). GVB - Garibaldi Volcanic Belt.

the seismicity shallows and this correlates with increased heat flow [*Lewis et al.*, 1992].

Historically (i.e. before 1975), there have been earthquakes larger than magnitude 4.5

	M	latitude	longitude
Oct 29, 1846	5.5	48.75N	123.25W
Aug 25, 1865	5.0	48.5 N	123.5 W
Feb 6, 1896	5.0	48.3 N	124.3 W
Aug 18, 1915	5.6	48.5 N	121.4 W
Dec 6, 1918*	7.0	49.8 N	126.5 W
Jan 24, 1920	5.5	48.6 N	123.0 W
Sept 17, 1926	5.5	50.0 N	123.0 W
Sept 22, 1926	5.0	50.22N	121.89W
Dec 4, 1926	5.0	48.5 N	123.0 W
May 7, 1927	5.5	50.15N	127.85W
Feb 9, 1928	5.8	49.0 N	125.3 W
Nov 3, 1934	4.9	48.0 N	121.0 W
Nov 29, 1943	4.8	48.4 N	122.9 W
Oct 21, 1945	4.5	50.23N	127.37W
Jun 23, 1946*	7.3	49.8 N	125.3 W
Jul 5, 1946	4.5	49.83N	125.5 W
Jan 26, 1957	5.0	48.12N	123.04W
Jun 23, 1963	4.5	50.31N	127.74W
Nov 1, 1968*	4.9	51.0 N	124.1 W
Nov 30, 1975*	4.9	49.2 N	123.6 W

Table 1.1 Larger historical earthquakes from Canadian Earthquake Epicentre File (CEEF). Dates with asterisks indicate events for which focal mechanism solutions were calculated [*Rogers*, 1979].

in the North America plate (figure 1.6, table 1.1). Rogers [1979] compiled focal mechanisms for four of these events and discussed their tectonic significance. The focal mechanism solutions indicate a north/south direction for the maximum regional compressive stress which is consistent with subsequent studies from Washington State and the results from this thesis.

This thesis deals entirely with the seismicity within the continental North America plate in southwestern British Columbia. Figure 1.7 shows the North America plate earthquakes, from Geological Survey of Canada (GSC) files, of all magnitudes from 1975-1991. The largest event

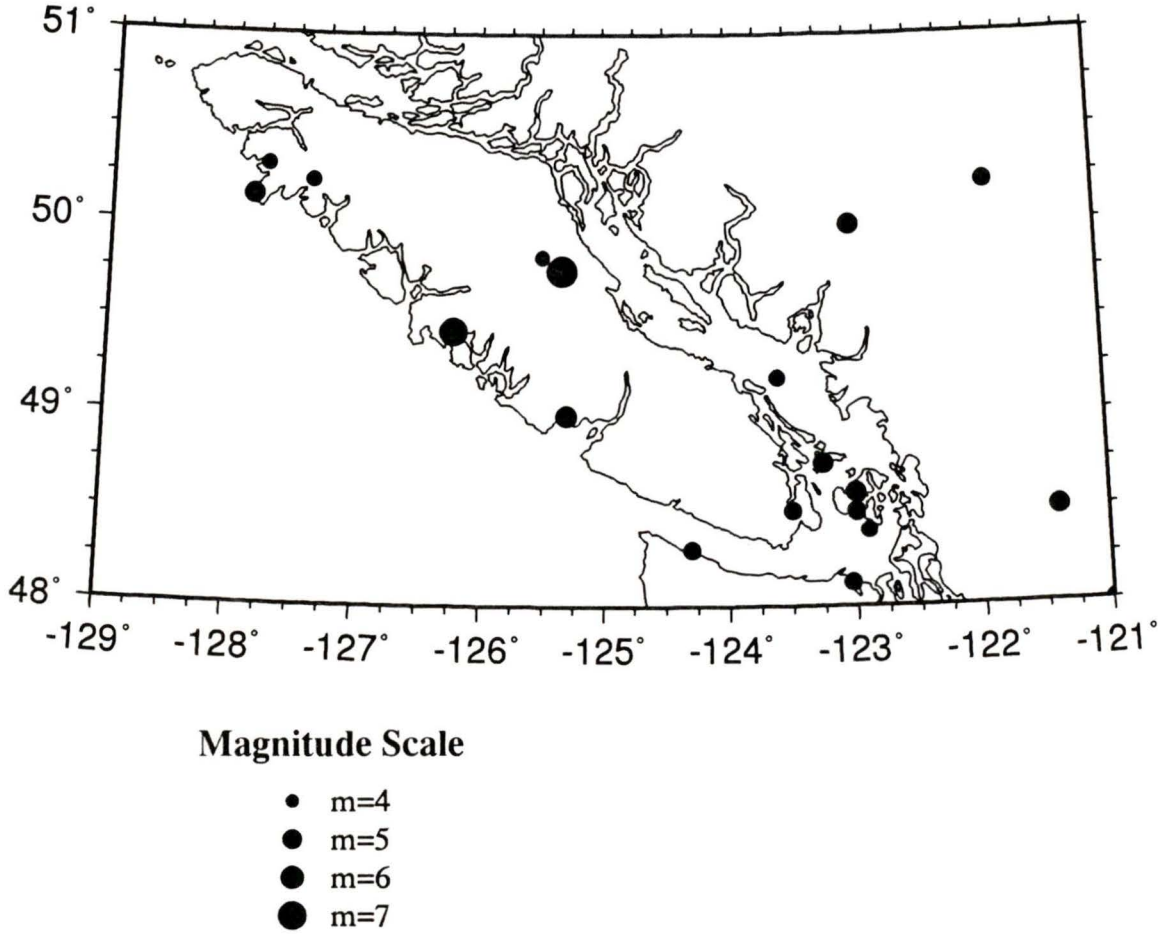

Figure 1.6 These are large (M ≥ 4.5) historic earthquakes within the North America plate occurring between 1900 and 1975. Epicentres are listed in table 2.1.

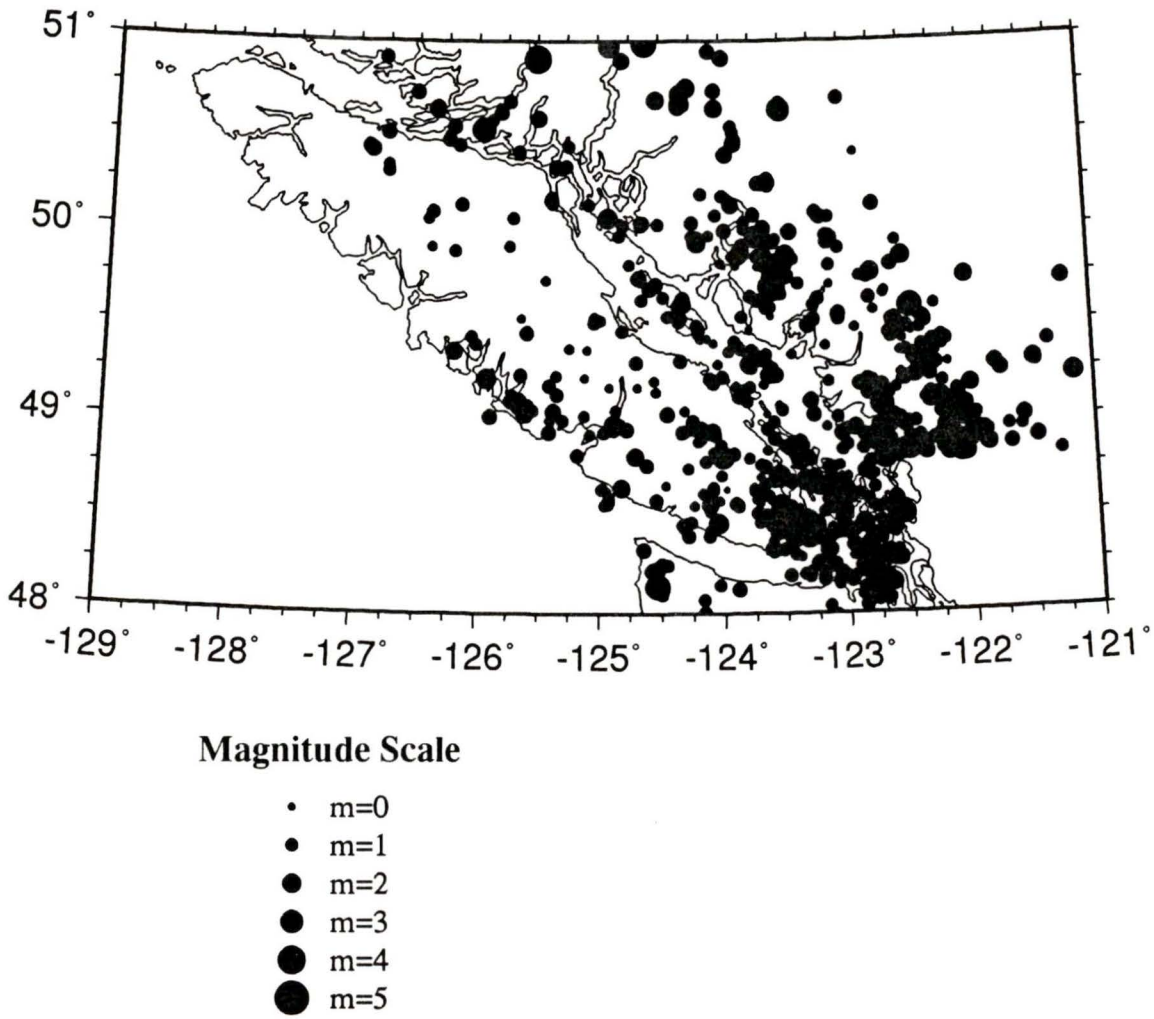

Figure 1.7 North America plate seismicity (from GSC files) from 1975-1991. These earthquakes include all magnitudes which occurred during this time period but are only complete from approximately m= ≥1 (most small events of fixed depth were removed); the largest event is m=3.9. The GSC routinely locates earthquakes within 25 km of the border, thus the lower right hand corner of the plot is artificially devoid of earthquakes.

during this time was magnitude 3.9 which occurred in the Coast Plutonic Complex in 1987.

1.5 THESIS OUTLINE

In southwestern British Columbia the continental crust of the North America plate overlies the subducting Juan de Fuca plate and is the site of frequent earthquake activity. Detailed seismic monitoring of the region began in 1984, and since then a decade of data exists to study this area. The aim of this thesis is to study the earthquakes within the North America plate in the region of southwestern British Columbia in order to understand the character of the seismicity and its possible causes. Recurrence relations, correlation of seismicity with topography and geology, correlation of seismicity with gravity and magnetic data, correlation of seismicity with rheology, regional stress regime, and Poisson's ratio are all examined and are presented in the following chapters.

CHAPTER 2

NORTH AMERICA PLATE SEISMICITY

2.1 DATA SELECTION

Digital seismic data in southwestern B.C. have been collected since 1975 by the Western Canadian Telemetered Network (WCTN) and the University of British Columbia (UBC). Seismic station coverage is shown in figure 2.1. Within the network (i.e. southern Vancouver Island, Georgia Strait, and adjacent mainland), event location accuracies are generally within 3 km horizontally and 5 km vertically. The ability to detect and accurately locate earthquakes decreases with distance from the network. All events were taken from the Canadian Earthquake Epicentre File (CEEF). Since the depth distribution of earthquakes was important in this study, only events which had data at four or more stations and depth errors of less than 7 km were included in the data set for analysis. For the majority of events, these criteria were met. Earthquakes which did not fit these criteria were generally less than magnitude 1. This makes the data set incomplete for earthquakes $< m=1$ inside the seismic array. It is assumed to be complete for $m \geq 1$. Most of the events are from 1981 onwards since that is when the network

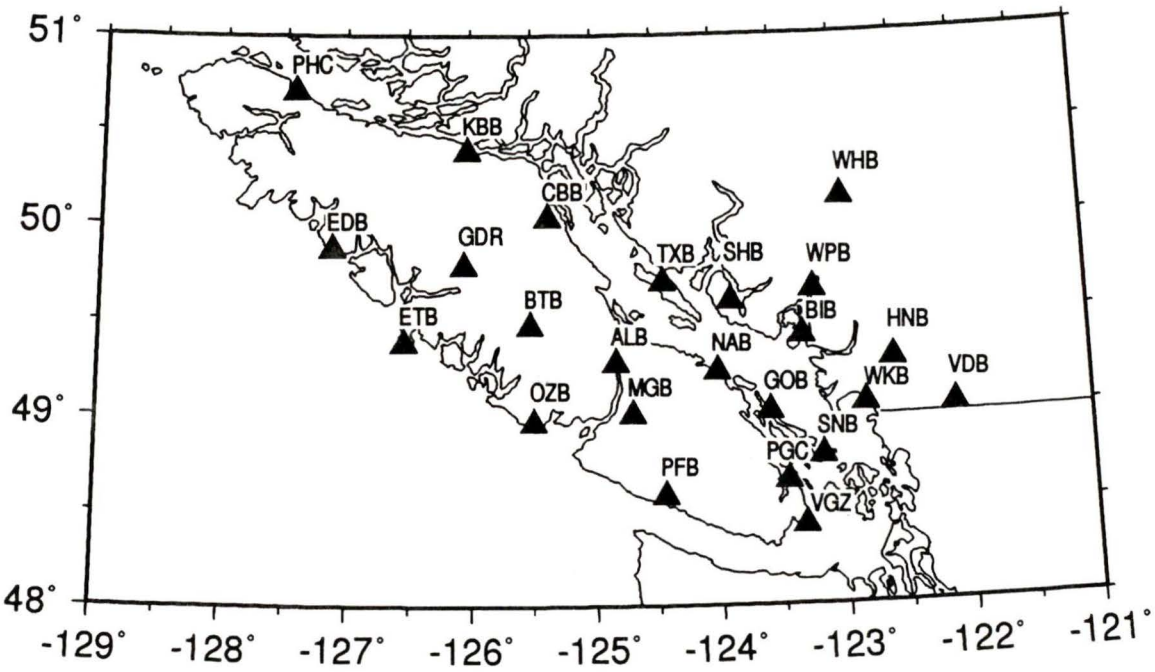

Figure 2.1 Seismic station coverage since 1984. From 1975 to 1984, ALB and stations near HNB (HYC), SNB (PIB), and PGC (VIC) were the four stations covering the region. Station coverage expanded significantly in 1984 resulting in a dramatic increase in event detection and accuracy of location.

expanded and consequently event detection increased.

Events determined to be within the oceanic Juan de Fuca plate were removed from this data set. The position of the subducting Juan de Fuca plate was previously determined by earthquake epicentres [*Rogers*, 1994] and seismic reflection data [*Clowes et al.*, 1987]. For events that lie within the oceanic plate, or within approximately 10 km above it, their depths and errors in depth were checked. Events which were constrained within their errors to lie 1 km or more above the oceanic plate were determined to belong to the North America plate. Events constrained to lie within the Juan de Fuca plate or 1 km above the plate were removed from the data set considered here.

A problem also arose with events which were located with fixed depths since when they were plotted on cross-section they showed artificial trends at these depths. Due to the sparse seismic station coverage prior to 1981, there was little depth control on earthquake hypocentre locations, particularly for earthquake located outside the seismic network. An arbitrary depth of 18 km, half the model crustal thickness, was selected as a default fixed depth for the majority of these events. The decision was made to omit these fixed depth events from the data set prior to 1981 since they would bias the data distribution at those depths. This left a few fixed depth events which occurred after 1980, on the assumption that depth control was better and that the fixed depth events were a good approximation to the "real" depth instead of just being an arbitrarily chosen depth as was the case prior to 1980. For the most part the fixed depth events in the North America plate which were retained, occurred to the east of Vancouver Island, outside the seismic array, and were small (less than magnitude 1). Because there is a lower rate of seismicity in this area and poorer seismic station coverage (figure 2.1) it was decided to keep as many of these events as possible.

2.2 DEPTH DISTRIBUTION OF SEISMICITY

Figure 2.2 shows the bimodal depth distribution of the earthquakes within the North America plate. There is a concentration of shallow events which decrease to a minimum between 8 and 10 km. The number of events increases to a maximum at a depth of 20 km, and then decreases again to essentially zero at 30 km. Figure 2.3 shows depth uncertainty histograms for all earthquakes in the North America plate. The majority of earthquakes have uncertainties of 4 km or less. The shallow earthquakes (less than 10 km) have a slightly greater uncertainty range (most up to 5 km or less) than the deeper earthquakes, implying that the deeper earthquakes, in general, are better located. Shallow earthquakes are more difficult to locate since the waves come in at very shallow angles and are likely to be more subject to time delays from travelling through longer sections of the inhomogeneous upper crust than would the waves from deeper earthquakes.

To confirm that there are no major trends in earthquake location errors with respect to depth, figure 2.4 shows a plot of error in depth location versus depth for all earthquakes. This is plotted next to the crustal model used to locate earthquakes. The only visible trend is the one that reflects the general distribution of earthquakes with depth, with the number of earthquakes dying off from 6-10 km and again after 30 km. Since the crustal model has an increase in velocity at 6 km depth, there was concern that the decrease in the bimodal earthquake distribution was a result of the model. Earthquakes from the culled data set which occurred in 1990 were relocated with a crustal model with no velocity increase at 6 km (an average of the velocity above and below the 6 km boundary was used) and with latitude and longitude held constant. There was no significant difference in the bimodal earthquake distribution within the depth uncertainties involved (figure 2.5). In addition, the majority of the shallow earthquakes occur within the Coast

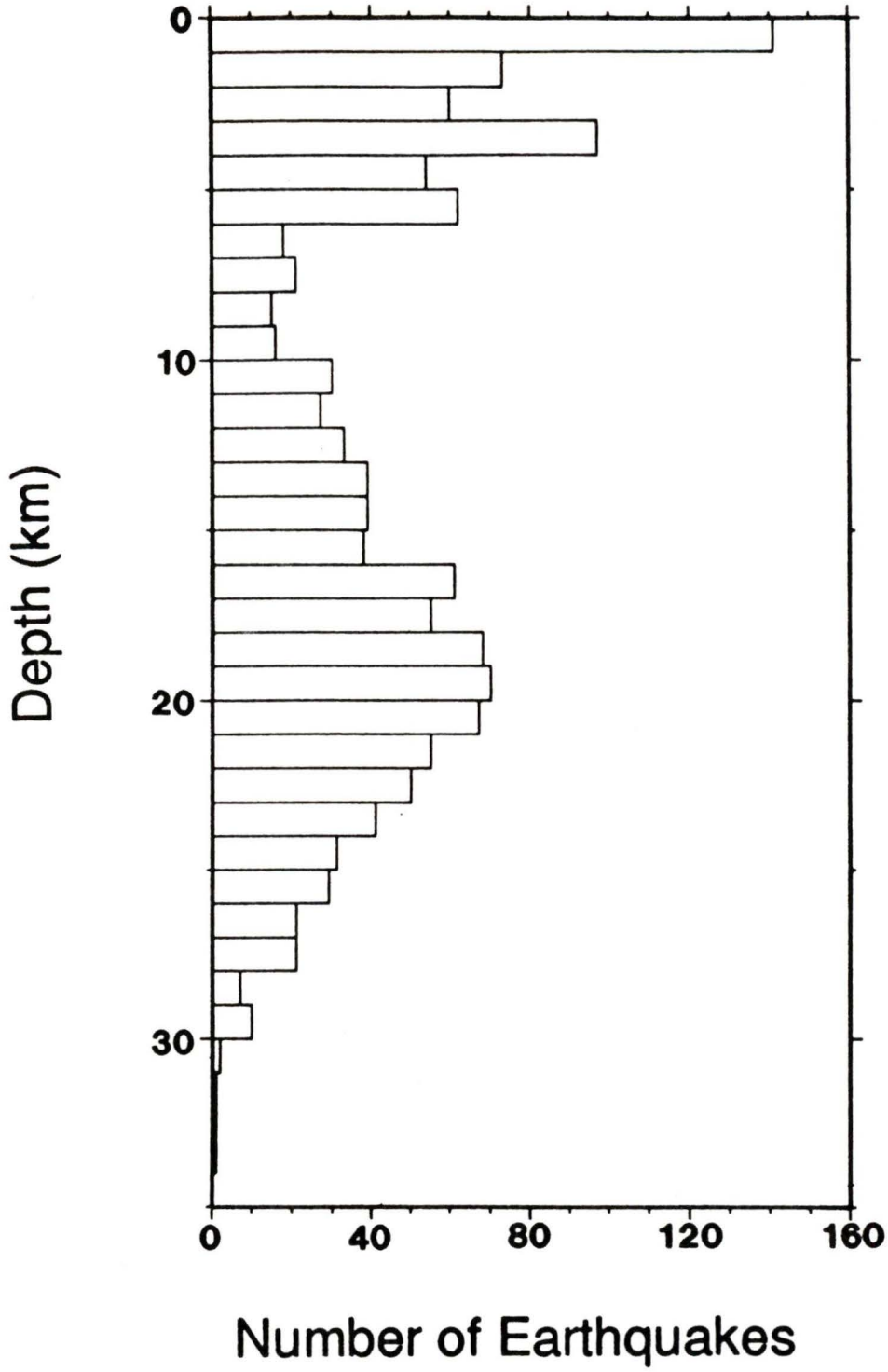

Figure 2.2 Histogram of earthquake depths for North America plate earthquakes. Note bimodal distribution with depth. The number of earthquakes decreases to a minimum between 6 and 10 km, increases from 10 to 20 km, and then decreases from 20 to 30 km.

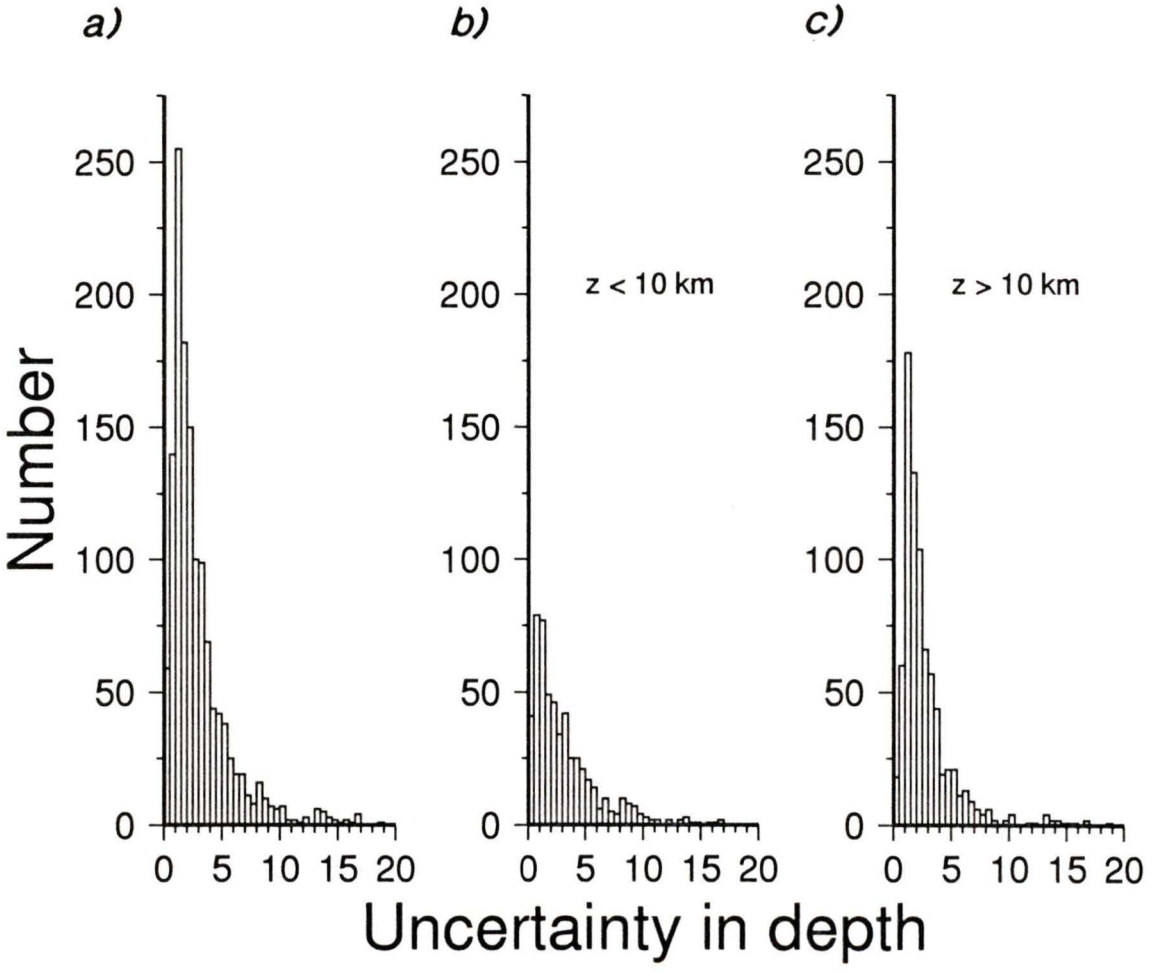

Figure 2.3 Depth error histogram for a) all earthquakes in the North America plate b) earthquakes less than 10 km depth c) earthquakes greater than or equal to 10 km depth.

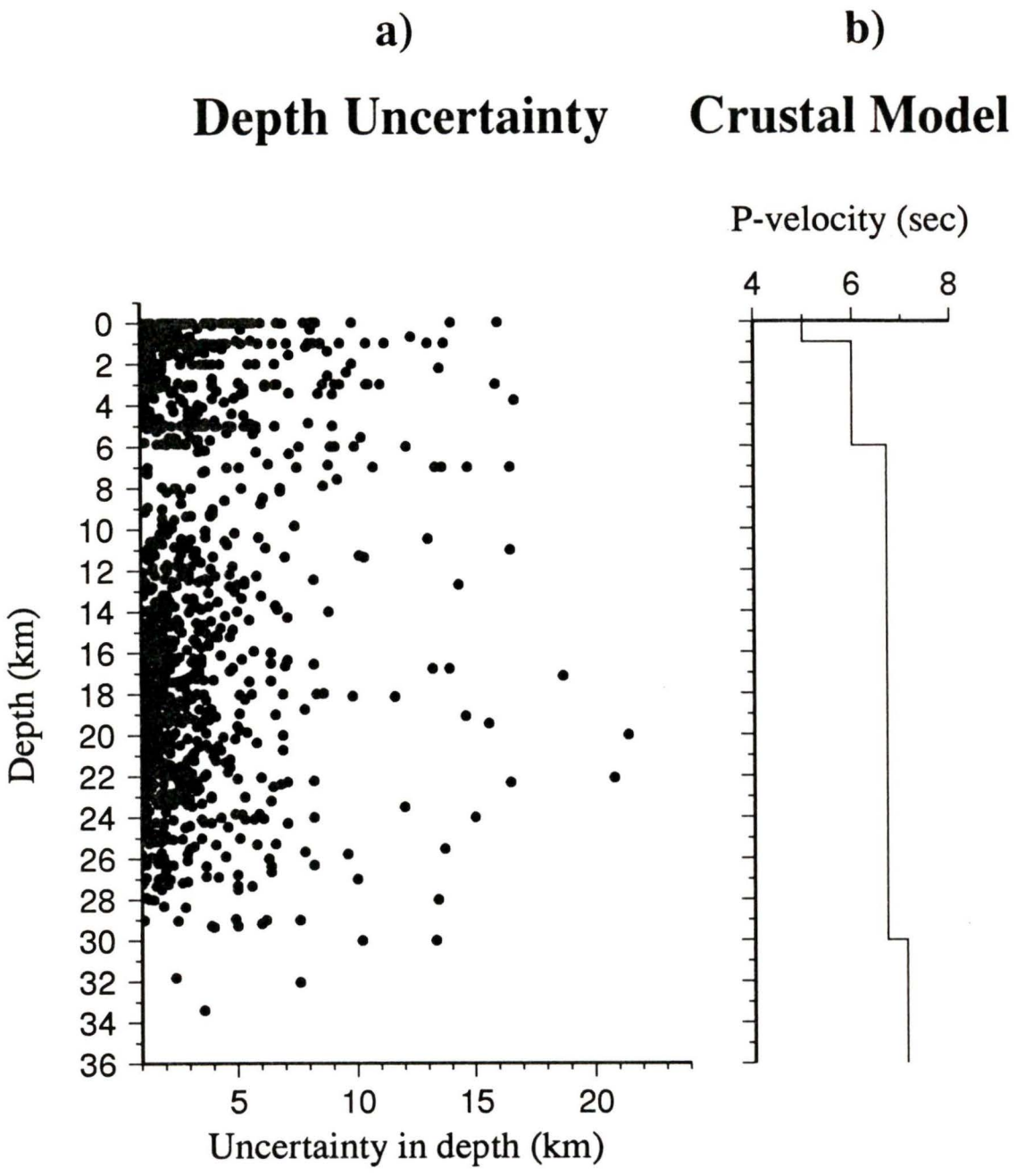

Figure 2.4 a) Scatter plot of error in depth location *vs* depth for North America plate seismicity. All magnitudes are included. The horizontal trends at 0 and 5 km are earthquakes of fixed depth that were not removed from the data set due to their magnitude and location with respect to the seismic network. b) Crustal model of depth *vs* velocity for comparison to scatter plot.

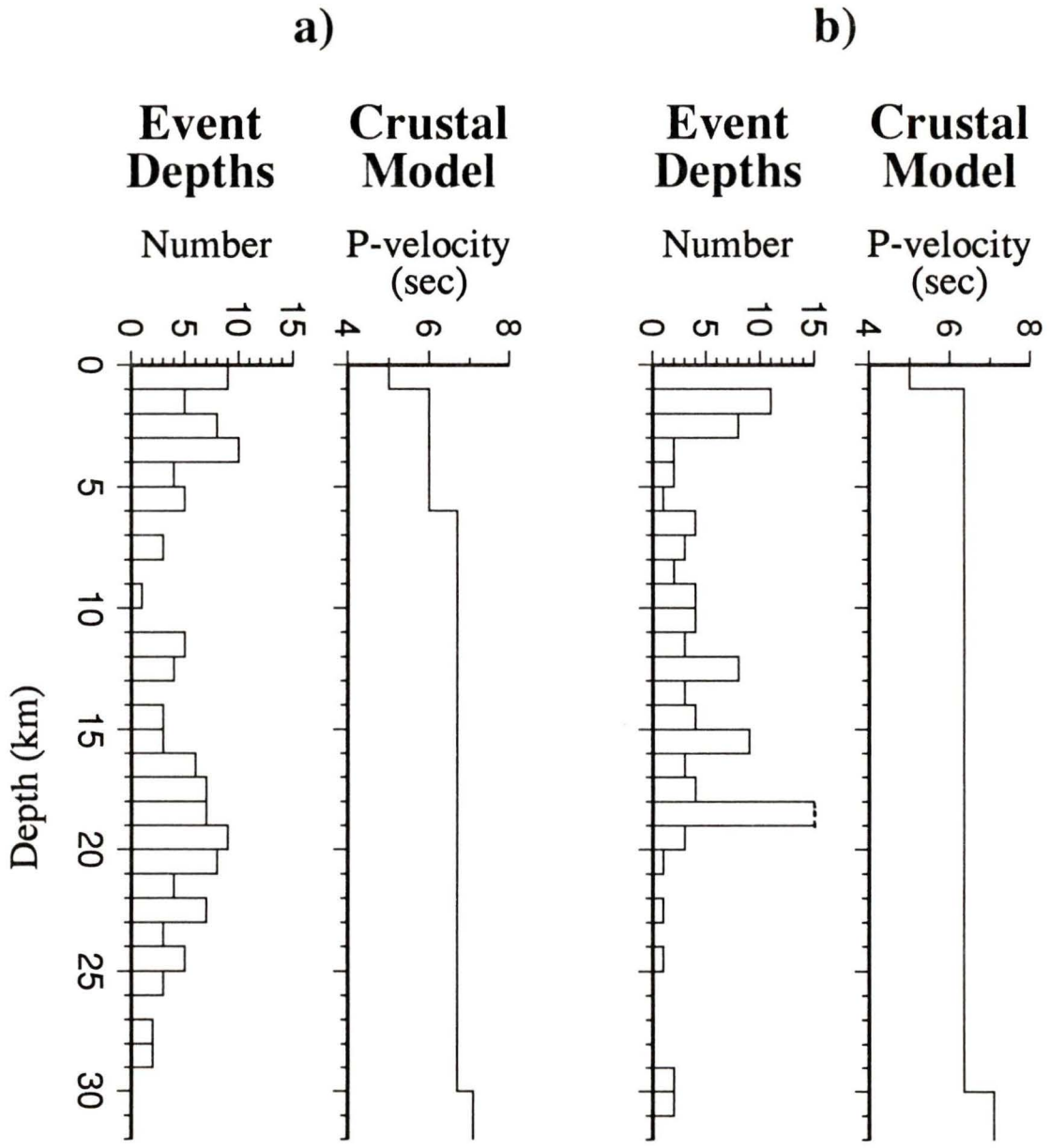

Figure 2.5 Histograms of 1990 earthquakes located with two different crustal models. a) Event depths and corresponding crustal model used in routine seismic processing with a velocity increase at 6 km depth. b) Event depths and corresponding crustal model with no velocity increase at 6 km depth. The relocation of these events with a different crustal model does not change the existence of the bimodal earthquake distribution.

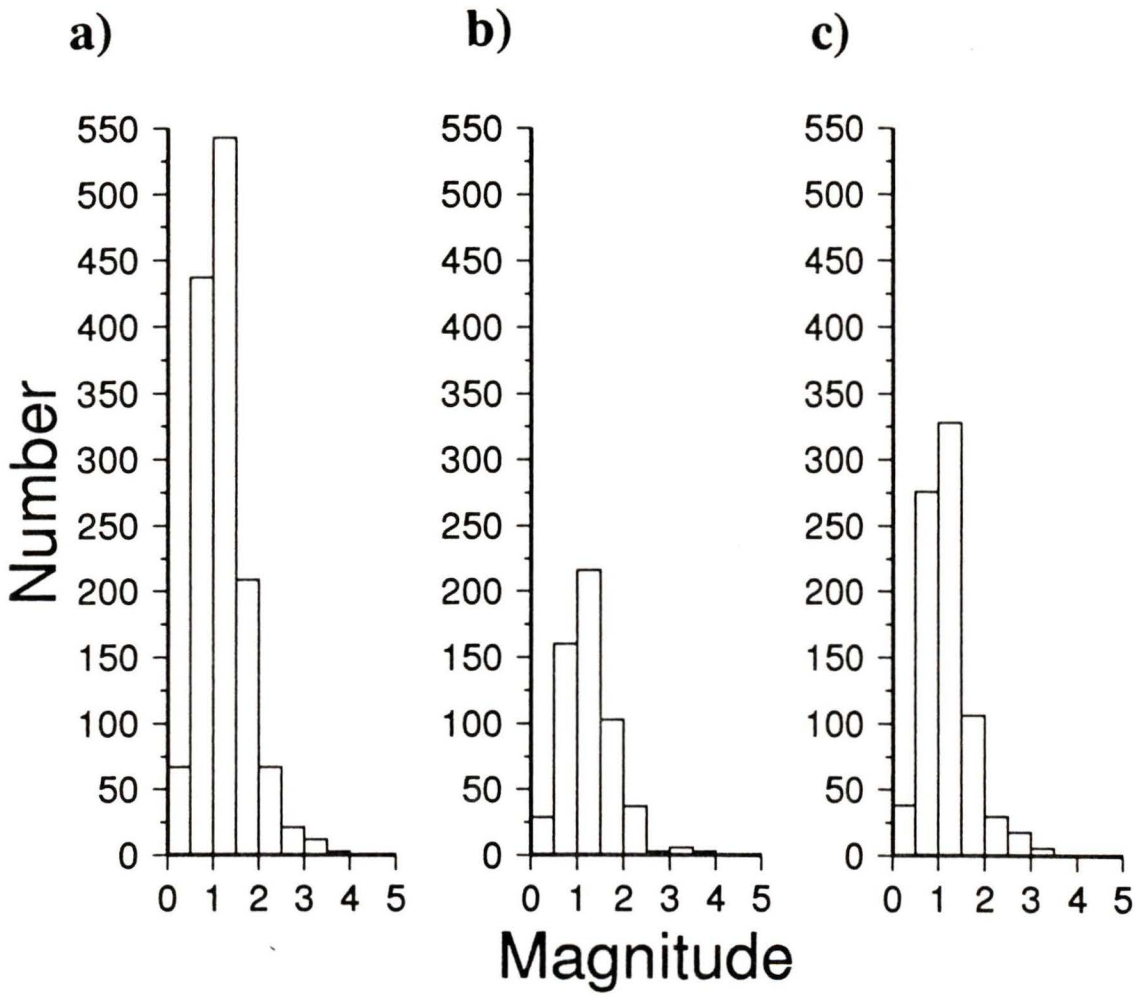

Figure 2.6 Histograms of magnitude distribution of seismicity for a) all depths b) shallow depth (< 10 km) and c) deep depth (≥ 10 km). For all depth distributions there are a large number of small earthquakes which peak from magnitudes 1 to 1.5 at which point the number of earthquakes rapidly dies off to zero by magnitude 4.

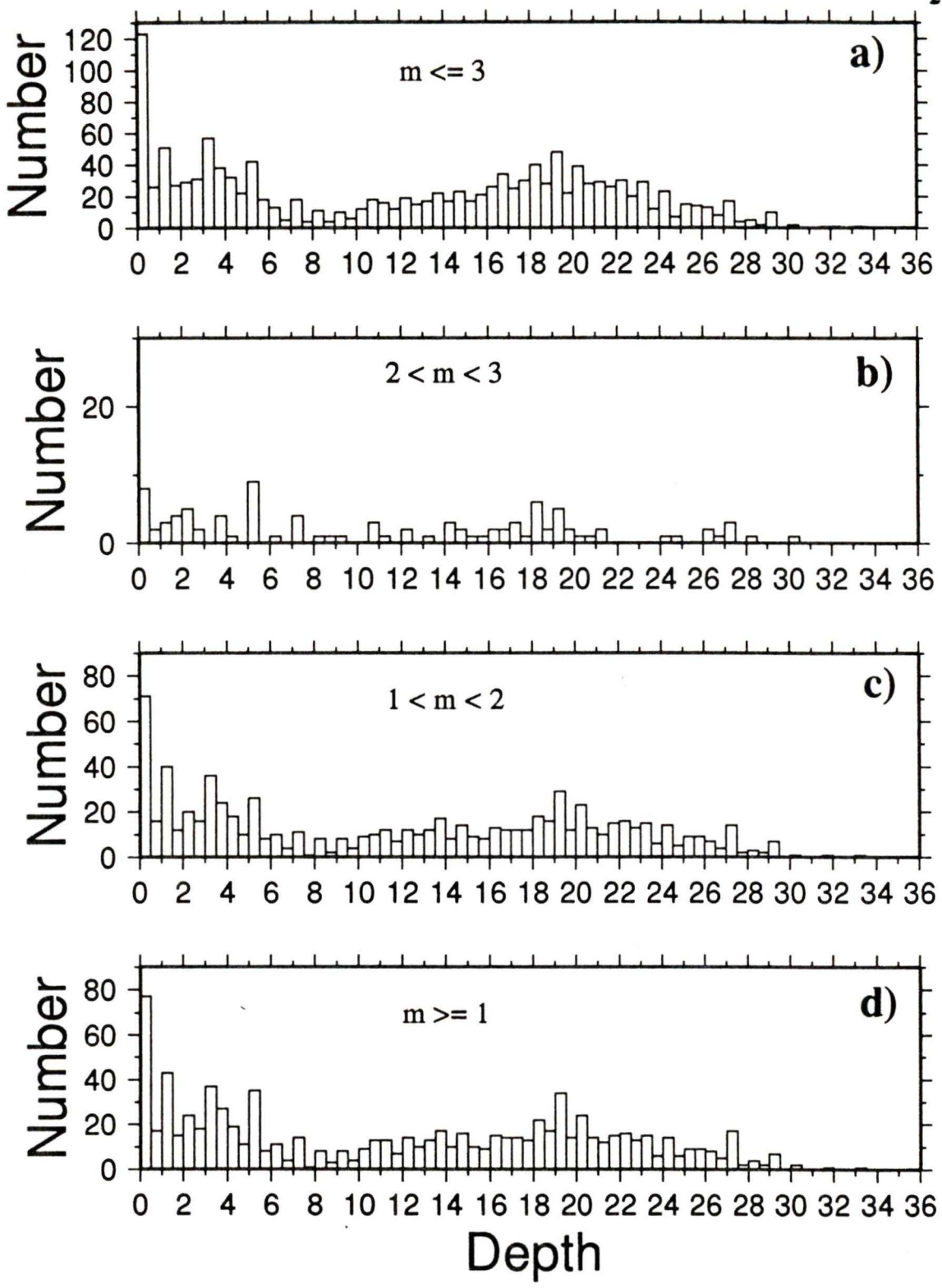

Figure 2.7 Histograms of magnitude distribution with depth for a) $m \leq 3$ b) $2 < m < 3$ c) $1 < m < 2$ d) $m \geq 1$. The bimodal earthquake distribution is reflected at all magnitudes. All magnitudes occur at all depths.

Plutonic Complex and the majority of deeper earthquakes occur beneath Vancouver Island (see figure 1.5).

To examine how magnitude is distributed with depth, events were separated into different magnitude regimes. From histograms of magnitude distribution with depth (figures 2.6 and 2.7) there is no discernable pattern; all magnitudes occur at all depths and there is no preference for, say, smaller magnitude events at shallower depths and larger magnitude events at greater depths. The bimodal depth distribution is reflected at all magnitudes.

2.3 RECURRENCE RELATIONS

The frequency of occurrence of earthquakes in a given region is always a question of concern. Usually, the larger the earthquake magnitude, the longer the time period between successive reoccurrences of another earthquake of that magnitude. For a given data set, a plot of the logarithm of the number of earthquakes within a given time period versus their magnitude can be fit to a straight line. The slope of this line has absolute value b and its intercept with the y-axis is a. Gutenberg and Richter [1949] empirically defined the recurrence relationship for earthquakes from this type of plot:

$$\log N = a - bm$$

where N is the number of earthquakes of magnitude m in a given time period and a and b are constants. Several workers [*Gutenberg and Richter*, 1949; *Mogi*, 1967; *Scholz*, 1968; *Wyss*, 1973] have examined the variability of the slope, or b-value. They have compared it to various physical parameters and have noticed that the average b-value varies from region to region, with an overall average value around 1. Mogi [1962, 1967] relates his experimental results on rock fracturing to the heterogeneity of the medium; homogeneous bodies exhibit lower b-values that

a more heterogeneously fractured body. From microfracturing experiments Scholz [1968] found that the frequency-magnitude relationship sharply distinguishes between two processes [*Scholz*, 1968]; that of low stress, which is characterized by crack closing and frictional sliding and results in high observed b-values (> 1), and that of high stress ($\geq$ 50% of fracture strength), which is characterized by propagation of new fractures and results in lower b-values (< 1) which decrease as stress increases. Wyss [1973] noted that frictional resistance to failure increases with depth which implies decreasing b with depth. When a thermal gradient becomes a factor, the stresses resisting fracture may decrease until resistance to shear is so low that all deformation occurs as creep. This implies increasing b-value with increasing temperature [Wyss, 1973].

2.3.1 Data and Results

Recurrence relations, or b-values, were calculated using the program of Weichert [1980] assuming that the earthquakes sequences have a Poisson distribution. The program applies to a range of earthquakes with continuous magnitude values. It groups data into discrete magnitude classes (m=1 to 2, m=2 to 3, m=3 to 4, etc.). The data must be continuous, or complete, for a given minimum-maximum magnitude interval so a minimum magnitude must be specified for each data set. A maximum magnitude is determined from the data plot.

Data from the North America plate data set in southwestern British Columbia were used to calculate b-values. Events with fixed depths were included for calculations so that the magnitude range could be assumed to be complete over the 10 year time span from 1981 to 1991. Data was divided up into four regions, based on varying stress regimes and geological composition: all of southwestern British Columbia, Vancouver Island, Coast Plutonic Complex, and the seismicity concentration at the bend in the North America plate coastline (figure 2.8). Vancouver Island and the Coast Plutonic Complex represent two geologically distinct tectonic

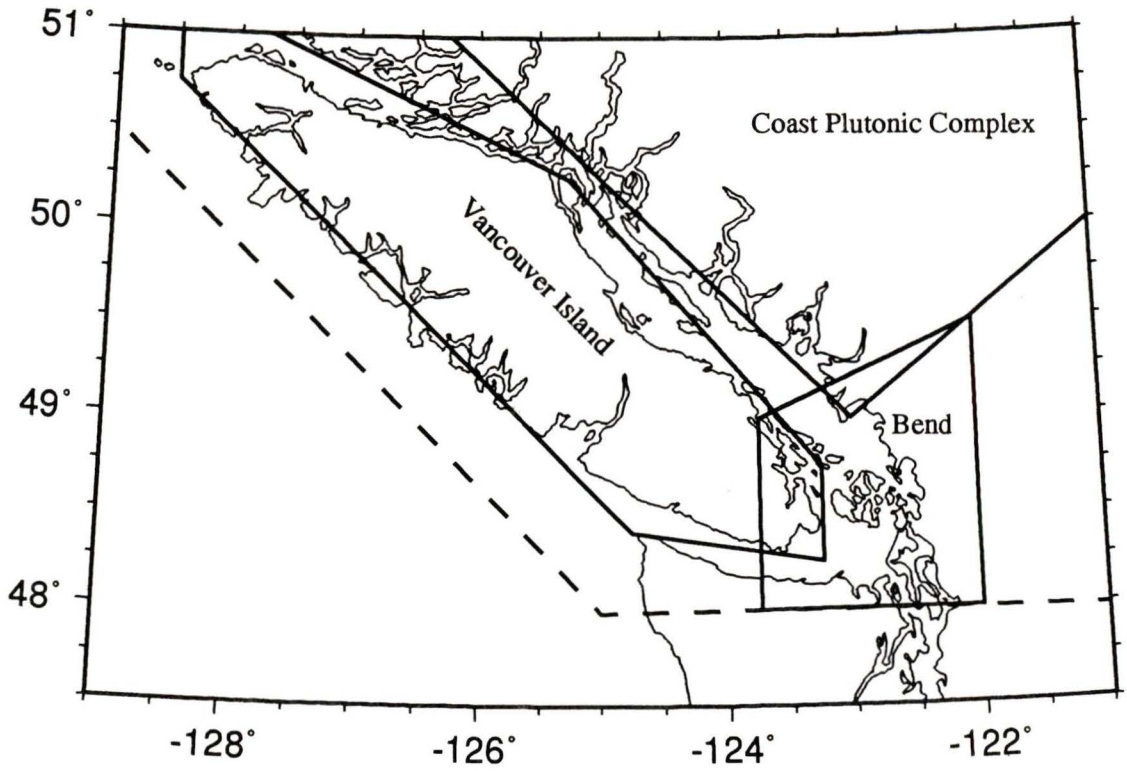

Figure 2.8 Regions for b-value calculations. Note the overlap between the regions. Southwestern British Columbia region encompasses all North America plate earthquakes with the study area as shown by the dashed line. The data were further subdivided into shallow (0-10 km) and deep (10-35 km) subsets for further comparisons. B-value results are listed in table 2.2.

Region	m_μ	m_x	b	Number of events
SW BC	1.0	4.5	0.875±0.030	1377
shallow	1.2	4.5	0.889±0.054	574
deep	1.1	4.0	0.990±0.050	803
Vancouver Island	1.0	4.0	1.037±0.076	368
shallow	1.0	3.0	1.221±0.194	86
deep	0.8	4.0	0.849±0.063	282
Coast Plutonic Complex	1.0	4.1	0.782±0.059	293
shallow	1.0	2.5	0.745±0.088	254
deep	1.1	2.8	0.848±0.227	39
North America bend	1.0	3.4	0.875±0.044	778
shallow	0.8	2.6	0.607±0.079	166
deep	1.1	4.0	0.973±0.059	612

Table 2.1 Calculated b-values for the given regions and minimum (m_μ) and maximum (m_x) magnitudes. Each region is further subdivided into shallow, ≤ 10 km depth, and deep, > 10 km depth, regimes.

regions which might reasonably be expected to respond differently to applied tectonic stresses. Many earthquakes appear inland from the bend in the coastline of the North America plate, possibly related to a high concentration of regional tectonic stress due to this bend [*Rogers*, 1983]. The four regions were further subdivided by depth into shallow (≤ 10 km) and deep (> 10 km) regimes based on the bimodal distribution of earthquakes with depth. After inspection of each subdivided data set a minimum magnitude was assigned. When the data were plotted in the form log *N* versus *m*, the maximum magnitude was determined by the magnitude at which N=0. Figure 2.9 shows histograms of log *N* versus *m* for the four regions and table 2.1 shows the tabulated results. During the time span of this study a greater number of earthquakes occurred beneath Vancouver Island (368 earthquakes ⇒ $9.4 \cdot 10^{-3}$ earthquakes/km^2) than in the Coast Plutonic Complex (293 ⇒ $6.0 \cdot 10^{-3}$ earthquakes/km^2), which may be a reflection of the difference in temperature.

The bend in the North America plate, like Vancouver Island, also shows a strong

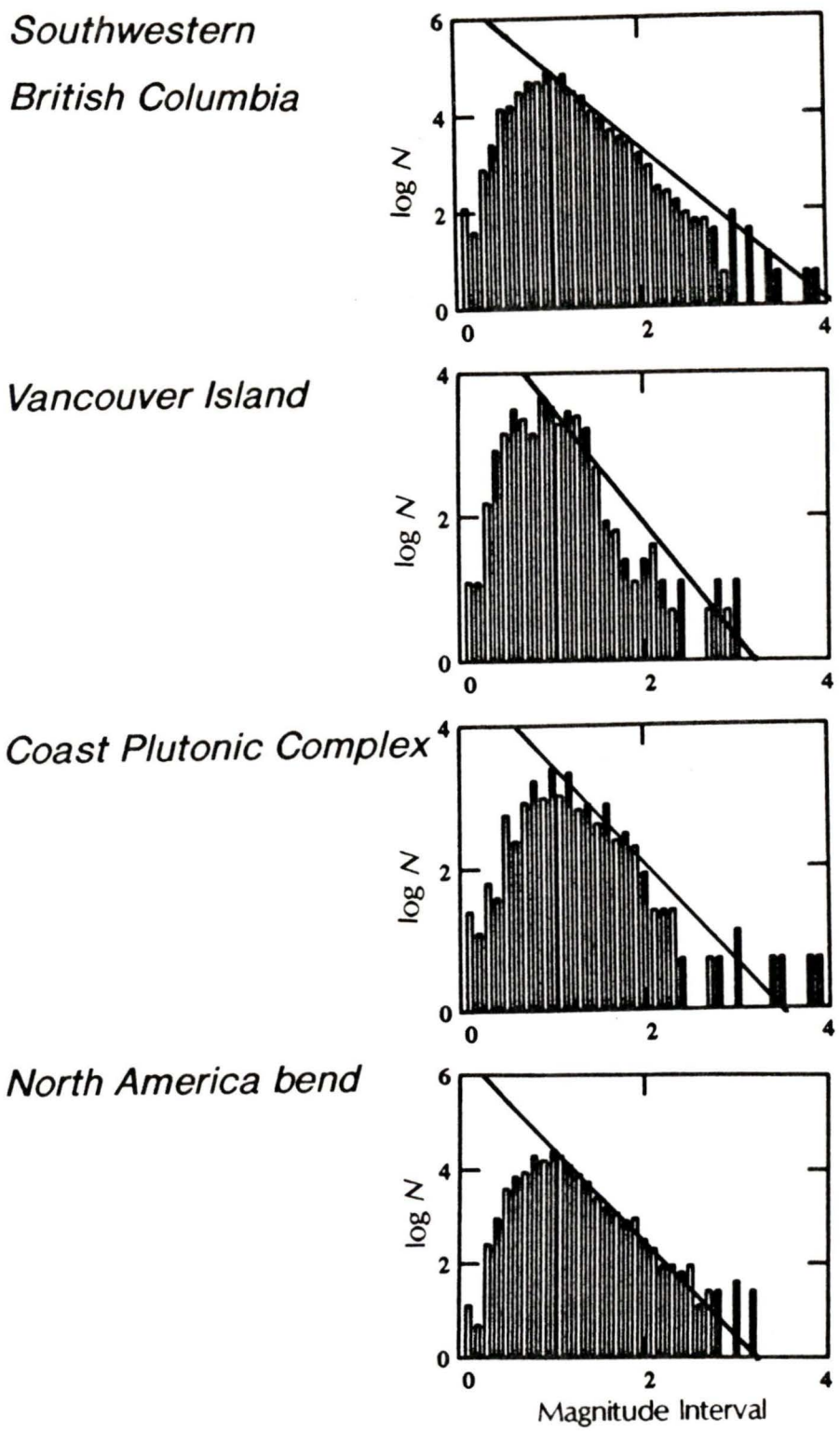

Figure 2.9 Histograms of log N vs m data for recurrence relationships; the linear best fit line for each data set is also shown. These plots illustrate for which magnitude intervals the data are nearly complete, for each of the four major data groupings. The b-values are listed in table 2.2. Regions are as discussed in text and as shown in figure 2.8.

separation between shallow and deep events with the majority of the events being deeper than 10 km (612 deep events compared to 166 shallow events). The deeper events have a significantly higher b-value (0.97) than the shallow events (0.61).

2.3.2 Discussion

The b-values shown in table 2.1 can be compared with those previously determined by other researchers. Variations in b-value have been associated with stress, rate of change of stress [*Scholz*, 1968], heterogeneity of material [*Mogi*, 1962, 1967], and temperature [as discussed in *Wyss*, 1973].

Rogers [1983] and Crosson [1981] have both calculated b-values for this general region of the Pacific Northwest. Rogers [1983] determined a b-value of 0.38 for central Vancouver Island (magnitude range 4-7 from 1900-1978). This is significantly different from the b-value of 1.04 determined for Vancouver Island; however Roger's data spans a magnitude range of $4 \leq m \leq 7$ while the data in this study spans a magnitude range of $1 \leq m \leq 4$. In addition, this study encompassed the whole of Vancouver Island (data mainly concentrated within the southern half) while Rogers' study concentrated on central Vancouver Island (where there are very few small earthquakes (see figure 1.7). Crosson [1981] determined a b-value of 1.02 for Puget Sound (magnitude range $0 \leq m \leq 4.8$ from 1970-1978). This favourably agrees with the b-values of 1.04 for Vancouver Island and 0.88 for the bend in the North America plate from this study. Crosson's data set encompasses a similar magnitude range over roughly the same time period as the data set in this study so the b-values can be compared with meaning.

There are several factors which influence the seismicity, and hence b-values, of a region. Scholz [1968] concluded from his microfracturing experiments that b-values significantly decrease with an increase in stress. If this is true, then from table 2.1 it could be concluded that stress

increases inland, away from the subduction zone since the b-value decreases from Vancouver Island to the San Juan Islands to the B.C. mainland (the Coast Plutonic Complex). However, from heat flow values [*Lewis*, 1991; *Lewis et al.*, 1992] this region also gets increasingly warmer from west to east and if temperature was a dominating factor then b-values could be expected to increase [*Wyss*, 1973] inland in this region. Since b-values decrease, it is unlikely that temperature is the dominating factor in the stress regime here. There is also a significant change in geology from Vancouver Island (Wrangellia terrane - basalts) to the mainland (Coast Plutonic Complex - granodiorites) which may be the greatest factor influencing the b-values. Both upper Wrangellia, as defined by Zelt *et al.* [1993], and the Coast Plutonic Complex extend to approximately 10 or 15 km depth [*Clowes et al.*, 1987; *Dehler and Clowes*, 1992]. Zelt *et al.* define middle Wrangellia as lying below (depth approximately 12 to 20 km) upper Wrangellia and extending eastward, beneath the Coast Plutonic Complex, possibly as far as the Harrison Lake Fault. The b-values reflect the differences between the upper 12 km of Vancouver Island (upper Wrangellia; $b=1.22$) and the Coast Plutonic Complex ($b=0.75$), and the similarities in geological structure between lower Vancouver Island (middle Wrangellia; $b=0.85$) and the "lower Coast Plutonic Complex" (also middle Wrangellia; $b=0.85$). Consequently, differences in stress and geology affect seismicity in the upper portion of the crust. Variations in fluid content may also play a role, but little is known of fluid distribution in the crust at this time.

CHAPTER 3

CORRELATION OF SEISMICITY WITH TOPOGRAPHY AND GEOLOGY

3.1 INTRODUCTION

The topography and geology of western North America are intimately related to the past and present tectonic motions along this coast. The majority of the morphological and geological features are a result of past tectonic motions, with the geology constraining the rheology of the area which in turn constrains the current seismicity. All the seismic events recorded are due to contemporary tectonic geometry and motions and are partially constrained by the geological boundaries formed during past tectonic events.

3.2 TOPOGRAPHY

The subduction trench offshore and paralleling Vancouver Island, which is filled with

thick sediments, occurs at a maximum water depth of 2.5 km. East of the trench, the western coast of Vancouver Island rises above sea level to a local topographic high on the mountains of Vancouver Island. East of these mountains the topography drops to a low in the Georgia Strait area between Vancouver Island and the mainland. This topographic low continues to the south into Washington State where it is called the Puget Sound lowlands. Farther inland the Coast Mountains rise to a topographic high [*Tiffin and Seeman*, 1985].

Precise levelling and gravity surveys, examination of tide-gauge data [*Dragert and Lisowski*, 1990], and continuous GPS monitoring [*Dragert and Hyndman*, 1995] show rapid uplift ($\sim$9.5 mm/yr) of the region north of central Vancouver Island, consistent with overriding of the young, buoyant Explorer plate. Uplift, at a less rapid rate ($\sim$3 mm/yr), also occurs south of this region to the Olympic Peninsula north to Campbell River [*Dragert and Lisowski*, 1990]. Dragert and Lisowski [1990] attribute changes in vertical and horizontal deformation to differential plate motions across the underlying Nootka fault. There appears to be very little seismicity in the northern half of central Vancouver Island which does not appear to agree with Dragert and Lisowski's determination of rapid uplift in this region, unless uplift was occurring aseismically. It is possible that this lack of seismicity is a problem of earthquake detection. An inspection of the seismic network in figure 2.5 shows a paucity of seismic stations in northern Vancouver Island compared to southern Vancouver Island. The stations which are primarily relied upon for locating earthquakes in northern Vancouver Island are PHC, EDB, ETB, GDR, and CBB (see figure 2.1). EDB and ETB are coastal stations which are most affected by microseismic noise from wind and waves. Consequently the background noise at these stations is high, lowering the detection threshold. Furthermore, with no seismic station in central Vancouver Island between GDR and PHC, small earthquakes located in the centre of this region may not be recorded at a minimum of three stations from which an epicentre determination can be made. Nevertheless,

there is little doubt that the southern half of Vancouver Island has more seismicity than the northern half.

There are three positive correlations of seismicity with topography. These are:

1) Apparent correlation of seismicity (see figure 1.7) with the topographic low through Georgia Strait and Puget Sound. This topographic low is filled with basin and glacial deposits (see figure 1.3).

2) Apparent correlation of seismicity with the bend in the coastline. Seismicity is concentrated at the southern end of Vancouver Island and the adjacent mainland, and continues south into northernmost Washington state (see figures 1.4 and 1.7). There is significant overlap with the Georgia Strait and Puget Sound topographic low mentioned in (1).

3) Apparent correlation of northwest/southeast trends of seismicity (see figures 1.4 and 1.7) with the topographic high of the Coast Mountains. This band of seismicity borders the eastern edge of the main concentration of earthquakes. They are also correlated with increased heat flow to the east of the Garibaldi Volcanic Belt [*Lewis et al.*, 1992], marked by the location of volcanoes in figure 1.1.

3.3 GEOLOGY

The region of this study covers both the Insular and Coast tectonic belts (see figures 1.2 and 1.3) which are two distinct geological regions. Figures 3.1 and 3.2 compare shallow ($z < 10$ km) and deep ($10 \leq z < 30$ km) seismicity with the geologic terranes and mapped surface

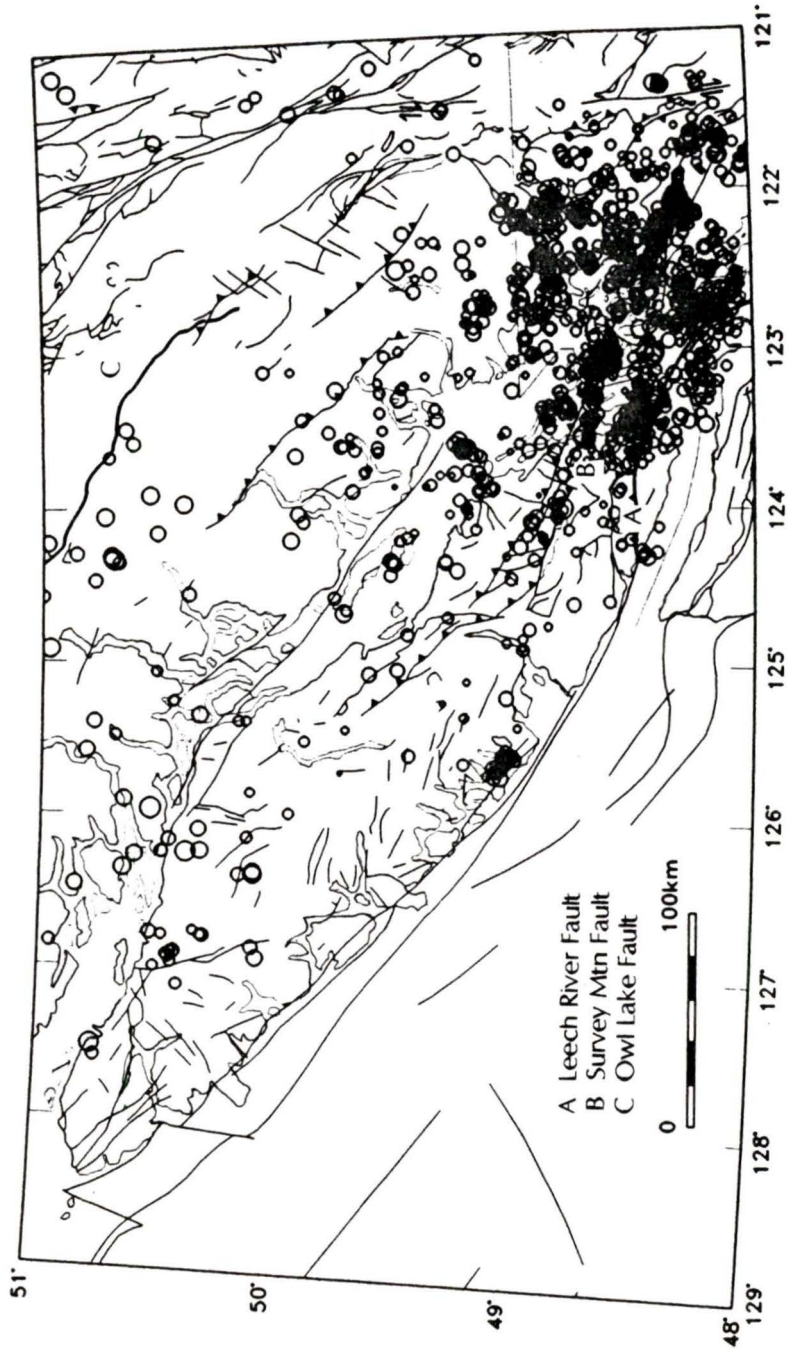

Figure 3.1 Fault map of southwestern British Columbia with shallow (< 10 km) earthquakes plotted. Faults taken from Wheeler and McFeely [1991].

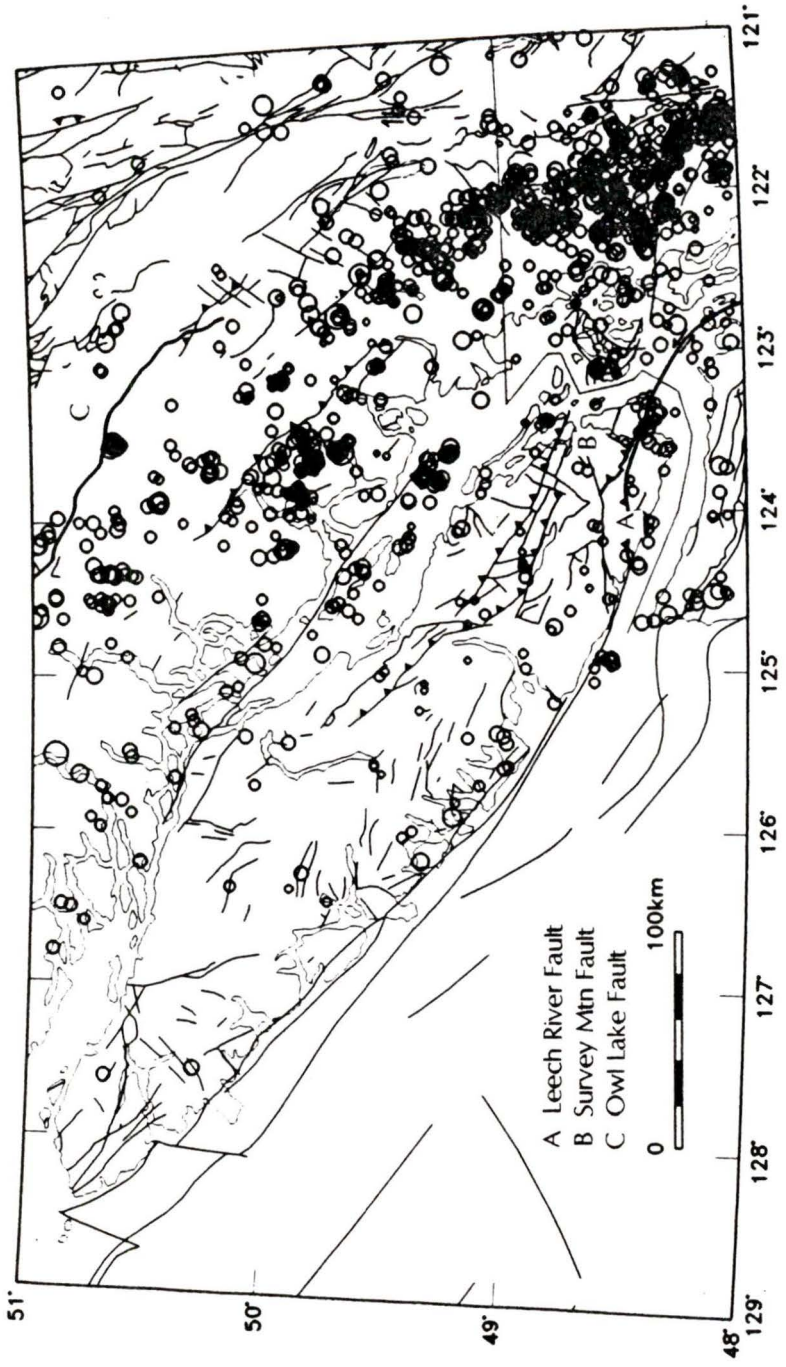

Figure 3.2 Fault map of southwestern British Columbia with deep (≥ 10 km) earthquakes plotted. Faults taken from Wheeler and McFeely [1991].

faults.

Most of the shallow seismicity (figure 3.1) clearly lies within the Coast belt, extending south down into the Cascades in Washington state. The earthquakes are not associated with any fault in particular but instead lie between the Strait of Georgia and Owl Lake fault. They predominantly show linear trends parallel to the Strait of Georgia with some smaller perpendicular (SW-NE) trends evident. There is very little shallow seismicity associated with either the Insular belt or the Intermontane belt. At the southern end of Vancouver Island, in the Victoria region, there are a group of shallow earthquakes in the region of the Leech River and Survey Mountain faults. This is examined in further detail in Chapter 8. There are also earthquakes which may be associated with faults in northern Washington state but these are outside the region studied in this thesis.

Most of the deep seismicity (figure 3.2) is concentrated in the southern end of Vancouver Island and the adjacent mainland at the "bend" in the North America plate from north-south in the US to northwest-southeast in Canada. No correlation between deep seismicity and exposed surface faults is expected; however some of the observed northwest-southeast linear trends of epicentres along the southern part of Vancouver Island have the same orientation as some of the near surface faults in the region. Again some of this seismicity occurs in the Leech River, Survey Mountain fault regions and is examined in more detail in Chapter 8. There is more deep than shallow seismicity in the Insular belt, but only a small amount of deep seismicity in the Coast belt. Very little seismicity occurs east of Owl Lake fault and in the Intermontane belt.

There is no direct correlation of seismic trends with mapped faults in this region of southwestern British Columbia (figures 3.1 and 3.2), implying that these faults can not be identified as active today. Consequently it appears that deformation, as inferred from earthquake distribution, is occurring within geological units and not along major pre-existing faults between

or within these units.

CHAPTER 4

SEISMICITY CORRELATION WITH GRAVITY AND MAGNETIC DATA

4.1 INTRODUCTION

Along with seismicity, which provides information concerning the strength of the earth's crust and the stress it is subjected to, potential field data provide additional information on deep earth structure. Both gravity and magnetic methods attempt to measure small differences in a relatively huge force field. Due to the nature of the bipolar magnetic field, secular variations, and the influence the solar wind has on the geomagnetic field, magnetic maps tend to be more complex than gravity maps and variations in the magnetic field are more erratic and localized [*Telford et al.*, 1976].

Gravity is a natural source method in which local variations in the density of rocks near the earth's surface cause minute changes in the main monopolar gravity field [*Telford et al.*, 1976]. The gravity map shows mainly regional effects. Unprocessed gravity data reflect a combination of elevation, density, thickness of the earth's crust, and nearby topography changes. For the "free-air gravity anomaly", the gravity data is processed so that all the readings are

reduced to a common datum (mean sea-level). However, the free-air correction does not account for the material between the datum and the measuring site, so the free-air map also reflects changes in elevation as well as density and crustal thickness. The free-air anomaly map is usually used over very flat surfaces such as over water where there is no question of added or missing land mass. The "Bouger gravity anomaly" corrects for the extra land mass which is above the datum, or missing land mass if the reading was taken below the datum. Bouger anomaly maps reflect variations in density and crustal thickness.

The magnetic method also relies on a natural source field, but one which changes over time. Large variations in the magnetization of rocks near the earth's surface cause changes in the measured magnetic field [*Telford et al.*, 1976]. The magnetic response of rocks is determined by the amount of magnetic minerals they contain, which have susceptibilities far greater than the components themselves. Magnetic susceptibility is the degree to which a body is magnetized; it is the ratio of induced magnetization to the strength of the magnetic field causing the magnetization. Susceptibility is affected by temperature; an increase in temperature causes a decrease in susceptibility until the material reaches the Curie point (which varies for different minerals) and becomes demagnetized. Coles and Currie [1977] found that the Curie point for samples of Coast Plutonic rocks was between 565°C-580°C. Lewis *et al.*'s [1992] heat flow profile indicates that the Curie point is reached at an approximate depth of 25 km on the western side of Vancouver Island and increases to approximately 45 km just west of the Garibaldi Volcanic Belt. This exceeds the base of the brittle portion of the North America plate, as determined from seismicity, so it is safe to assume that the temperature of the entire North America plate in southwestern British Columbia is below the Curie point and that the magnetic data reflect structures from the base of the North America plate to the surface.

4.2 DATA PROCESSING

In the gravity data presented here, a free-air anomaly was used at sea and a Bouger anomaly was used on land with all units in mGals (1 Gal = 1 cm/sec^2, the unit of acceleration of gravity); the data was supplied by the National Geophysical Data Centre (NRCan, Ottawa). A data processing package called GEOSOFT [1992] was used to process both the subsequent gravity (figure 4.1a) and magnetic (figure 4.1b) data. For both data sets the data were converted to a Lambert Conformal projection, Fourier transformed to the frequency domain, filtered, and inverse Fourier transformed back to the spacial domain. Due to the bimodal distribution of seismicity (see figure 2.6) it was decided to split the seismic, gravity, and magnetic data sets into shallow (0 to 10 km) and deep (between 10 to 30 km) regimes for comparison purposes. Figures 4.2 and 4.3 show the distribution of shallow and deep seismicity, respectively, with trends in the seismicity outlined and numbered for reference. Both the gravity and magnetic data were filtered using a gaussian filter for shallow, 0 to 10 km depth, and for deep, 10 to 30 km depth, wavelengths. A gaussian filter is a highpass filter which uses the standard deviation for a gaussian distribution ($1/\lambda$) to determine the shape of the cutoff curve between low and high frequencies. A bandpass type filter can be obtained by combining gaussian filters centred on different frequencies. Wavelengths (λ) of twice the desired depth (0 km and 20 km for the shallow filter, 20 km to 60 km for the deep filter) were used to filter for the signals desired. The resulting gravity and magnetic maps were overlain by the corresponding seismicity: 0 - 10 km depth seismic events for the shallow data and 10.1 - 30 km depth events for the deep data. First derivatives of both the shallow and deep data for gravity and magnetics were also computed in order to highlight rapid changes in the data which might reflect subsurface structure, but the results did not show any features or trends that were not visible from the simple Gaussian depth filtered plots. The majority of the seismicity occurred in the southern half of Vancouver Island

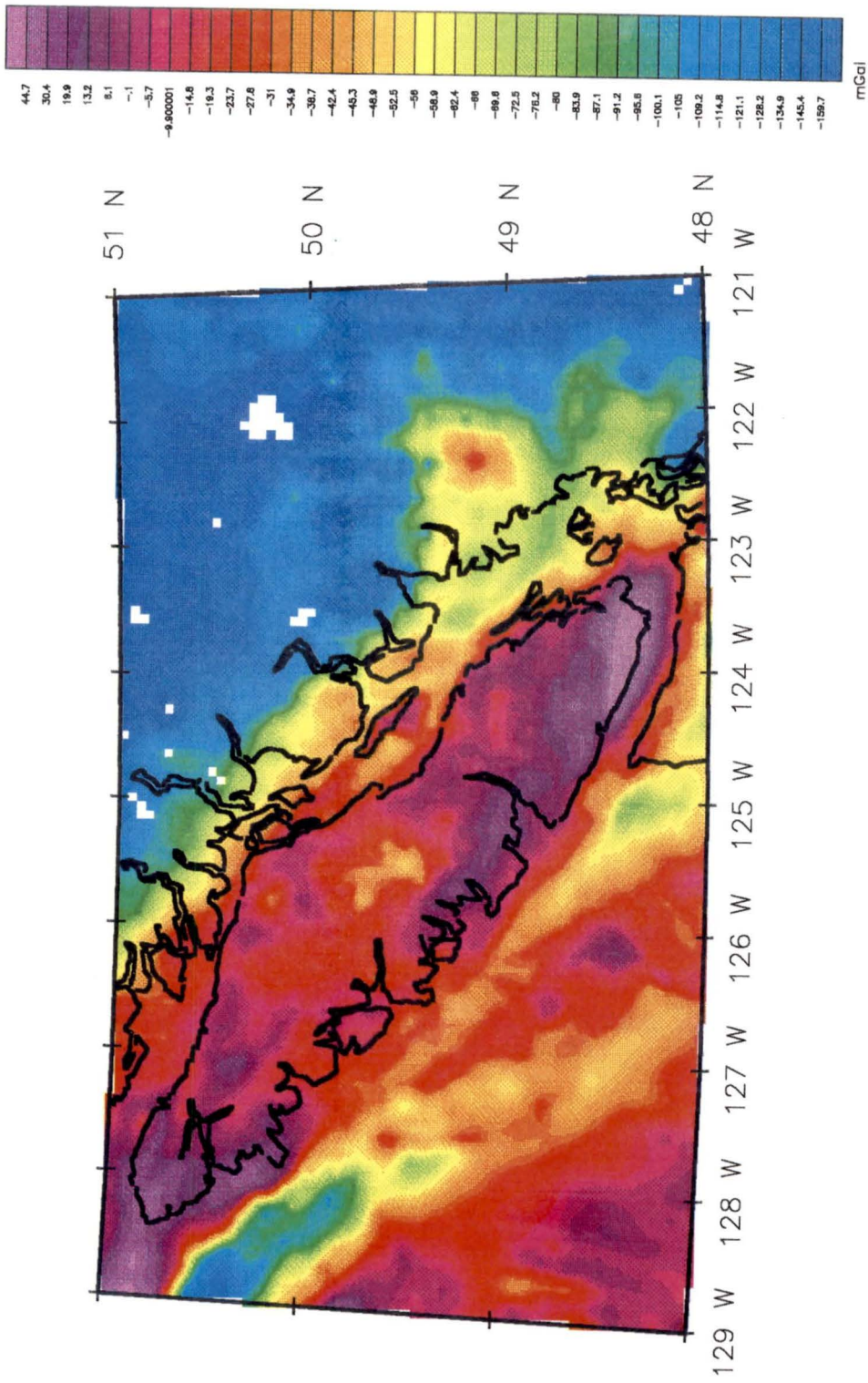

Figure 4.1a Unfiltered gravity map for southwestern British Columbia. Free-air gravity data over sea, Bouger gravity data over land. Note subduction zone pattern of high, low, high, low from west (offshore, oceanic Juan de Fuca plate) to east (onshore, overlying North America plate).

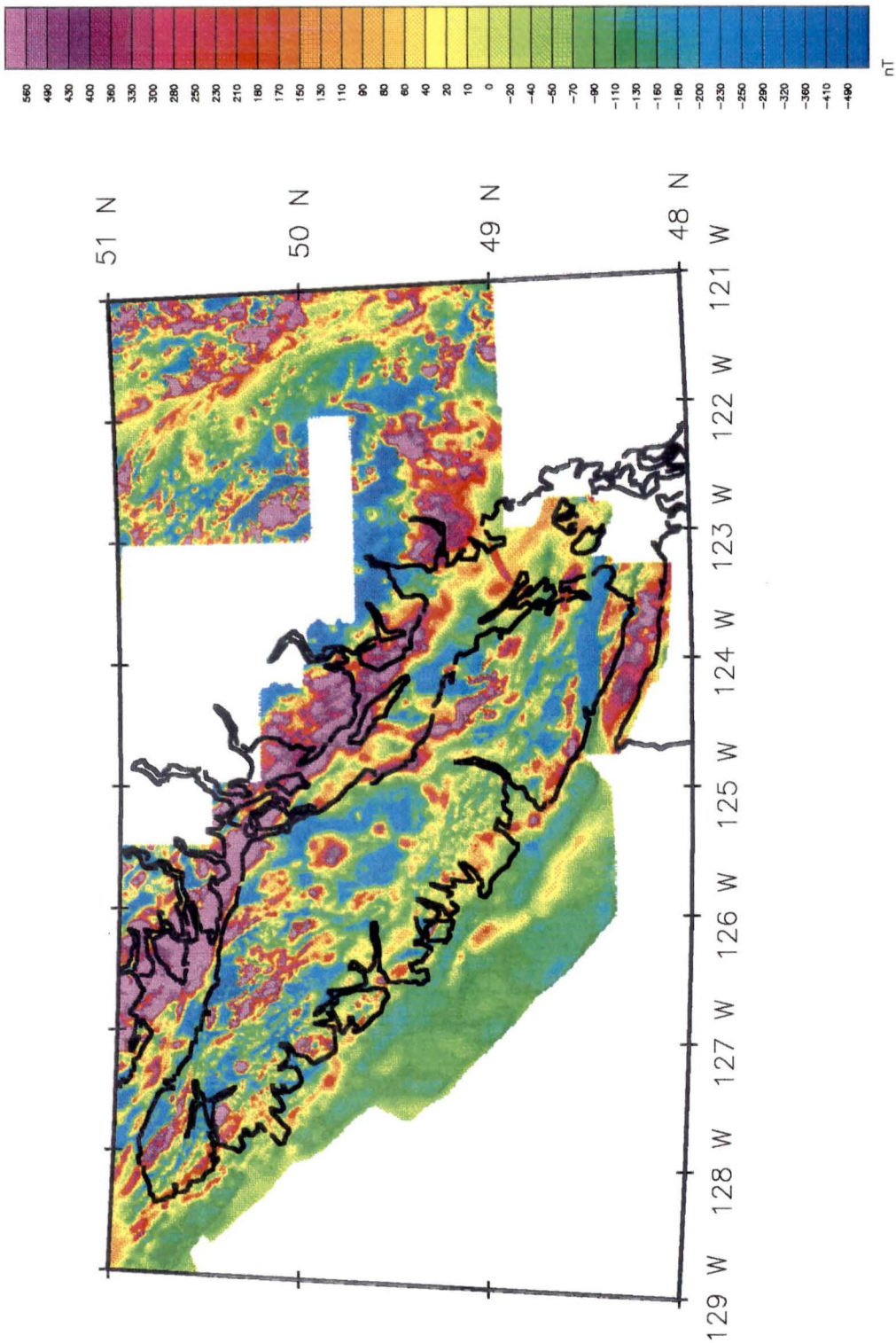

Figure 4.1b Unfiltered magnetic map. Major fault zones such as Leech River fault (see figure 3.1) in the southern tip of Vancouver Island and a series of north-northwest/south-southeast running faults (such as the Hope fault and Fraser fault systems) on the far eastern side of the map are clearly evident.

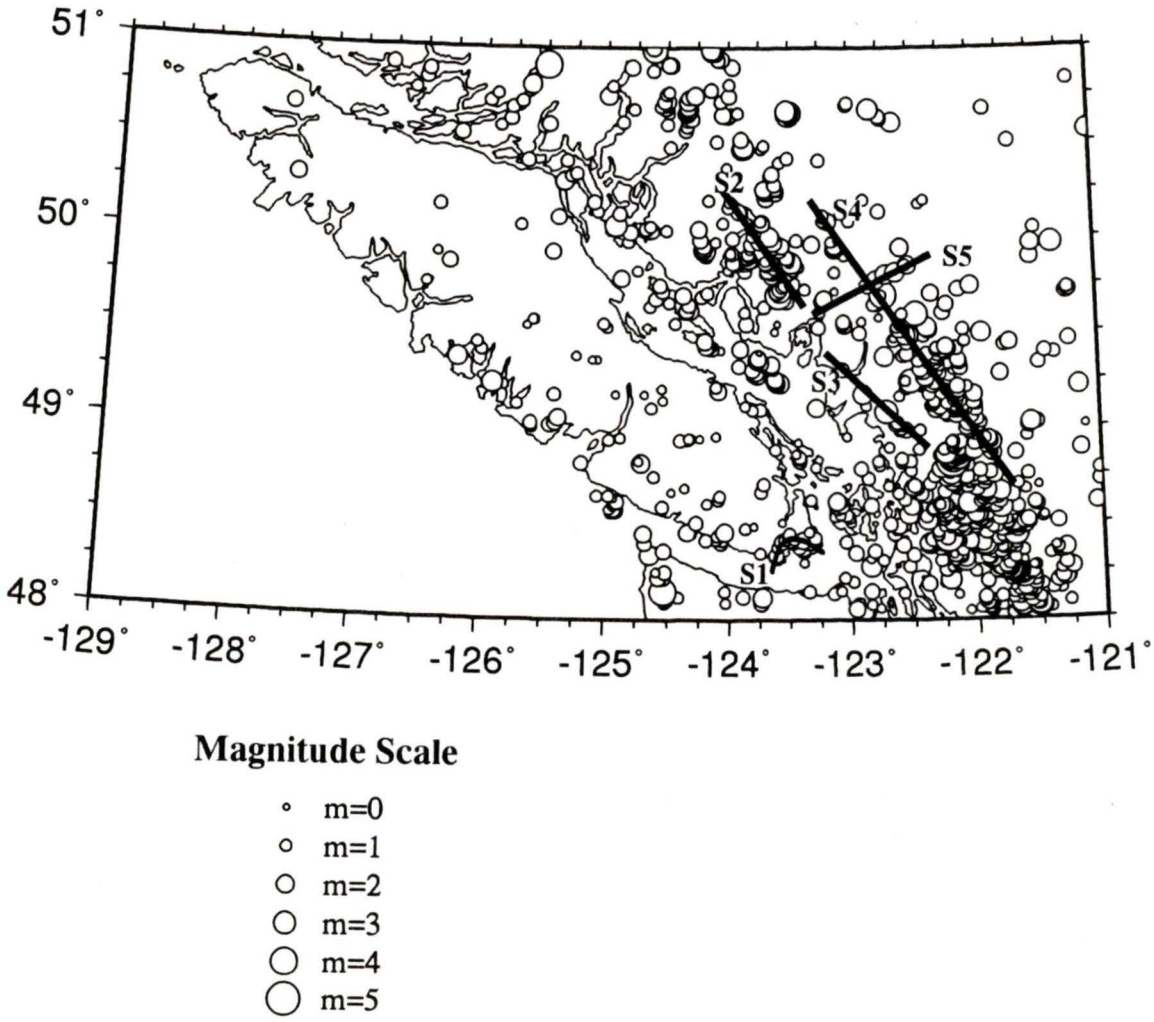

Figure 4.2 North America plate seismicity for depths: $0 \leq z \leq 10$ km. Seismicity trends S1, S2, S3, S4, and S5, as discussed in text, are marked by heavy black lines. These trends are used for comparison with gravity and magnetic data as shown in figures 4.4a, b, c, and d.

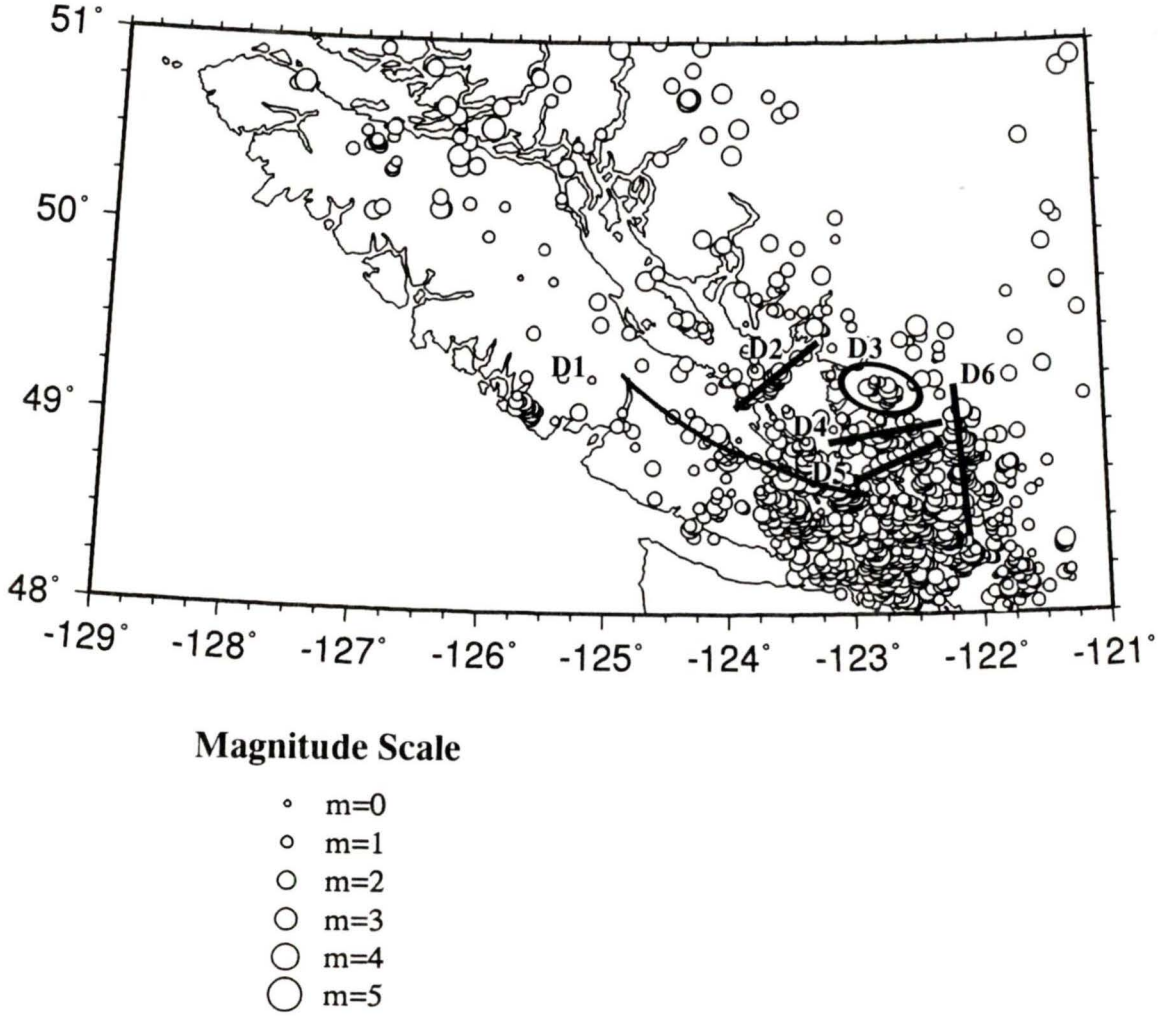

Figure 4.3 North America plate seismicity for depths: 10 km < z ≤ 30 km. Seismicity trends D1, D2, D3, D4, D5, and D6, as discussed in text, are marked by heavy black lines. These trends are used for comparison to gravity and magnetic data as shown in figures 4.4a, b, c, and d.

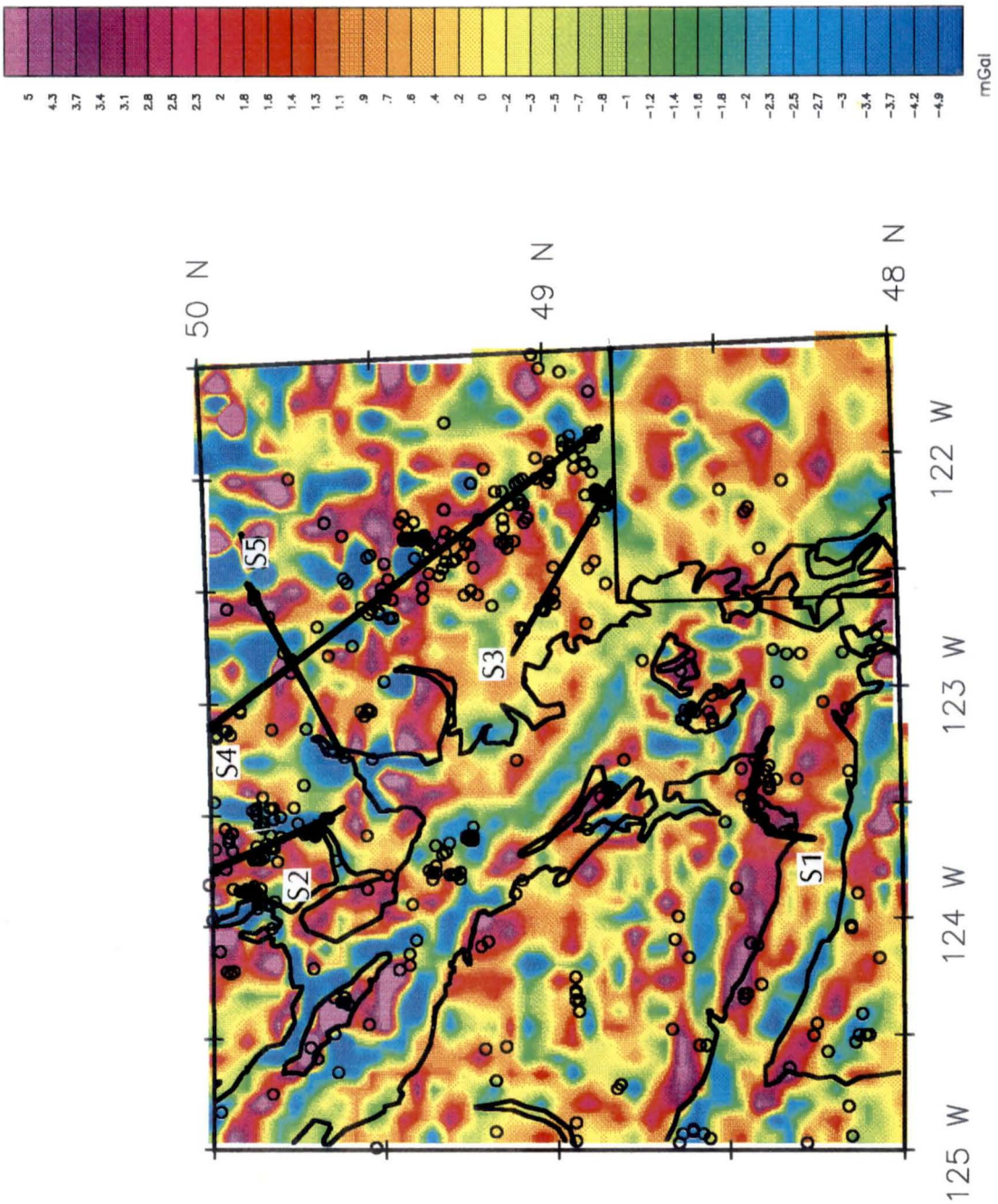

Figure 4.4a Filtered gravity data, cutoff wavelength of 10 km, for the southern end of Vancouver Island and adjacent mainland. Long wavelength components of shallow sources are also present. Heavy black lines indicate observed earthquake trends noted in figure 4.2.

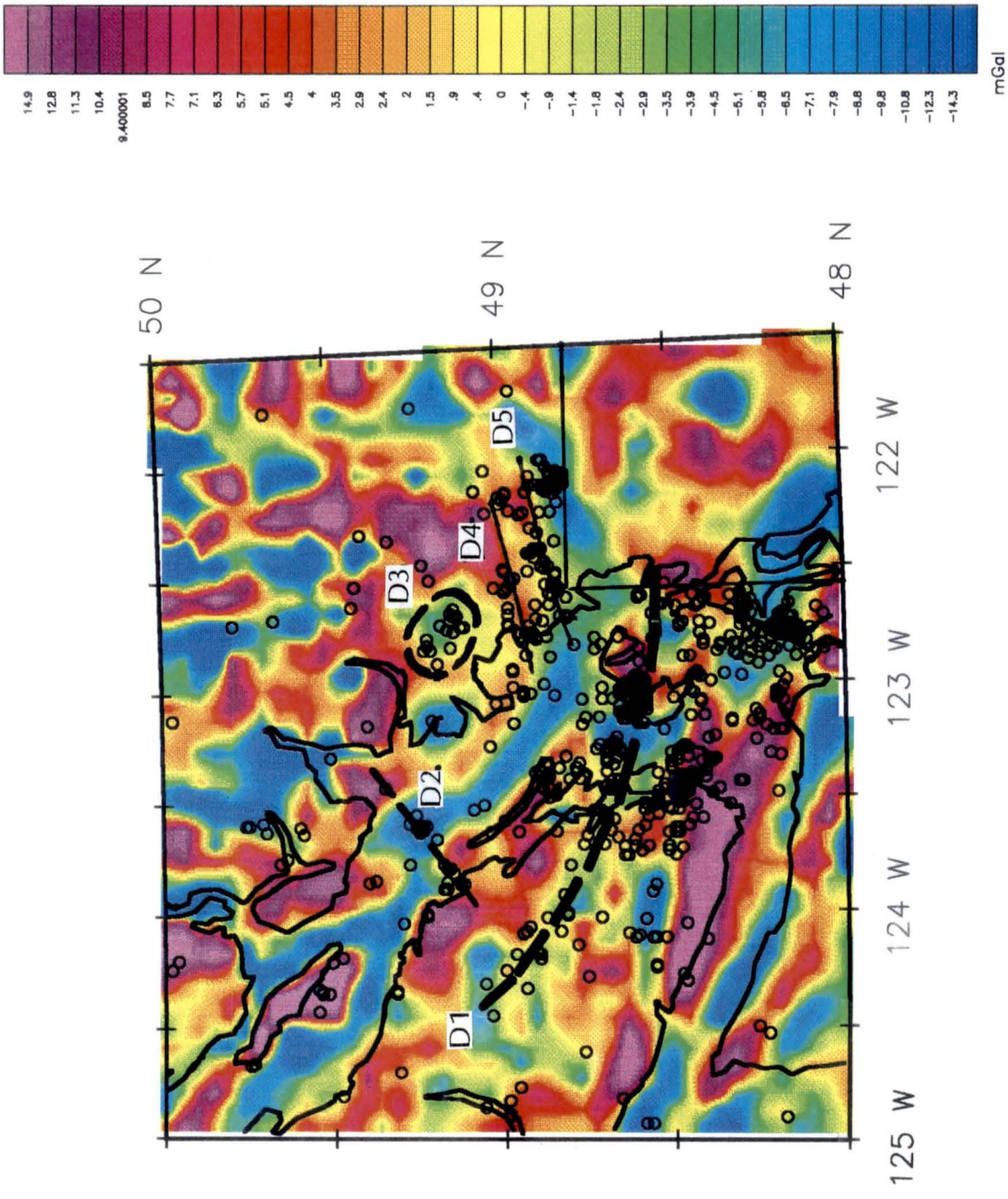

Figure 4.4b Filtered gravity data, cutoff wavelengths of 10 to 30 km, for the southern end of Vancouver Island and adjacent mainland. Short wavelength components of deeper sources are also present. Heavy black lines indicate observed earthquake trends noted in figure 4.3.

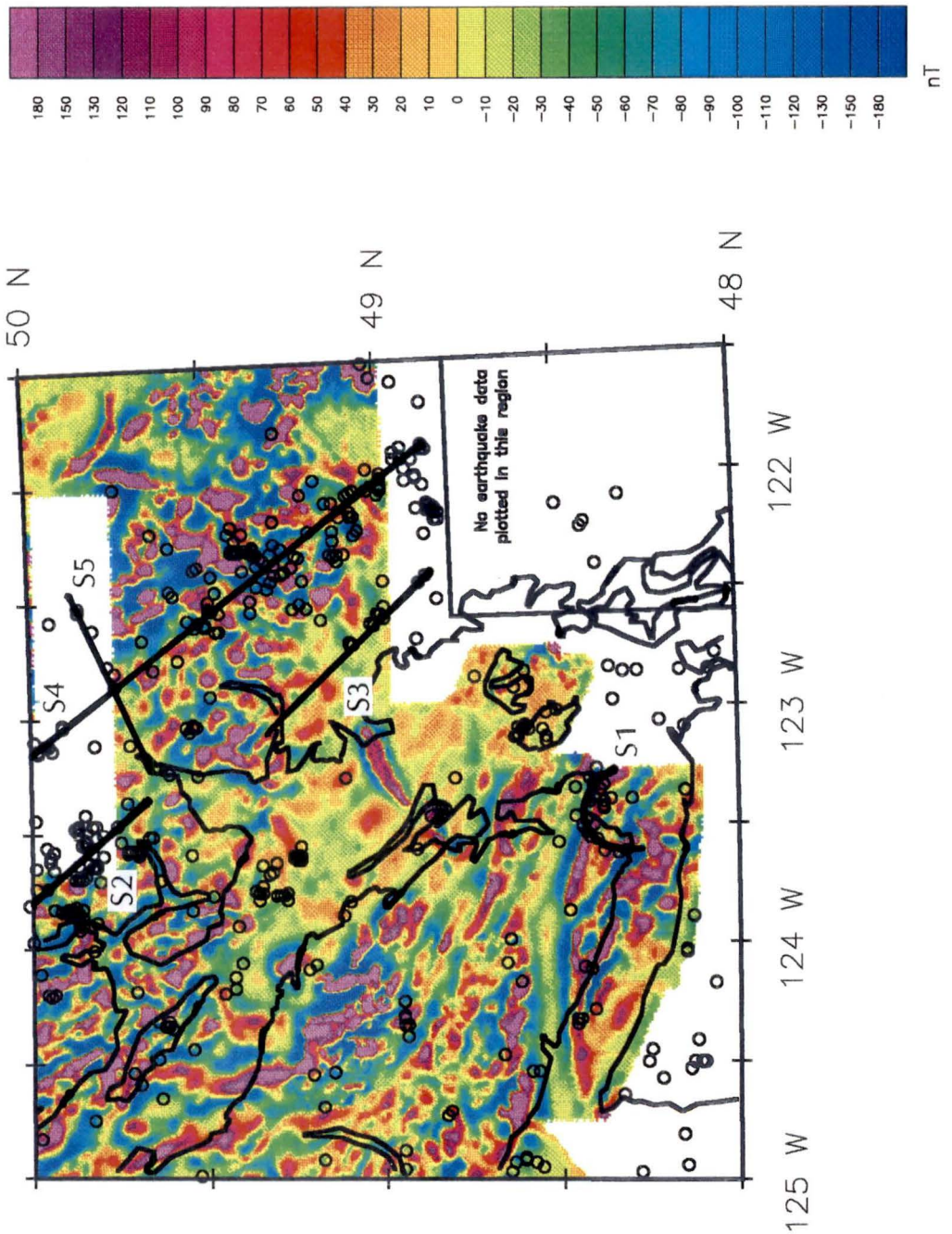

Figure 4.4c Filtered magnetic data, cutoff wavelength of 10 km, for the southern end of Vancouver Island and adjacent mainland. Long wavelength components of shallow sources are also present. Heavy black lines indicate observed earthquake trends noted in figure 4.2.

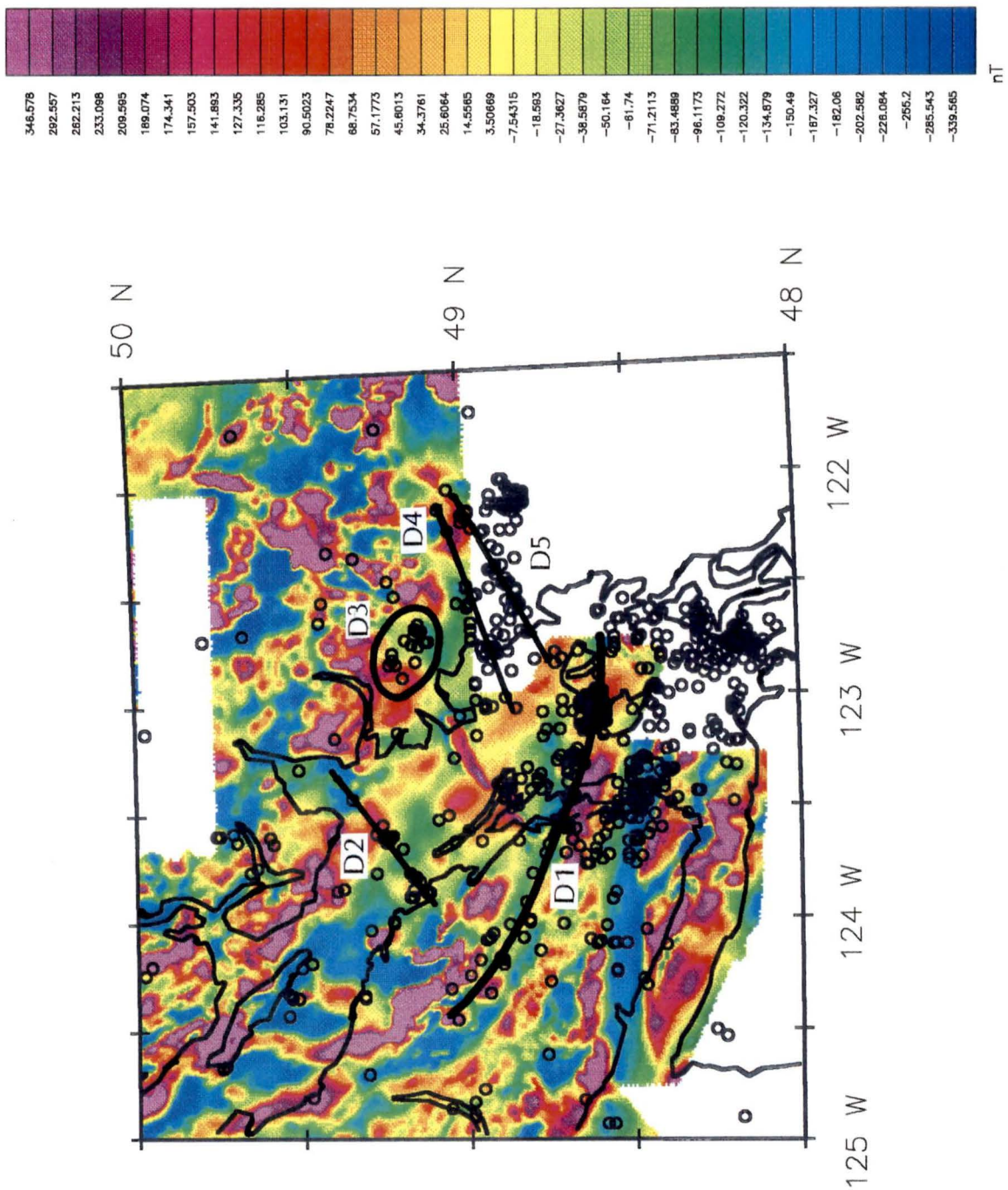

Figure 4.4d Filtered magnetic data, cutoff wavelengths of 10 to 30 km, for the southern end of Vancouver Island and adjacent mainland. Short wavelength components of deeper sources are also present. Heavy black lines indicate observed earthquake trends noted in figure 4.3.

and the adjacent mainland so that area was enlarged for a clearer examination of the data (figures 4.4 a, b, c, and d).

4.3 DISCUSSION

4.3.1 Gravity data

As observed and interpreted by Stacey [1973], the gravity data (figure 4.1a) shows a typical subduction zone gravity signature, from offshore to onshore of low, high, low. The offshore low over the Juan de Fuca plate and trench reflects thick low-density sediments above the downgoing plate. Over Vancouver Island, the gravity high reflects the North America plate with slivers of stranded dense oceanic crust embedded in the lower crust [*Riddihough*, 1977; *Dehler and Clowes*, 1992]. Farther east, the low over the mainland, east of the Garibaldi Volcanic belt, reflects only the less dense, continental North America plate.

By comparing trends noted in both the shallow and deep seismicity maps (figures 4.2 and 4.3) with gravity data plotted at a larger scale, it can be seen that any correlation of seismicity with the gravity data is somewhat tenuous. In figure 4.4a, the shallow gravity data with superimposed shallow earthquakes, the only correlation appears to be the semi-circular arc of earthquakes (S1) atop a small gravity high (1.6 mGal to 2.8 mGal) on the southern tip of Vancouver Island. Other features of note in this gravity map are the Pacific Rim and Crescent terranes of the Cascadia belt (see figure 3.1 for terrane boundaries) which correlate with a lenticular gravity low (-3 mGal) and an adjacent high (5 mGal) through the southern end of Vancouver Island and Juan de Fuca Strait. This marks an abrupt change in lithology, bounded by major faults; the gravity low, south of the volcanic rocks of Wrangellia, occurs over the

sedimentary rocks of the Pacific Rim terrane, while the gravity high occurs over the higher density basalts of the Crescent terrane. In addition, there is also a gravity low associated with the Georgia basin, a topographic low filled with sediment to a depth of approximately 5 km [*White and Clowes*, 1982]. There is seismicity which also runs down the Strait of Georgia (fig 4.2), but inspection of figure 4.4a indicates no specific correlations with gravity lows or highs. It must be noted that these gravity maps cannot be interpreted to too fine a structure due to the 5 km cell size used to grid the data. Many of the small, discrete high and low "blobs" are a result of the data griding.

In figure 4.4b, the deep gravity data with superimposed deep earthquakes, there is a correlation of a low amplitude (-0.4 mGal to -6.5 mGal) gravity low with a patch of events at approximately 49.2°N, 122.8°W (D3). There may also possibly be a correlation of a series of low amplitude gravity lows (-0.4 mGal to -8.8 mGal) with a long arc of seismicity running through the southeastern section of Vancouver Island and the Gulf and San Juan Islands to the U.S. mainland (D1). In this longer wavelength gravity plot, the features related to the Strait of Georgia, Pacific Rim terrane, and especially the Crescent terrane are even more marked here than in the shorter wavelength plot. It is possible that these three groupings of earthquakes are associated with some variation in density or crustal layer thickness with depth. Overall there is no consistent correlation of seismicity with gravity.

4.3.2 Magnetic data

Correlation with the magnetic data is a bit more encouraging. Figure 4.4c shows no apparent correlation of shallow seismicity with the shallow magnetic data; this generally corresponds to no correlation of seismicity with surface faults in this region. However, there is a possible correlation of deep seismicity (D2, figure 4.4d) with boundaries of magnetic changes

(i.e., faults) across the Strait of Georgia. As well, there appears to be a positive correlation of a magnetic structure with the arc of seismicity through the southeastern part of Vancouver Island, the Gulf and San Juan Islands (D1). This could mark a fault or change in lithology between 10 and 30 km depth running along that arc.

CHAPTER 5

CORRELATION OF SEISMICITY WITH RHEOLOGY

5.1 INTRODUCTION

Rheology is the study of the deformation and flow of matter [*Bates and Jackson*, 1984]. The rheological behaviour of rocks is highly dependent upon their temperature and density and the regional stresses involved. The significance of a rheological profile is that it provides information about the material properties of the rocks at depth and how they must behave in order to give the observed regions of brittle failure and creep flow. Earthquakes within continental plates are a result of brittle deformation, or failure, which occurs when the regional stresses overcome the frictional and creep strength of the lithosphere. Therefore, any valid model of the rheological strength of the North America plate must also reflect the current earthquake distribution with depth for the model to be valid. In this chapter the method and data used to determine a representative rheological model for the North America plate in southwestern British Columbia will be presented.

5.2 METHOD AND RESULTS

Frictional failure is a pressure-dependent failure mechanism which occurs at shallow depths where pressure (p) and temperature (T) conditions are low to moderate, as is the case for the southwestern British Columbia portion of the North America plate. The variables involved in frictional failure are predominantly stress difference, overburden (or lithostatic) pressure, and pore fluid pressure [*Sibson*, 1974]:

$$\sigma_1 - \sigma_3 \geq \beta \rho g z (1 - \lambda)$$

where σ_1 and σ_3 are the maximum and minimum compressive stresses, respectively, ρ is density, g is the acceleration of gravity, λ is the pore fluid factor ($= 1/\rho$), and β is a fault parameter which is *3*, *1.2*, or *0.75* for thrust, strike-slip, or normal faulting, respectively. In this model the density, ρ, values were obtained from modelling of gravity and magnetic data by Dehler and Clowes [*1992* and *1995*] (figure 5.1). The fault parameter, β, was assumed to be 3 as the predominant faulting mechanisms in this area are a combination of strike-slip and thrust faulting, and the limiting stress difference (σ_1-σ_2) for thrust faulting (β=3) is much larger than that for strike-slip faulting (β=1.2).

Ductile flow is predominantly a temperature-dependent failure mechanism. In order for flow to occur, the stress applied to the rock must exceed the creep strength, defined as the stress difference needed to achieve a given strain rate. The creep strength decreases as temperature increases; hence when rocks deform ductilely, i.e., at depths greater than 10 km, the temperature is sufficiently high for steady-state flow to occur. The variation of creep strength with depth can be derived from the following relationship [*Kirby*, 1983]:

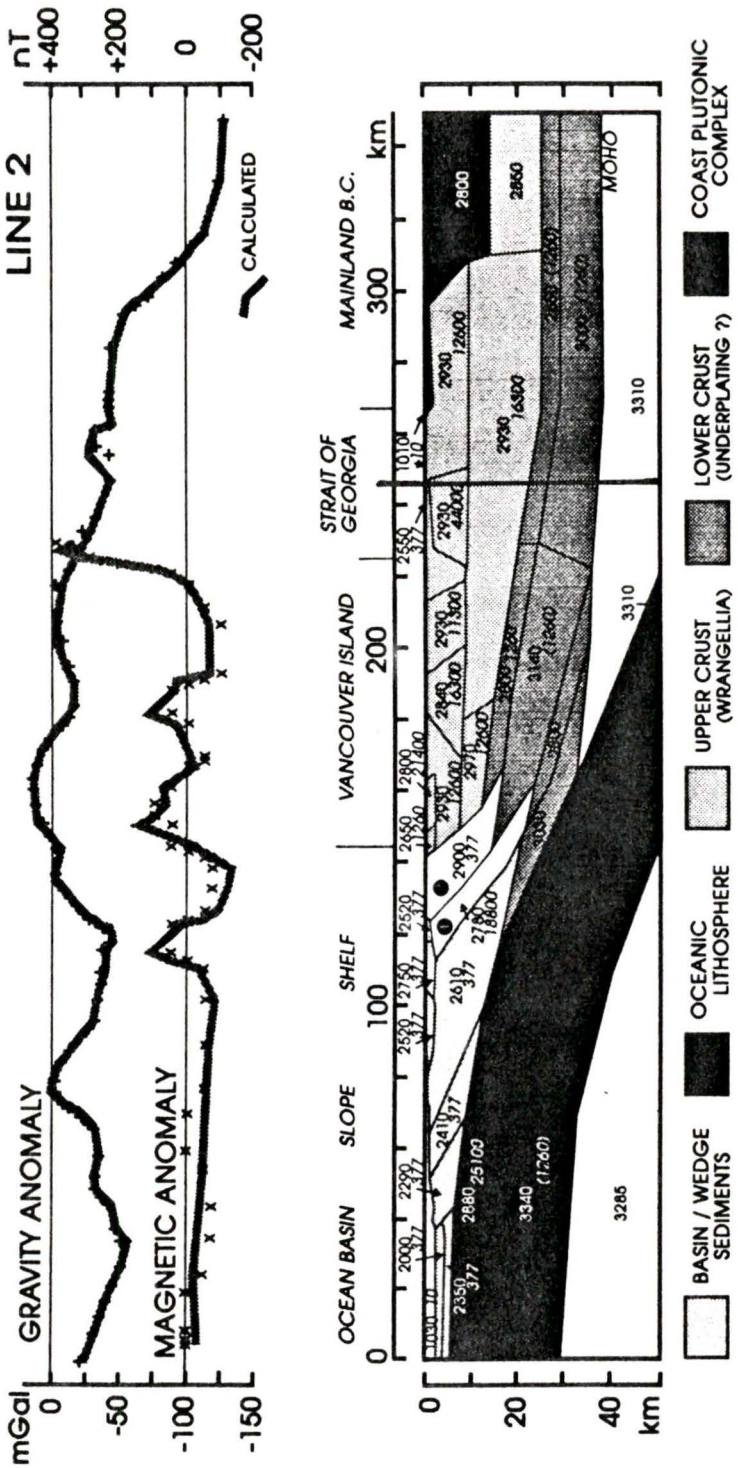

Figure 5.1 Dehler and Clowes' [*1995*] density model across the Juan de Fuca/North America plate subduction region. The solid vertical line through the middle of the Strait of Georgia indicates the location of the rheological profile (figure 5.3a). Density values used in the rheological model were obtained from this cross-section.

$$\sigma_1 - \sigma_3 = (\dot{\epsilon}/A)^{1/n} \exp(Q/nRT)$$

where $\dot{\epsilon}$ is strain rate, A (parameter of dimensions), n (stress and temperature-independent parameter, $2<n<8$), Q (creep activation energy) are experimentally determined material parameters, R is the gas constant, and T is the temperature in degrees Kelvin. For this expression of the flow law, the pressure dependence of creep is neglected since the error introduced is negligible at pressures less than a few GPa [*Ranalli and Murphy*, 1987] which is the situation in southwestern British Columbia. The strain rate, $\dot{\epsilon}$, is assumed to be 0.12μr/yr or 3.805×10^{-9}/s [*Dragert et al.*, 1994]; T is derived from the heat flow data and conductivity modelling of Lewis et al. [1992] (figure 5.2); A, n, Q are from Kirby [1983], Ranalli and Murphy [1987], and Lowe and Ranalli [1993]; and geological composition with depth is taken from the gravity and seismic modelling of Dehler and Clowes [1995] (figure 5.1), Clowes *et al.* [1987], and Zelt *et al.* [1993].

Frictional failure and creep strength values were calculated at 2 km depth intervals, for a profile through the middle of the Strait of Georgia, using the material parameters A, n, Q (table 5.1) which best approximated the inferred rock type at each depth. The profile location is indicated in figure 5.1. Initially, frictional failure and creep strength values were calculated assuming quartz diorite for the upper crust (Wrangellia; 0 - 22 km), and diabase for the lower

Rock type	A ($GPa^{-n} \cdot s^{-1}$)	n	Q ($kJ \cdot mol^{-1}$)
quartz diorite	$2.0 \cdot 10^4$	2.4	219
diabase	$3.2 \cdot 10^6$	3.3	268
granite	5.0	3.2	144
wet granite	$2.0 \cdot 10^2$	1.9	137

Table 5.1 Creep parameters for rheological calculations [from *Kirby*, 1983; *Ranalli and Murphy*, 1987; and *Lowe and Ranalli*, 1993].

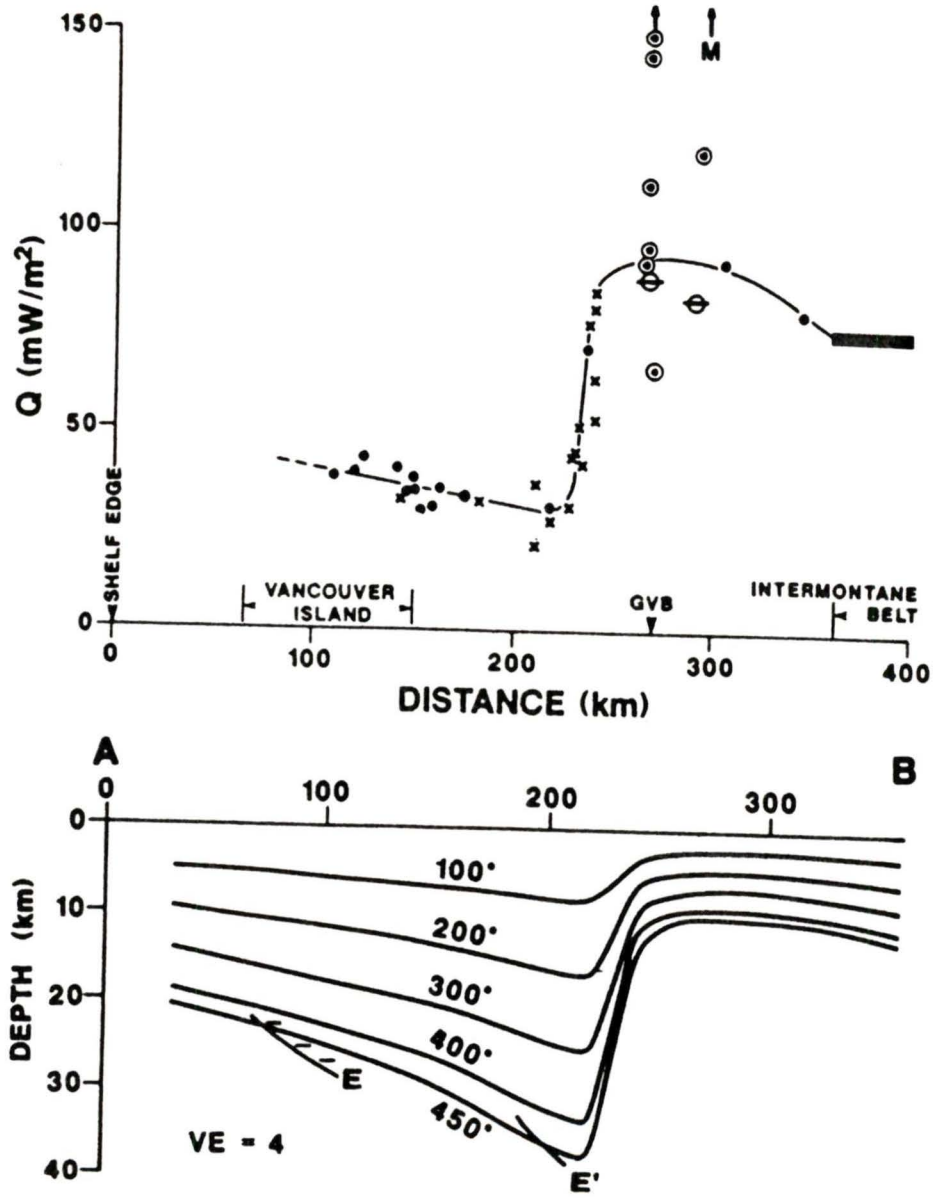

Figure 5.2 Heat flux and computed crustal temperatures across the southern half of Vancouver Island [after *Lewis et al.*, 1992]. Near the 450° isotherm beneath Vancouver Island, the line marked E is the top of the E-layer of seismic reflectors and its possible continuation beneath the mainland, and the three short horizontal lines are the top of the high electrical conductivity anomaly indicated by magnetotellurics.

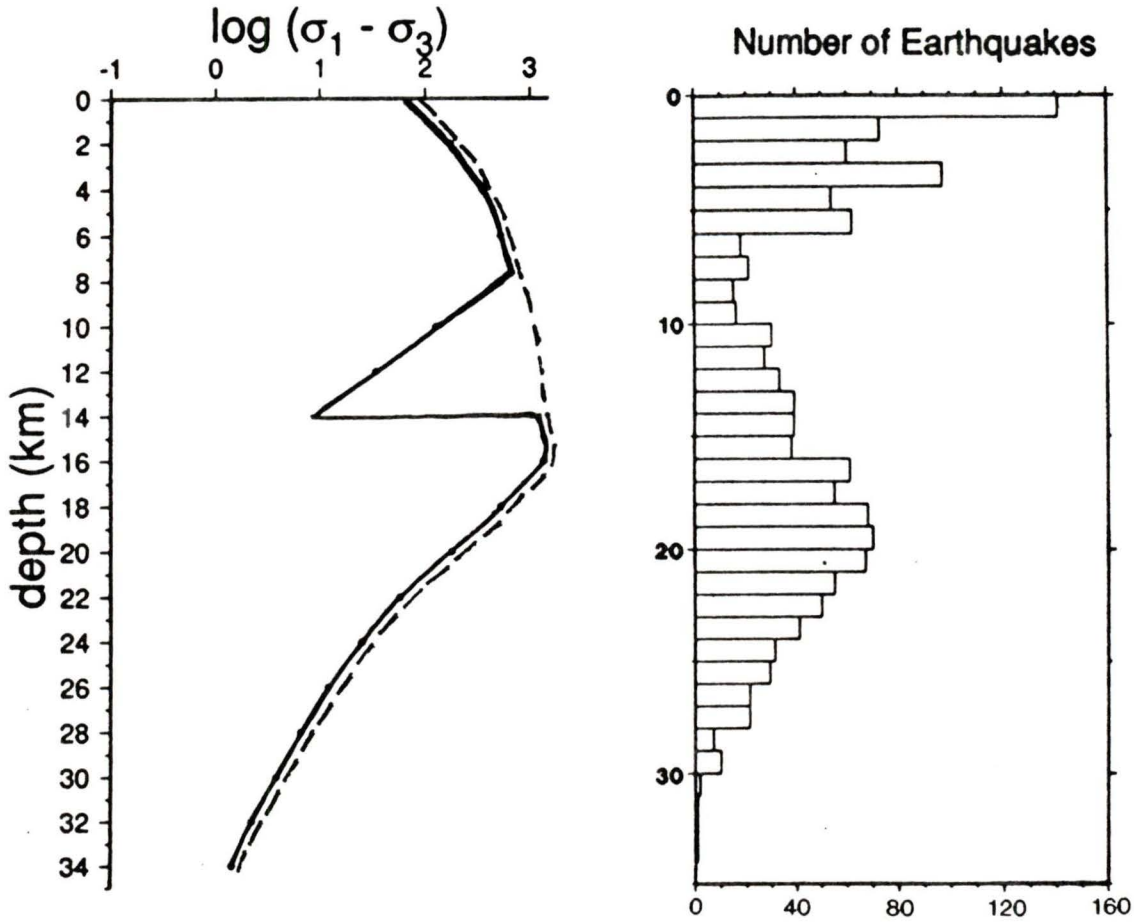

Figure 5.3 a) Rheological profile for the middle of Strait of Georgia, see figure 5.1 for location of profile. Dashed line represents a two-layer crustal model, assuming a quartz diorite upper crust and a diabase lower crust. This gives a brittle regime extending to ~16 km depth, with creep failure predominating at depths ≥16 km. The solid line represents a three-layer crustal model with a layer of "wet" granite inserted in the upper crust to reflect the region of low seismicity shown in figure 5.3b. The "wet" granite region models creep failure predominating between depths of 8 to 14 km. b) Depth distribution of North America plate earthquakes. Seismicity virtually ceases after 30 km.

crust (24 - 34 km). This gave the rheological profile indicated by the dashed line in figure 5.3a, but the profile does not adequately explain the observed earthquake distribution (figure 5.3b). Discrepancies can be related to several sources (a) incorrect ρ, T values (b) incorrect A, Q, n values (c) oversimplified earth model. To model the decrease in seismicity between 6 and 10 km a layer of wet granite was assumed in this upper crustal region. The wet granite is ductile at depths of 8 to 14 km, and the resulting rheological profile (indicated by the solid line in figure 5.3a) adequately modeled the observed earthquake distribution.

5.3 DISCUSSION

Earthquakes at crustal depths are a result of brittle failure (i.e. frictional faulting) of the crust. Decreases in seismicity at crustal depths are a result of ductile flow beginning to dominate over brittle failure. The bimodal seismicity distribution shown in figure 5.3b reflects brittle failure dominating at depths of 0 to 6 km; ductile flow beginning to occur at depths of 6 to 10 km, which models the decrease in seismicity; brittle failure again dominating at depths of 10 to 20 km; and finally ductile flow processes occurring again at depths greater than 20 km, where seismicity once again begins to decrease, until ductile flow dominates completely and seismicity ceases to occur around 30 km depth. Given the two layer geological model of an upper and lower crust [*Dehler and Clowes*, 1992; *Clowes et al.*, 1987], the experimentally determined material parameters (A, n, and Q) available in the literature for various rock types, and the possible presence of fluids (modelled as wet granite) at shallow depths in the upper crust, the "best" geologically reasonable rheological model gives a brittle region (positive slope in figure 5.3a) from 0 to 8 km, a ductile region where ductile process start to occur (negative slope

in figure 5.3a) from 8 to 14 km, a brittle region from 14 to 16 km, and finally another ductile region from 16 km downwards. This rheological model of a quartz diorite upper crust (0 to 22 km), a diabase lower crust (24 to 34 km), with a fluid rich region from 8 to 14 km, matches the observed earthquake distribution within the uncertainties of the earthquake depth locations. This study shows that a two-layer crust does not adequately explain the observed earthquake distribution. A better explanation is provided by a three-layer crustal model or by the presence of fluids at depths of approximately 6 to 10 km.

CHAPTER 6

FOCAL MECHANISMS AND REGIONAL STRESS ORIENTATIONS

6.1 INTRODUCTION

Seismicity over the past ten years reveals more than just the outlines of tectonic plates. Focal mechanism analysis allows for the determination of the stress directions causing a particular earthquake. If enough focal mechanisms from a given region are combined together one can determine a statistically meaningful orientation of the regional stress regime. Any stress regime can be divided into its principal components of σ_1 - the maximum compressive stress, σ_2 - the intermediate compressive stress, and σ_3 - the minimum compressive stress. This principal axis system is rotated to fit the observed stress regime. Focal mechanism analysis from earthquake data can determine P (pressure), B, and T (tension) axes (the observed stress directions) which can correspond to σ_1, σ_2, and σ_3 axes (taken here to mean the regional stress regime).

Focal mechanism analysis can determine the location of two nodal planes (one of which represents the fracture plane) which divide the first arrival data from an earthquake into compressional and dilatational (tensional) quadrants when data from various stations are plotted on a lower hemisphere stereographic projection. The pressure axis (P-axis) is taken to be 45° from both nodal planes and positioned through the tensional quadrants and the tension axis (T-axis) is also taken to be 45° from both nodal planes but positioned through the compressional quadrants. However, McKenzie [1969] pointed out that if slip occurs along a pre-existing plane of weakness that the focal mechanism data will not reflect the true principal stress. McKenzie also noted that if the coefficient of friction varies in different rock types that the principal stress directions may lie at less than 45° to the slip plane so that, again, the P and T-axes determined from focal mechanisms would no longer reflect the true regional principal stress regime, σ_1 and σ_2.

It might be expected that with strong plate coupling the P-axes from a group of North America plate earthquakes will reflect compression in the direction of plate convergence [*Ma et al.*, 1991]. Previous work in Washington state (immediately to the south of the region studied here) by Crosson [1972], Yelin and Crosson [1982], Malone *et al.* [1975], Crosson [1983], Ma *et al.* [1991], and Quamar [1992] indicates that this is not the case in the North America plate with respect to the subducting Juan de Fuca plate. The direction of relative plate motion between the Juan de Fuca plate and the North America plate is in a northeasterly direction [*Atwater*, 1970], yet the composite P-axes plot of Washington state data indicates that σ_1 is oriented in a north-south direction and the T-axes plot indicates that σ_3 is oriented in a girdle in an east-west direction (figure 6.1).

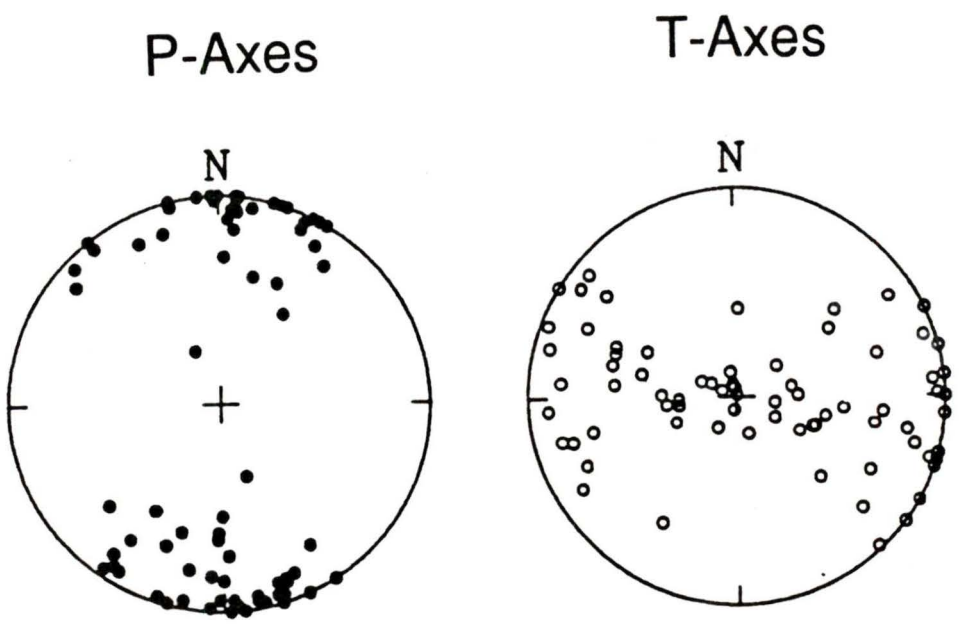

Figure 6.1 North America plate events in the Puget Sound region of Washington state. The composite P-axes plot indicates that σ_1, the maximum regional compressive stress, is oriented approximately north/south in a predominantly horizontal attitude. The composite T-axes plot indicates that σ_3, the minimum regional compressive stress, is oriented in a roughly east/west direction, but its inclination varies from horizontal to vertical in a girdle distribution [From *Ma et al.*, 1991].

6.2 FOCAL MECHANISMS

Focal mechanism solutions for events with first motion data (figure 6.2) were obtained through two programs, the USGS program FPFIT (Reasenberg and Oppenheimer, 1985) and FOCMEC (Snoke *et al.*, 1984).

FPFIT determines the double-couple fault-plane solution, or source model, that best fits the given first motion P polarities for an earthquake. The source model is determined by minimizing a normalized, weighted sum of first motion polarity discrepancies. Weighting is based on two criteria, the estimated variance of the data and the theoretical P wave radiation amplitude with lesser weight applied to observations near nodal planes and greater weight to observations near radiation lobes. FPFIT formally estimates the uncertainty in the strike, dip, rake of the solution and calculates a uniformly distributed set of solutions within the range of estimated uncertainty. FOCMEC also determines the fault plane solution due to a double-couple source. However, it can incorporate SH and SV polarities and SH/P, SV/SH, and SV/P amplitude ratios along with the P-wave first motion data to provide further constraints on the focal mechanism solution. For the SV/P amplitude ratios, one need only to be able to read the P and S amplitude data to within 10% on the vertical component, short period seismograms. FOCMEC also allows a choice between weighted and non-weighted solutions. Weighting is by theoretical radiation amplitudes for P, SV, and SH waves.

All the first motion data was initially run through FPFIT which requires a minimum of six first motions for a given event to compute a focal mechanism. The resulting data were inspected to select between alternate solutions and to check for solutions FPFIT may have missed. Viable fault-plane solutions with an uncertainty of less than $\pm 45°$ were kept since the direction of maximum compression can be anywhere in the dilatational quadrant and the P axis could differ

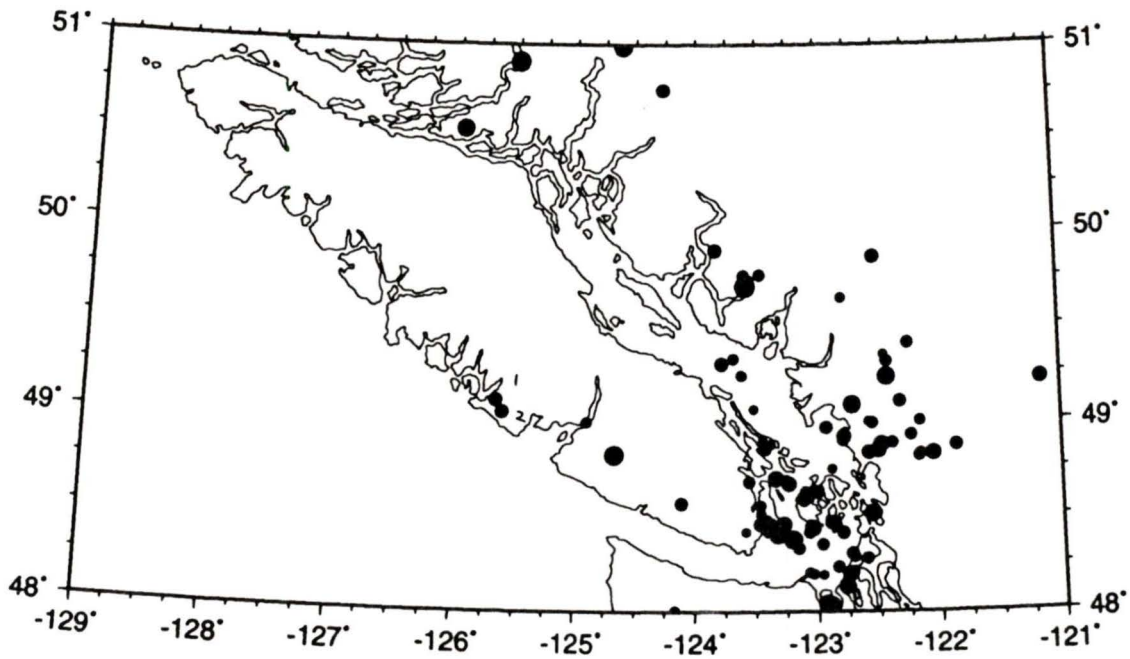

Figure 6.2 111 earthquakes for which focal mechanisms were able to be calculated.

from the true maximum stress direction by as much as 45° [*McKenzie*, 1969]. Solutions with first motion discrepancies (such as a compressional observation in a computed dilatational quadrant) were checked for stations that receive refracted rays across a nodal plane and for stations with reversed polarity. Each solution was assigned a quality factor, Q, which varied from 1 to 5. The quality of each solution depended on the number of data points, their distribution, the number of discrepancies, possible other solutions, and the actual range of distribution of P and T-axes (the goodness of fit - how tightly constrained the solution is by the data). The quality factor is a subjective determination, depending on how well constrained the solution is and if the constraints are believable. Events which are constrained solely on the basis of one first motion reading (which is not supported by other data points on the same quadrant) will have a low Q (i.e. $Q \geq 3$). The following guide was used to determine the quality, but it was not strictly adhered to if the data implied a better or worse solution:

1	excellent	$\pm 10°$, no discrepancies, no alternate solutions
2	good	$\pm 15°$, zero to one discrepancy depending on data distribution and quantity
3	average	$\pm 20°$, one to two discrepancies
4	poor	$\pm 25°$, two or more discrepancies
5	bad	$\pm 30°$, two or more discrepancies

The degree variation refers to the clustering of the P and/or T-axes, i.e. the "slop" in the fit of the nodal planes; discrepancies refer to discrepant observations within a compressional or dilatational quadrant. If an adequate solution could not be obtained with first motion data through FPFIT (too many discrepancies, poor distribution of stations, or less than 6 first motion readings) then the solution was obtained through the program FOCMEC after examination of the waveforms, where available, to determine SV/P amplitude ratios. In some instances SV/P amplitude ratios did not help constrain the data. In these cases the FPFIT solution was often used since it corresponds to the best fit solution, whereas FOCMEC determines a range of possible solutions without indicating any preferential solution. Amplitude ratios alone cannot distinguish

normal from reverse faults or left-lateral or right-lateral motion on a given plane. The resolution of fault strike for near-vertical strike-slip faults is weak and depends strongly on the availability of data from stations at particular azimuths for which the amplitude ratio is either very high or very low [*Kisslinger*, 1980].

In total, 111 focal mechanisms with reliable solutions were obtained, with the majority clustered near the south-southeast tip of Vancouver Island, the Gulf and San Juan Islands, and the adjacent mainland. For comparable event magnitude and azimuthal coverage, shallow depth earthquakes tend to have more poorly constrained focal mechanism solutions than deeper earthquakes. Shallow earthquakes usually yield very poor focal mechanisms since waves arrive at stations at very shallow angles. In this case the station readings are around the edge of the stereoplot with very few readings towards the centre of the plot to help constrain the solution. With a large number of first motion readings from several azimuths, the solution can be determined quite adequately. On the other hand, if the earthquakes is large enough, deep focal mechanisms solutions are generally quite well constrained due to the take-off angles from the hypocentre having a distribution between 0° to 90°. However, since the waves may not be received at as many stations as for a shallow earthquake of equal magnitude, the deeper earthquakes may have fewer data points with a better distribution.

6.3 DETERMINATION OF STRESS ORIENTATION

The resulting focal mechanism data were assessed, through statistical analysis and through an inversion program FMSI [*Gephart*, 1990a], to obtain an approximation to the regional stress tensor. Composite plots of the P and T axes were made and plotted on an equal area lower

hemisphere projection (figure 6.3). Fisher spherical statistics were initially used [*Enkin*, 1990] to determine the mean and error in the mean for each plot. The P-axes data have a bi-polar distribution with a mean trend of 332°, an inclination of 1°, and a 95% confidence interval of 7° in the mean trend. The T axes data have a girdle distribution with a mean trend of 242°, an inclination of 4°, and a 95% confidence interval of 7° in the mean trend. The Fisher distribution function gives the probability per unit angular area of finding a direction within an angular area, dA, centred at an angle θ from the true mean.

All the focal mechanism solutions were subsequently run through FMSI. FMSI is a program that determines a best-fitting four parameter stress tensor and estimates of uncertainty from populations of focal mechanisms and fault/slickenside data [*Gephart and Forsyth*, 1984; *Gephart*, 1985; *Gephart*, 1990a; *Gephart*, 1990b]. The four parameter stress tensor consists of three principal stress directions expressed by the three Euler angles Θ, Ψ, and Φ and one measure of relative stress magnitudes, R. The angles Θ, Ψ, and Φ are, respectively, the plunge and azimuth of σ_1 and the rake of σ_3 (in a plane normal to σ_1); and $R=(\sigma_2-\sigma_1)/(\sigma_3-\sigma_1)$. For input to FMSI the plunge and azimuth of the individual P and T-axes are needed along with the range of stress directions to be explored about the initial primary and secondary stress directions, and an initial guess (starting point) for σ_1 and σ_3. The previous results from the Fisher spherical analysis were used for the initial guess of σ_1 and σ_3. It was determined from a visual inspection of the data (figure 6.3) that an acceptable model must fit in the following regions:

σ_1	azimuth	310°-350°	plunge	00°-12°
σ_3	azimuth	030°-080°	plunge	00°-90°
R	0.5-1.0			

FMSI is run with weighted input. The best-fit model with equal weighting is $\sigma_1=10°/173°$, $\sigma_2=06°/082°$, $\sigma_3=78°/322°$, $R=0.4$. The inversion was also run for weighted data with weights assigned to P and T-axes based on the quality of each focal mechanism solution. The best quality

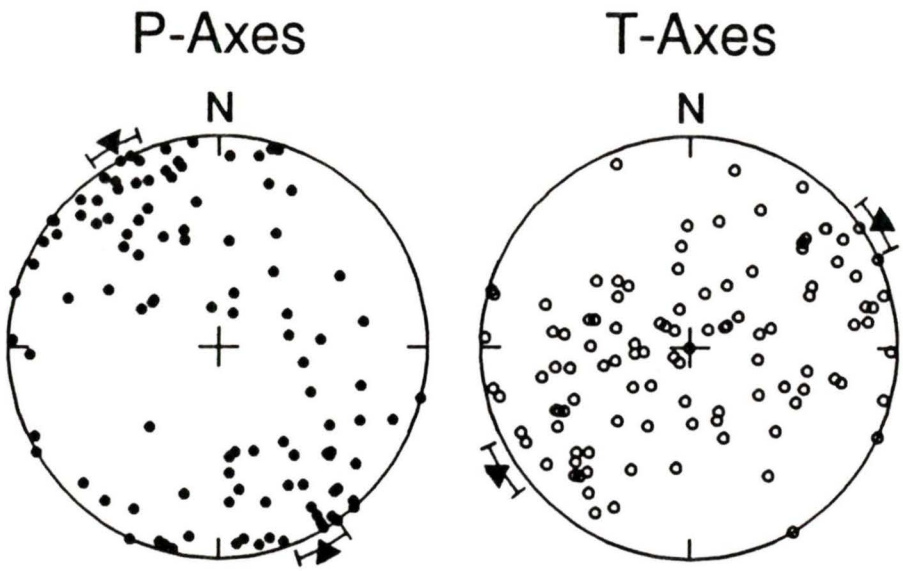

Figure 6.3 Composite P and T-axes plots for the 111 earthquakes shown in figure 6.2. The P-axes dominate the stress solution, being oriented in a north-northwest direction and constrained to lie nearly horizontally (01° → 332° ± 7°). The T-axes are oriented east-northeast (242° ± 7°) and vary from vertical to horizontal. The inclination of the P and T-axes agrees with the Washington state data, but the azimuthal directions are significantly rotated to the west (counter-clockwise).

	σ_1	σ_2	σ_3	R
Fisher statistics	01° / 332° ±7°		04° / 242° ±7°	
Exact solution				
FMSI no weights	10° / 173°	06° / 082°	78° / 322°	0.4
FMSI weights	10° / 173°	06° / 082°	78° / 322°	0.4

Table 6.1 Regional stress field orientations for southwestern British Columbia.

weighted model gave the same solution. The results are summarized in Table 6.1. Figure 6.4 shows the composite plot of P and T-axes according to their quality; this shows that the orientation is similar for both P and T-axes regardless of their quality, so that the stress solution is not skewed towards the poor quality solutions. Figure 6.5 shows the map distribution of P and T-axes according to their quality; this shows that the best quality solutions are located within the seismic network (see figure 2.5) and the poorer quality solutions are located near the edges of the seismic network as would be expected.

It is useful to examine the P and T-axes distributions on a map projection (figure 6.6) in order to note any spatial trends. For the two events on the west coast of Vancouver Island, the P-axes are aligned with the convergence direction. It is possible that because this portion of the North America plate is so close to the subducting Juan de Fuca plate that it is under compression due to subduction. This maximum compressive stress in the direction of subduction dominates indicating the effect of North America/Juan de Fuca coupling is stronger close to the trench. However, for all other events farther away from the trench, the P or T-axis directions are not consistent with the convergence direction. It was also thought that there might be a principal stress distribution trend with depth, but no preferential distribution was noted as can be seen in figures 6.7 and 6.8. The shallow events are at depths of 10 km or less and the deep events are at depth of greater than 10 km. This distinction was based on the North America plate earthquake depth histogram (figure 2.6) which shows a bimodal distribution with a decrease in

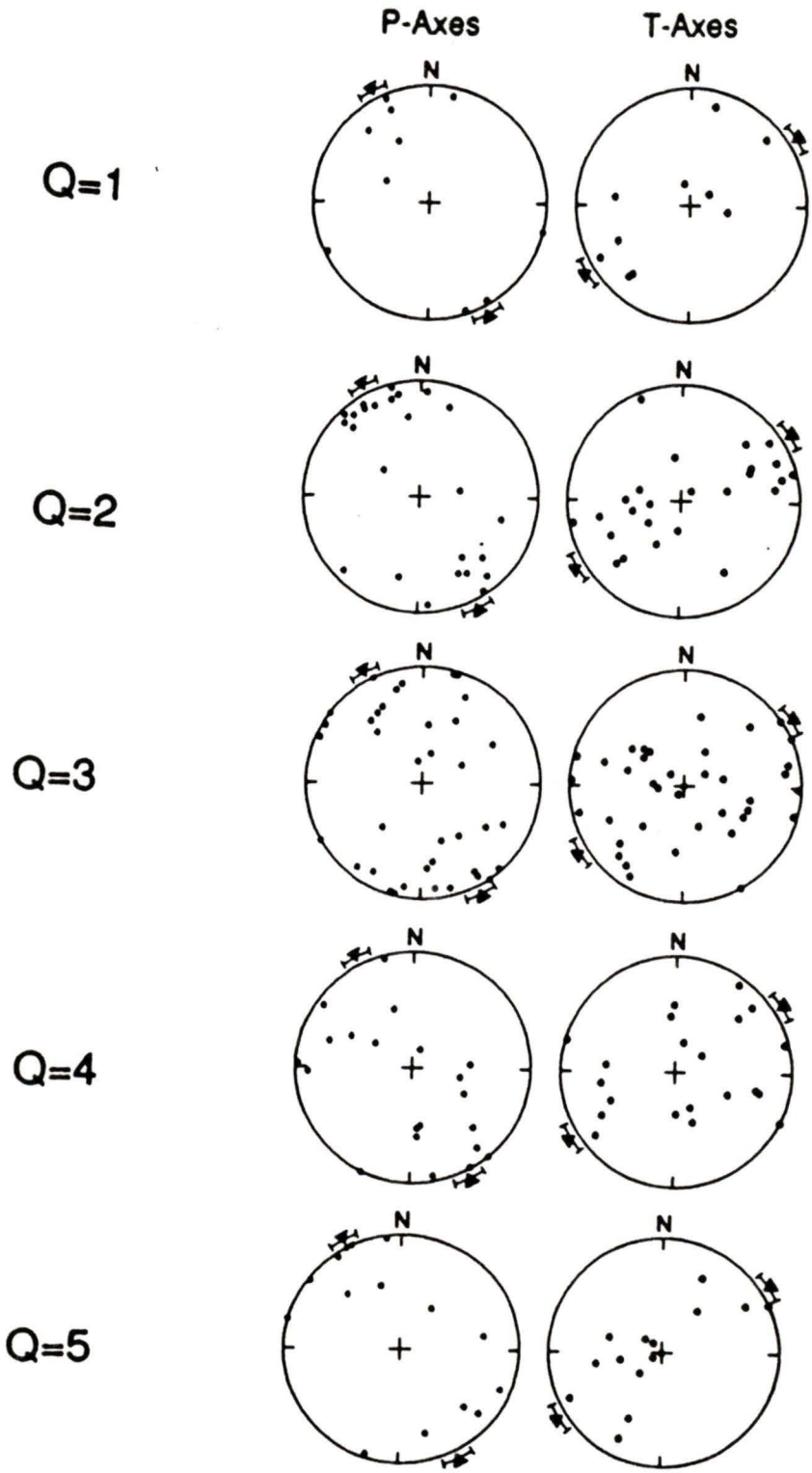

Figure 6.4 Composite plots of P and T-axes according to their quality, Q. Q=1 is excellent, Q=5 is very poor. The orientation of both P and T-axes remains the same regardless of the quality of the solution, so data is not being skewed by poor solutions.

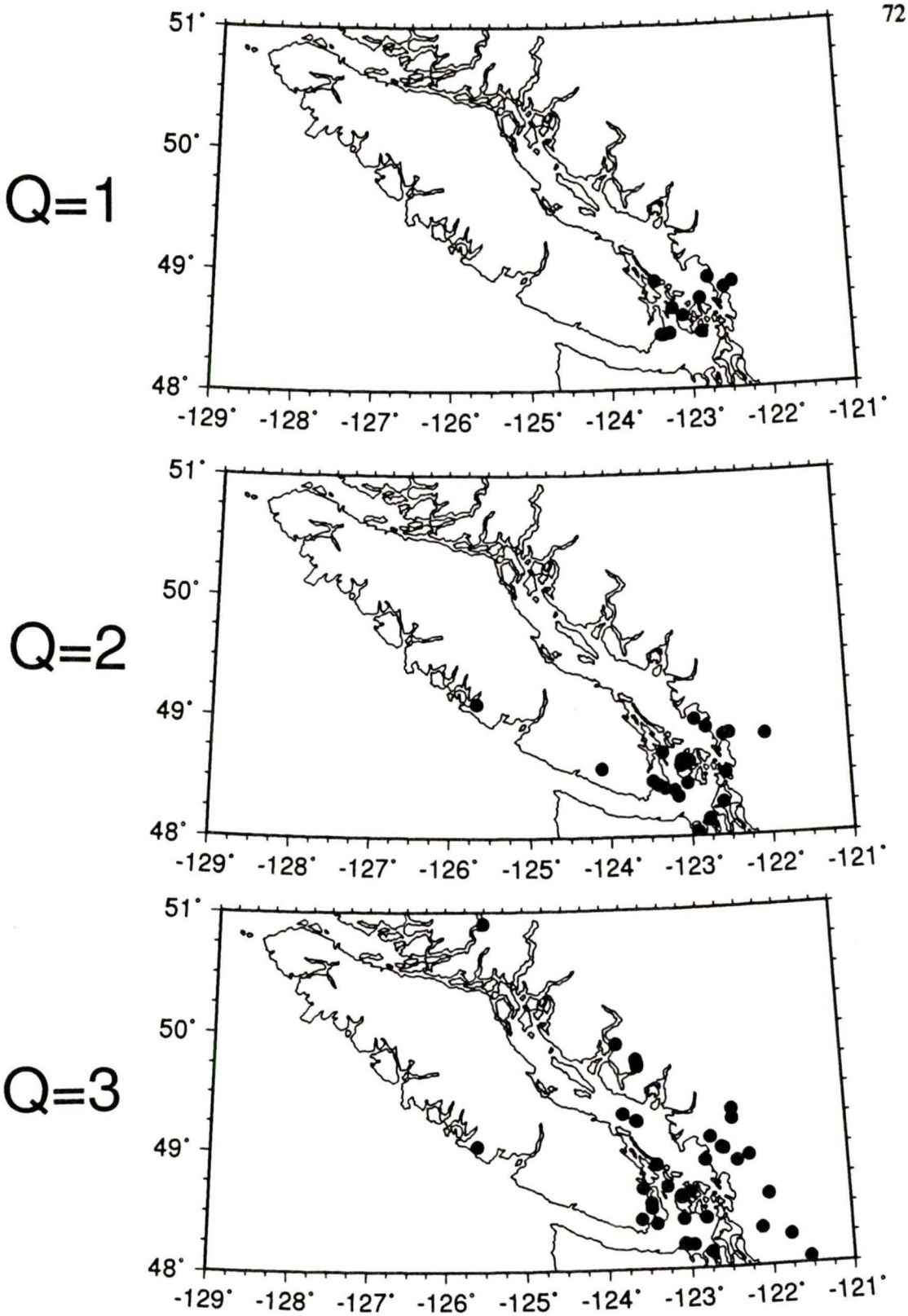

Figure 6.5 Map plot of P-axes according to assigned focal mechanism quality (1 is excellent, 5 is poor). The best (Q=1) solutions are located within the seismic network, the poorest (Q=5) on the edges of the network.

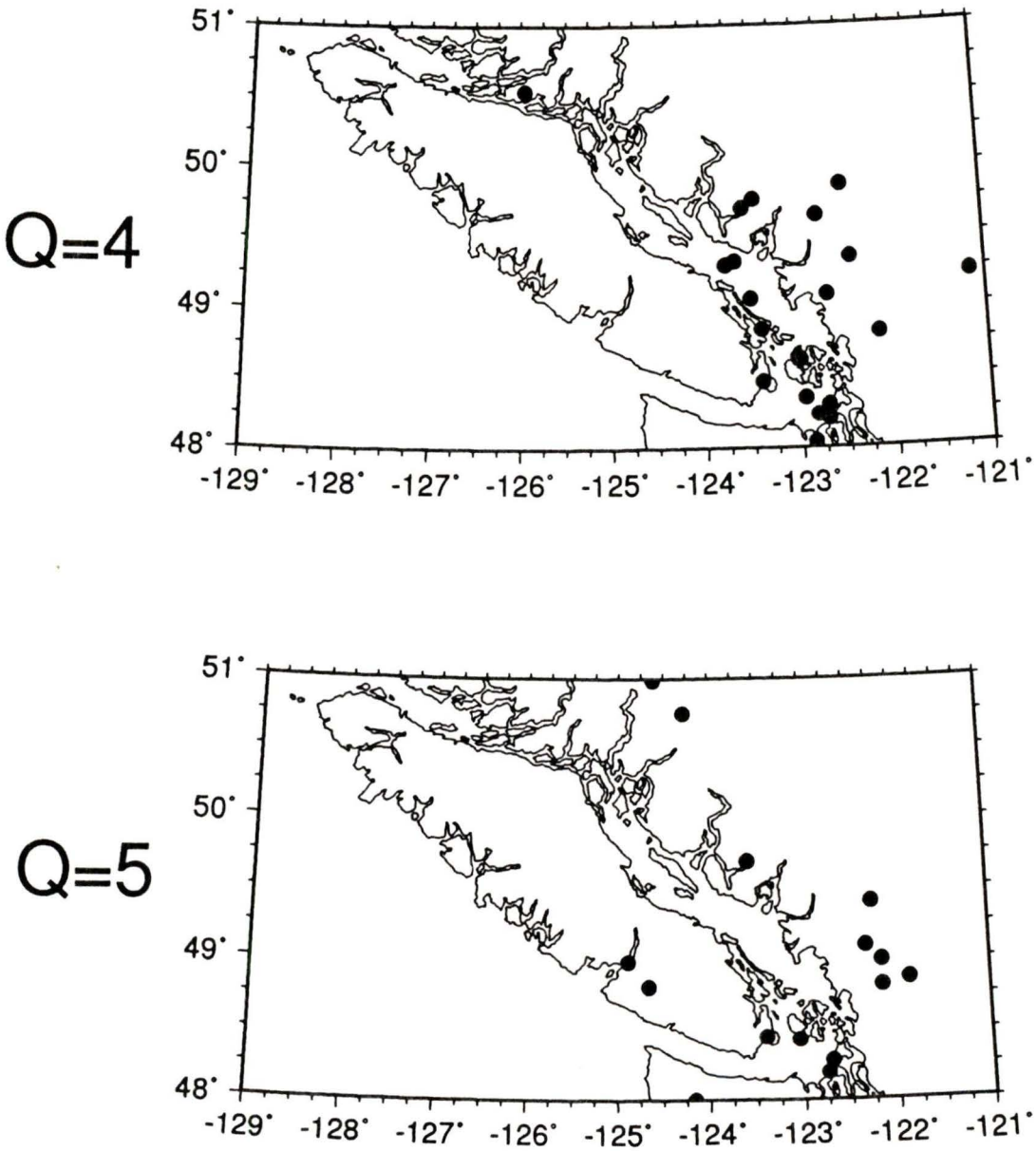

Figure 6.5 (continued) Map plot of P-axes according to assigned focal mechanism quality (1 is excellent, 5 is poor). The best (Q=1) solutions are located within the seismic network, the poorest (Q=5) on the edges of the network.

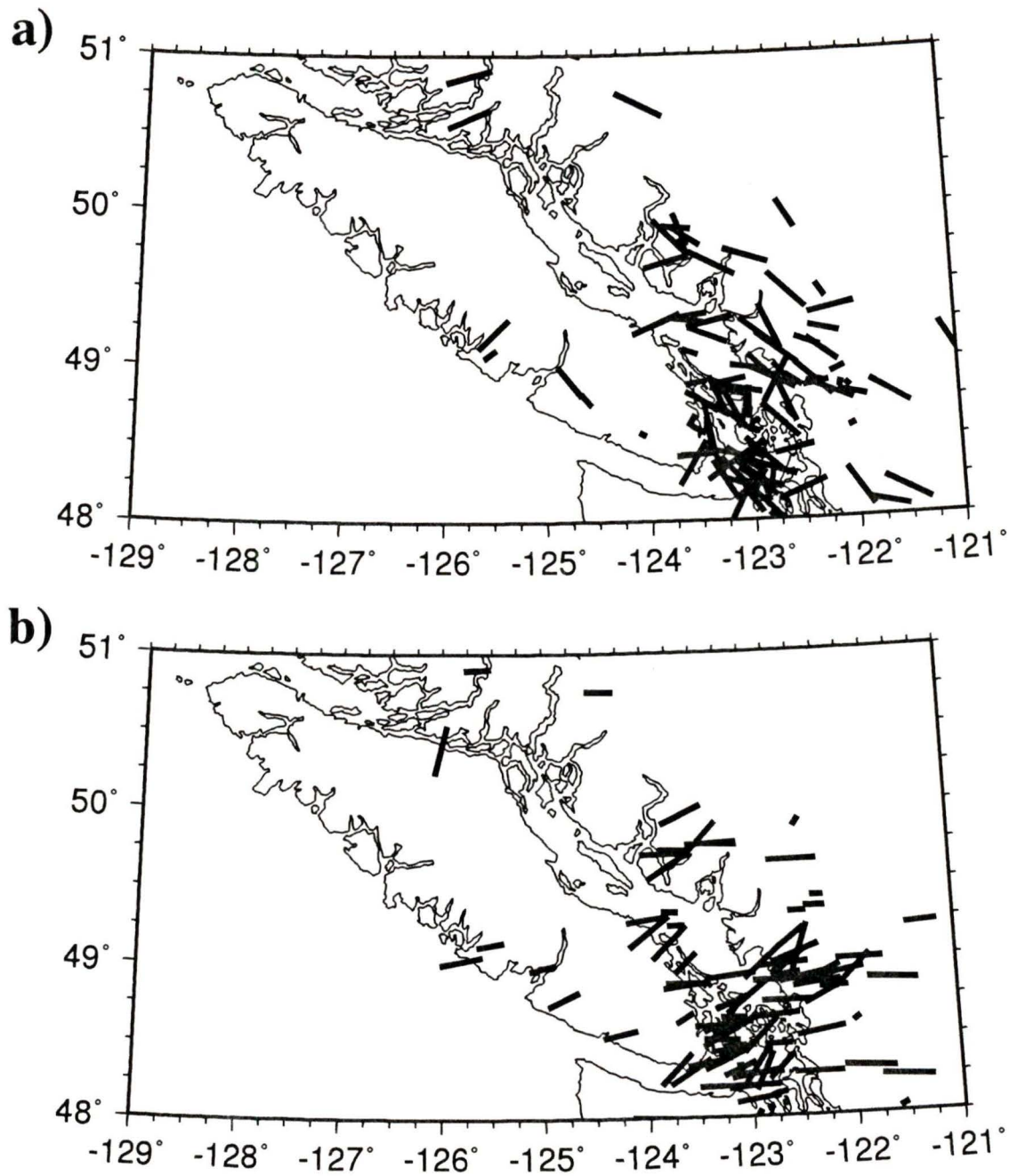

Figure 6.6 Map projection of a) P-axes and b) T-axes. The length of the bar is proportional to inclination; small dots are vertically oriented axes and the longest bars are horizontally oriented axes. Note the two events in (a) on the west coast of Vancouver Island which are oriented in the direction of subduction, perpendicular to the coastline. Because this portion of the North America plate is so close to the subducting Juan de Fuca plate, it is likely that compression in the direction of subduction dominates over the regional stress direction here.

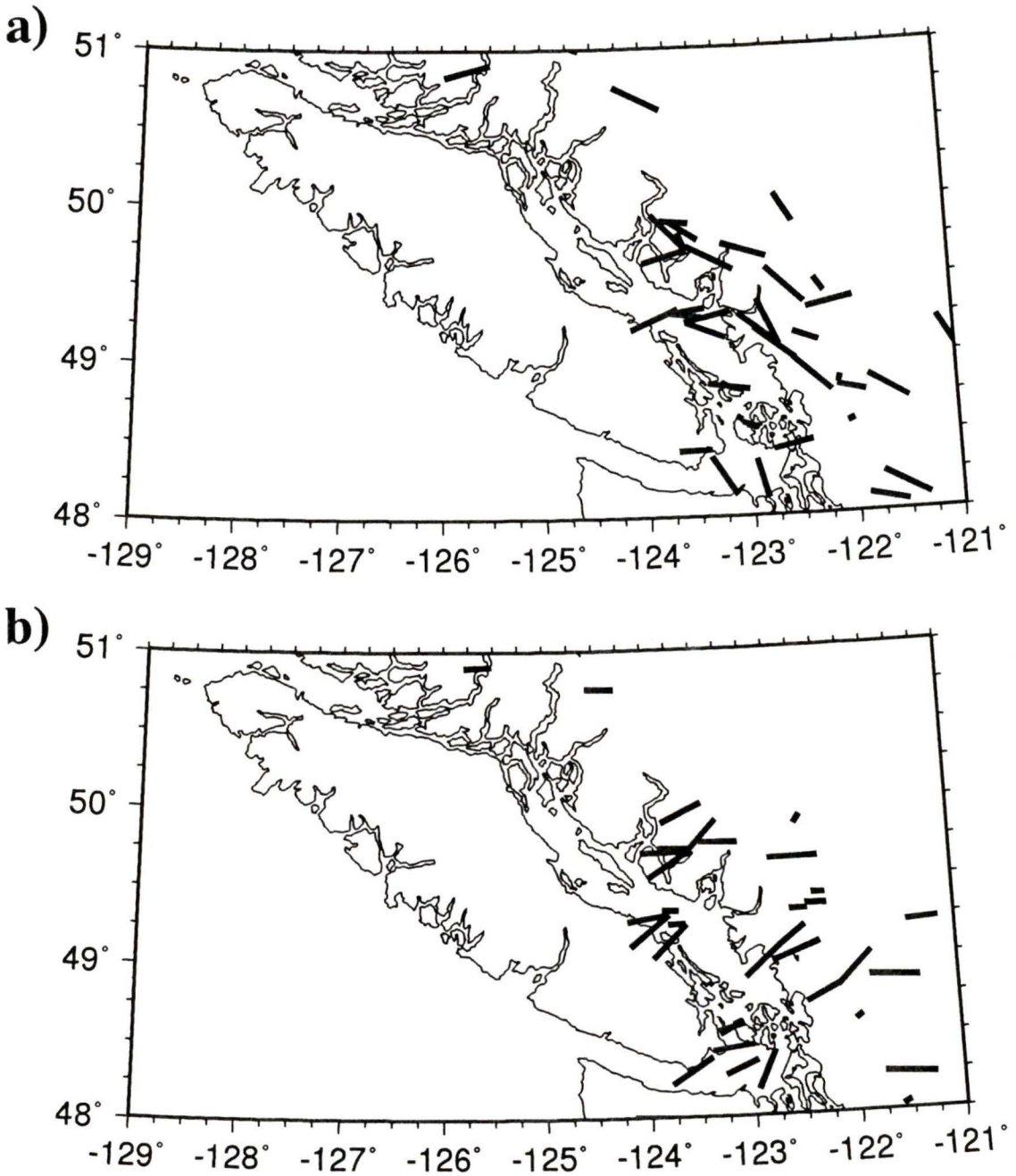

Figure 6.7 Map projection of (a) P-axes and (b) T-axes for shallow (≤ 10 km) events. Length of axes are proportional to dip as indicated in figure 6.6.

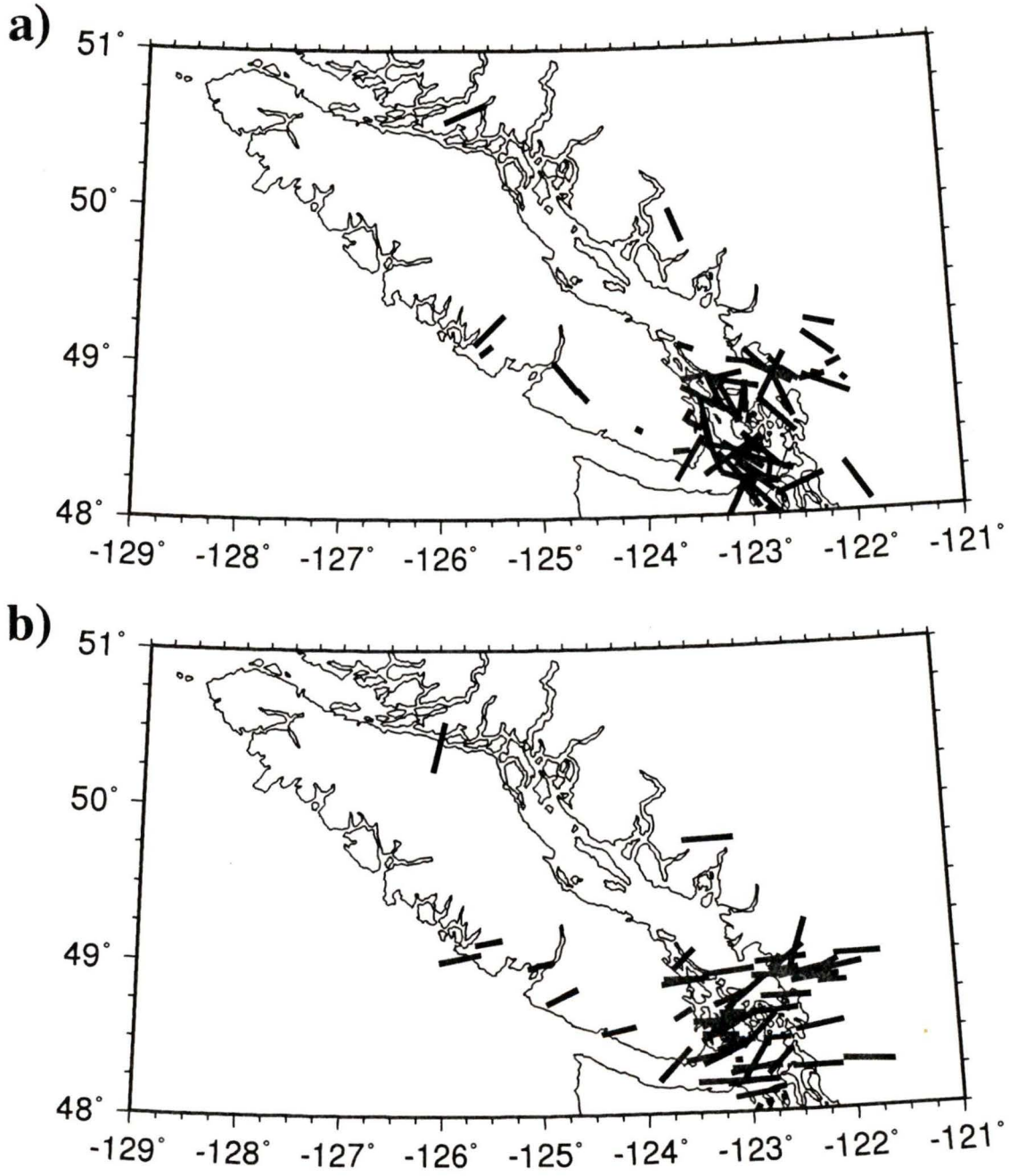

Figure 6.8 Map projection of (a) P-axes and (b) T-axes for deep ($10 < z \leq 30$ km) events. Length of axes are proportional to dip as indicated in figure 6.6.

events at 10 km depth and a cessation of seismic activity by 30 km depth.

6.4 CORRELATION WITH SEISMICITY PATTERNS

It is instructive to see if any focal mechanism solutions correspond to any trends of seismicity noted in Chapter 2. The trends chosen to compare with the gravity and magnetic data were the seismicity trends shown in figures 4.2 (shallow) and 4.3 (deep) for which focal mechanism solutions were determined. The primary objective of comparing seismicity trends with the available focal mechanism data was to determine if any of these trends are a result of a continuous sub-surface fault or indication of a localized stress regime within the regional stress field. If the focal mechanism solutions along a given trend are similar then an active fault could be identified, even without evidence of surface rupture.

6.4.1 Shallow (< 10 km) data

For the small semi-circular arc of shallow seismicity through the Victoria area, S1 (figure 6.9), there is an associated small gravity high arc (1.6-2.8 Mgal, figure 4.4c) but no magnetic anomaly which correlates with it. The magnetic map outlines surface (and sub-surface) faults such as the Leech River, Survey Mountain, and San Juan faults but there is no shallow seismicity correlation with these faults or correlation with the strike of the slip planes from the focal mechanism solutions.

There is also a north-northwesterly trending line of seismicity, S4 (figure 6.10), in the shallow data for which there are no associated gravity or magnetic trends (figure 4.4a and c). Three of the nine computed focal mechanisms have strikes in the direction of this seismicity

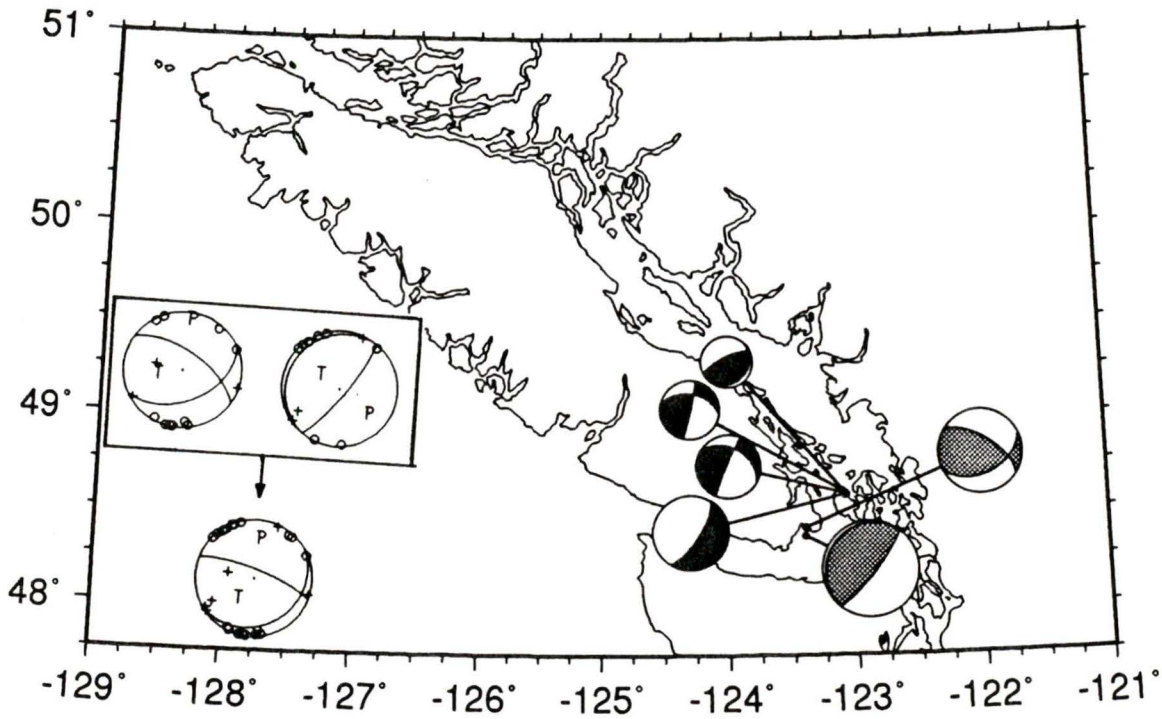

Figure 6.9 Shallow (≤ 10 km) focal mechanisms from events from trend S1 (see figure 4.2 for shallow seismicity trends). Data for the two grey shaded mechanisms are shown in inset. Composite solution with data is shown to right of inset. It is possible these two events are a result of similar stresses.

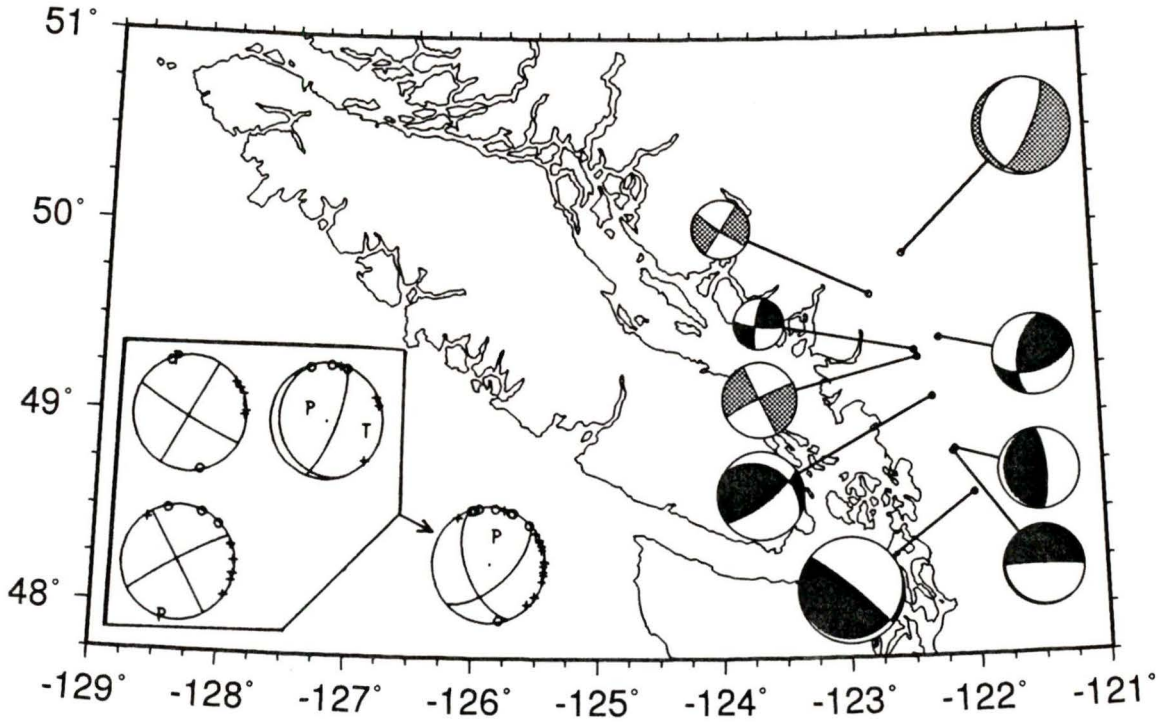

Figure 6.10 Shallow (≤ 10 km) focal mechanisms from events from trend S4 (see figure 4.2 for shallow seismicity trends). Data for the three grey shaded mechanisms are presented in inset to left; their strikes align with the general earthquake trend of north-northwest. Composite solution for these three events is also shown. It is possible these events ruptured along a pre-existing north-northwest oriented zone of weakness and are not a direct result of the regional stress.

trend. The inset in figure 6.10 shows a good composite solution of those three events (shaded) indicating a normal mechanism and a northerly (003°) P-axis. The P-axes (three individual plus one composite) are outliers on the overall regional P-axis trend (figure 6.3). These events may be initially caused by the regional stress, but then the rupture may have rotated to align itself in a direction of pre-existing weakness, whether it be a result of a fault, fluid zone in the upper crust, anisotropic trend (easier "grain" direction to rupture in), etc. Because there is no magnetic or geologic evidence in this region to support the idea of a major fault zone here, this trend of seismicity may be due to tectonic grain or a fluid-rich zone.

6.4.2 Deep (> 10 km) data

For the long north-west seismic arc trend through southern Vancouver Island and the Gulf and San Juan Islands, D1 (figure 6.11), there is a possible correlation with a series of low amplitude gravity lows (-0.4 to -8.8 mGals, figure 3.2c). There is a definite correlation of seismicity with magnetic data (figure 4.4d) along this seismic arc indicating either a change in susceptibility due to a fault zone or a change in lithology. There is only focal mechanism data for the east-south-eastern end of the arc: four out of thirteen fault plane solutions had fault planes which could line up with the south-eastern trend of the arc. These focal mechanism produce a high quality composite focal mechanism but the strike of the composite solution differs from the seismic trend by approximately 10-15°.

For the deep data there is also a north-easterly trending line of seismicity, D5 (figure 6.12), for which there is no gravity or magnetic correlation (figures 4.4 c and d). Three out of eight focal mechanisms have strikes in the northeast direction, all with similar mechanisms (thrust faulting). The composite solution shows a thrust fault with northeasterly strike (a few discrepancies, but mostly near nodal planes). The P-axis is in the mean direction for the region.

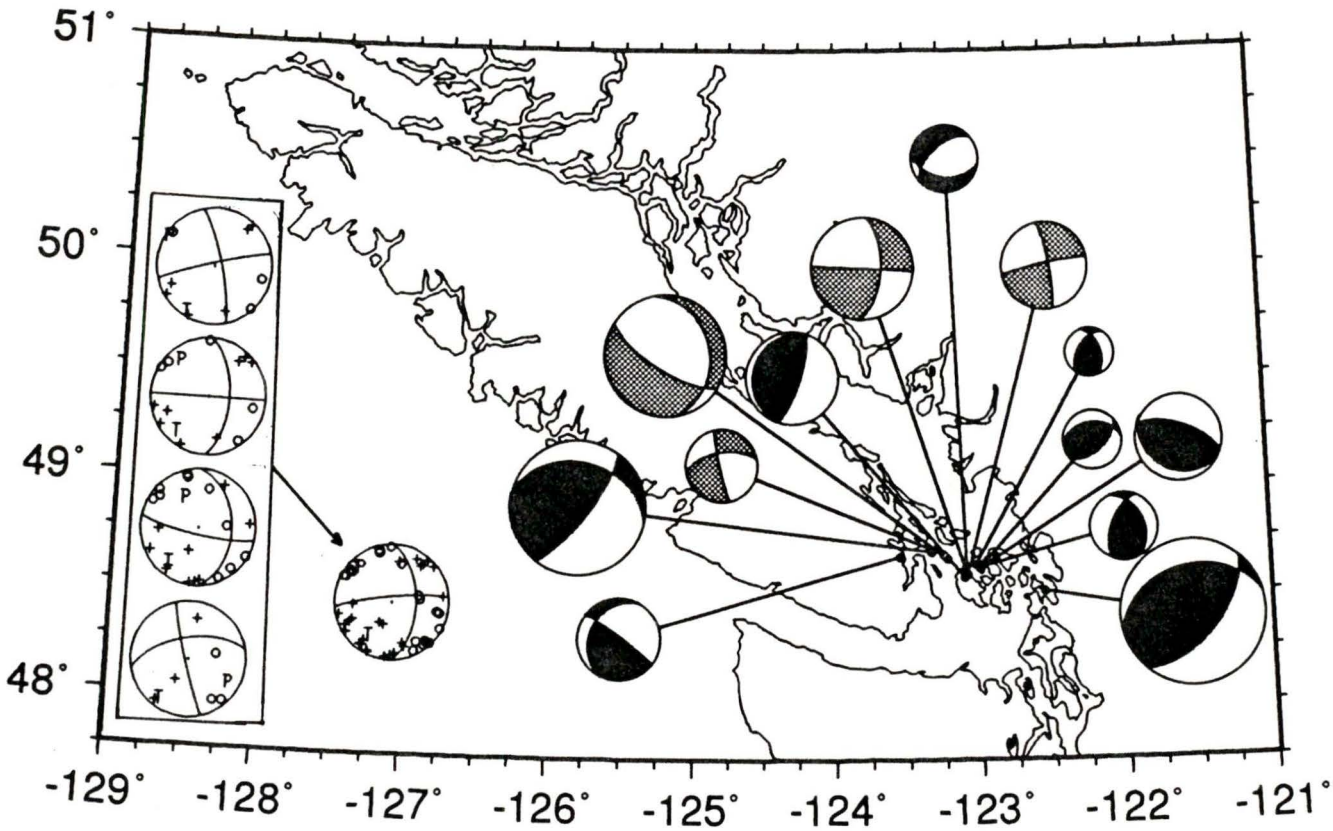

Figure 6.11 Deep (> 10 km) focal mechanisms from events from trend D1 (see figure 4.3 for shallow seismicity trends). Data for the grey shaded mechanisms are shown in inset at left; composite solution is to right of inset. Strike of events coincides with strike of seismic trend, but composite stride is 10-15° off.

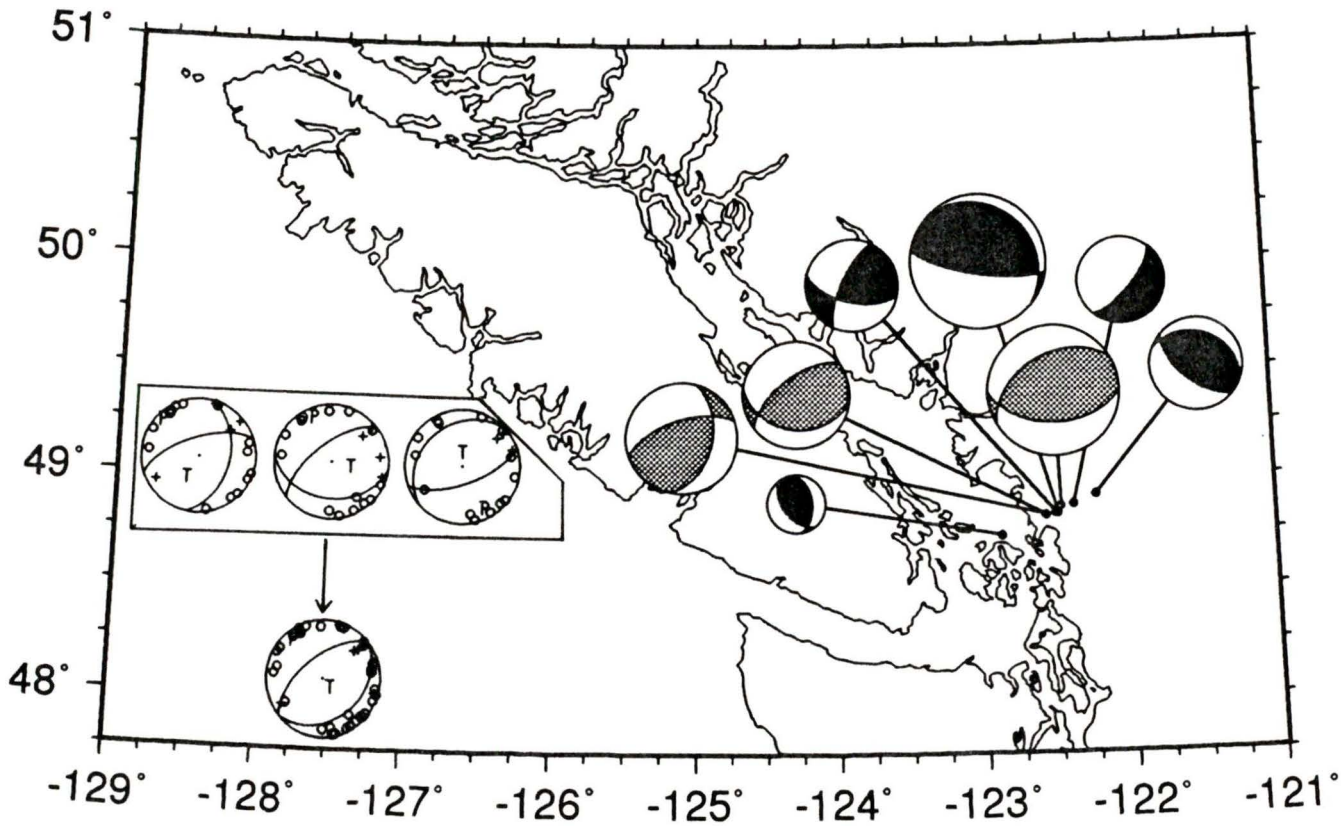

Figure 6.12 Deep (> 10 km) focal mechanisms from events from trend D5 (see figure 4.3 for shallow seismicity trends). Data for the grey shaded mechanisms are shown in inset at left; composite solution is below inset. Strike of events coincides with strike of seismic trend, the two events to the right may share a common fault plane while the left -hand shaded mechanism may be a result of similar stress to the other two, but the actual faulting mechanism is rotated slightly to the north.

6.5 DISCUSSION

From figure 6.3 the majority of P-axes are horizontal indicating maximum compression in a north-northwest/south-southeast direction. There are two notable exceptions to this north-northwest orientation with a horizontal inclination, and those two events lie in the accretionary wedge of the subduction zone (events labelled 1 and 2 in Fig 6.2). Their P-axes are perpendicular to the subduction margin indicating that here compressive stress from subduction dominates the regional stress field in this narrow area. The overall regional stress results obtained here agree in general with solutions from Washington state which are oriented in a slightly more northerly direction (see figure 6.1). This indicates a change in the regional stress direction around the bend in the North America plate margin, which parallels the plate's free edge.

The T-axes composite plot shows a south-southeasterly trend of 062° ± 7° and the axes vary in inclination from horizontal to vertical with little preference to angle of inclination (figure 6.3). Since σ_1 (P-axis) is confined to lie horizontally in the north-northwest direction, σ_2 and σ_3 (T-axis) must lie within the south-southeast oriented plane which is perpendicular to σ_1. Since the plunge of the T-axes show little preference for a given angle of inclination the intermediate stress, σ_2, also shows little preferential angle of inclination. This indicates that σ_2 and σ_3 must therefore be of similar magnitude; otherwise a preferential distribution for the angle of inclination of these regional stress axes would be observed. The value of R=0.4, the relative stress measure from program FMSI, indicates that σ_2 and σ_3 are not exactly the same magnitude although similar. This region of the Pacific rim has long been known to be a region of oblique

convergence between the subduction Juan de Fuca plate system and the overriding North American plate (*Atwater*, 1970), which complicates the issue of P and T-axes orientations. Together the regional stresses (and hence the focal mechanism solutions) show a mixture of strike slip and thrust faulting. However, no definite conclusions with respect to reactivating subsurface faults can be made from a comparison of focal mechanisms, gravity, and magnetic data.

There are three processes operating which affect the stress regime in southwestern British Columbia. Fitch [1972] proposed partitioning of slip into normal and margin parallel components at subduction zones. The margin parallel component can be taken up by right-lateral shear in the same direction. Sbar [1982] defined seismotectonic domains in the central and western United States; he attributed the observed state of stress in the majority of these seismotectonic domains as being due to north/south compression along the western coast of the United States from the Pacific plate pushing northwards against an abutting portion of the North America plate. Walcott [1993] proposed that opening of the Basin and Range province in the United States led to counterclockwise rotation of the Juan de Fuca subduction margin over the past 10 to 20 my, pivoting about a point near Seattle, Washington. All of these processes could lead to the observed P-axes orientations in southwestern British Columbia, with perhaps Fitch's [1972] model most directly accounting for margin parallel maximum compressive stress due to partitioning of slip from the Juan de Fuca plate. However, there is not enough evidence to rule out a significant contribution from Pacific/North America plate interaction which could result in north-northwest compression in southwestern British Columbia. It is unclear at this stage which of the above mentioned three processes is most significant in southwestern British Columbia tectonics.

In conclusion, the T-axes lie in a band which shows that σ_2 and σ_3 are close in value (the principal axes must be perpendicular to each other and since σ_1 is oriented NNW and horizontal, then the minimum stress, σ_3, must alternate with the intermediate stress, σ_2, in orientation since

there is no preferential alignment of the T-axis (σ_3) inclination). As a result, the compressional P-axes dominate the focal mechanism solutions, and therefore the regional stress regime, and are oriented horizontally in a north-northwest direction in southwestern British Columbia. This implies north-northwest compression or right lateral shear parallel to the plate margin.

CHAPTER 7

POISSON'S RATIO

7.1 INTRODUCTION

In the Canadian Cordillera velocity models of the upper crust have primarily been determined by calculating P-wave velocities and assuming a Poisson's ratio to define S-wave velocities. For Vancouver Island and the lower mainland region, little or no attention has been paid to independently determining an appropriate S-wave velocity model. As such, it is possible that earthquake hypocentre locations are biased towards the P-wave arrival readings so an independent estimate of the S-wave velocity (or equivalently, the P to S wave velocity ratio) is needed.

Rogers [1983] determined that a Poisson's ratio of 0.25, or a P to S velocity ratio of 1.73, faithfully reproduced the P-wave solution of Texada Island blasts when S-wave data were included. However, the results were not conclusive although they showed no trend which suggested that Poisson's ratio should be different from 0.25. Recently, Fallows [1994] determined values of Poisson's ratio for the upper 10 km of the North America plate in

Vancouver Island and the adjacent mainland by inverting arrivals from a refraction survey, SCoRE89, which had been recorded on seismic stations of the Western Canadian Telemetered Network (WCTN). However, his results are poorly resolved near the edges of his model and the values in any given part of his grid are affected by the adjacent grid values. Fallows' method results in reasonable averages of Poisson's ratio for a large region, but does not determine independently estimated values of Poisson's ratio for subsections of a given region. The earthquake data in southwestern British Columbia provide an independent estimate of P to S velocity ratios which does not depend on previous velocity model values.

Poisson's ratio can be expressed in terms of compressional and shear wave velocities for an elastic, isotropic medium

$$\sigma = \frac{1-\frac{1}{2}(V_p/V_s)^2}{1-(V_p/V_s)^2}$$

where σ is Poisson's ratio, V_P is compressional or P wave velocity, and V_S is shear or S wave velocity. The V_P/V_S ratio (and hence σ) provides information about the composition of the region through which the seismic rays travel. Most rock forming minerals have Poisson's ratio between 0.20 and 0.30 [*Anderson*, 1989 and *Holbrook et al.*, 1992].

7.2 COAST PLUTONIC COMPLEX

The Coast Plutonic Complex (CPC) lies within the Western Coast Belt and is comprised primarily of granodiorite, quartz diorite, and diorite intrusions of unknown age, with smaller regions of mafic and ultramafic, sometimes metamorphosed, plutonic rocks interspersed throughout the complex [*Douglas*, 1979]. Gravity and magnetic modelling by Dehler and Clowes

[1992] and EM modelling by Jones et al. [1992] indicated that the CPC extends to a depth of approximately 14 km. Hence two separate Poisson's ratios were calculated, one value which comprises an average σ from the surface down to a depth of 15 km and a second which comprises an average σ from the surface down to a depth of 30 km. Differences in arrival times for a given event between pairs of stations were used to obtain V_P/V_S using the expression

$$\frac{V_P}{V_S} = \frac{\Delta S}{\Delta P} = \frac{\Delta S_2 - \Delta S_1}{\Delta P_2 - \Delta P_1}$$

where ΔP and ΔS are the difference in travel times between a pair of stations for P and S waves respectively; ΔP_1, ΔS_1 are P and S wave arrival times at station 1; ΔP_2, ΔS_2 are P and S wave arrival times at station 2 (figure 7.1).

For the upper regime of the Coast Plutonic Complex, events at depths less than 15 km were used to obtain ΔP and ΔS travel time differences between pairs of stations. Care was taken to insure that all ray paths travelled only through the upper 15 km of the CPC region and that all take-off angles from the earthquake source were upward (no turning rays). The resulting V_P/V_S ratio was an average for the area the ray paths sampled. For the Poisson ratio data, travel times over shorter distances were not as accurate as travel times over longer distances, due to lateral and vertical inhomogeneities. A weighted mean of V_P/V_S and the standard error in the mean was determined for the upper 15 km of the Coast Plutonic Complex using the following statistical definitions for standard deviation (s_i), weighted mean ($\overline{X}$), and standard error of the weighted mean (s):

$$s_i^2 = \left(\frac{V_P}{V_S}\right) \left[\left(\frac{s_P}{\Delta P}\right)^2 + \left(\frac{s_S}{\Delta S}\right)^2 \right]$$

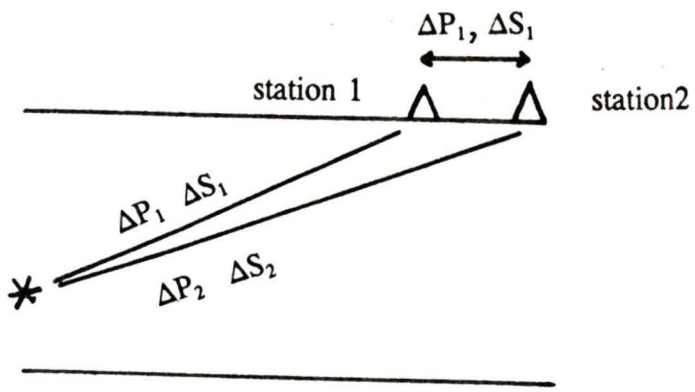

$$\frac{\Delta S}{\Delta P} = \frac{V_P}{V_S}$$

$$\sigma = \frac{1 - \frac{1}{2}\left(\frac{V_P}{V_S}\right)^2}{1 - \left(\frac{V_P}{V_S}\right)^2}$$

Figure 7.1 Idealized ray paths from an earthquake hypocentre to two stations at which arrivals were recorded. The difference in arrival times between the two stations is ΔP and ΔS for P and S-wave arrivals respectively. Equations show how Poisson's ration, σ, is obtained from ΔP and ΔS determinations.

$$\overline{X} = \frac{\sum_{i=1}^{n} \frac{(V_P/V_S)}{s_i^2}}{\sum_{i=1}^{n} \frac{1}{s_i^2}}$$

$$\frac{1}{s^2} = \sum_{i=1}^{n} \left(\frac{1}{s_i}\right)^2$$

where s_P=0.1 sec and s_S=0.2 sec are the errors in reading the P and S wave arrival times, respectively.

The same process was used to calculate a weighted V_P/V_S for the lower region. Events were constrained to lie between depths of 15 to 30 km and all ray paths had incident angles of $> 90°$, that is, no turning rays which sampled mantle material were used. The ray paths sampled the North American crust from the depth of the given event up to the surface giving an average travel time through this region. It was decided not to use events at depths less than 15 km in this calculation as it would heavily weight the region sampled in favour of the upper 15 km, since ray paths from the lower earthquakes and ray paths from the upper earthquakes both sample the upper 15 km. Figure 7.2 shows the location of stations and events used for the V_P/V_S calculation for the upper and lower sections of the Coast Plutonic Complex. Figure 7.3 shows ΔS versus ΔP data for the upper 15 km and for the upper 30 km of crust. For the upper 15 km of the CPC a total of 53 sets of station pairs were used and a weighted mean of 1.7099 $\pm$ 0.0068 was obtained corresponding to a Poisson's ratio of 0.2401 $\pm$ 0.0032. For 30 km of the crust of the CPC a total of 52 sets of station pairs were used and a weighted mean of 1.7061 $\pm$ 0.0083 was obtained with a Poisson's ratio of 0.2384 $\pm$ 0.0039. It must again be noted that these values represent an average Poisson's ratio down to the depth range mentioned.

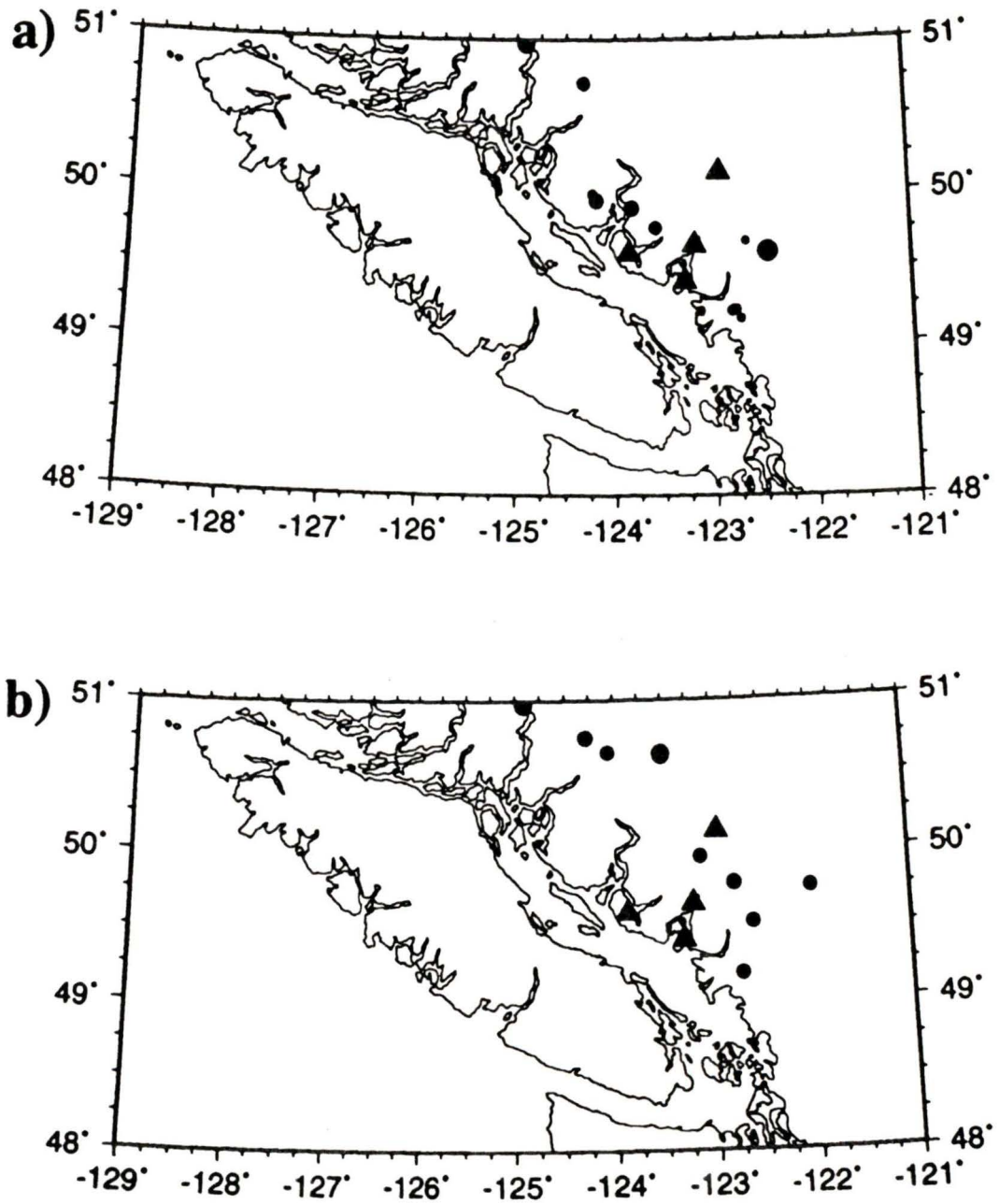

Figure 7.2 Location of stations (triangles) and events (circles) used to determine V_P/V_S (and hence σ) for the Coast Plutonic Complex (CPC) for a) the upper 15 km of crust and b) the entire crust upward from 30 km.

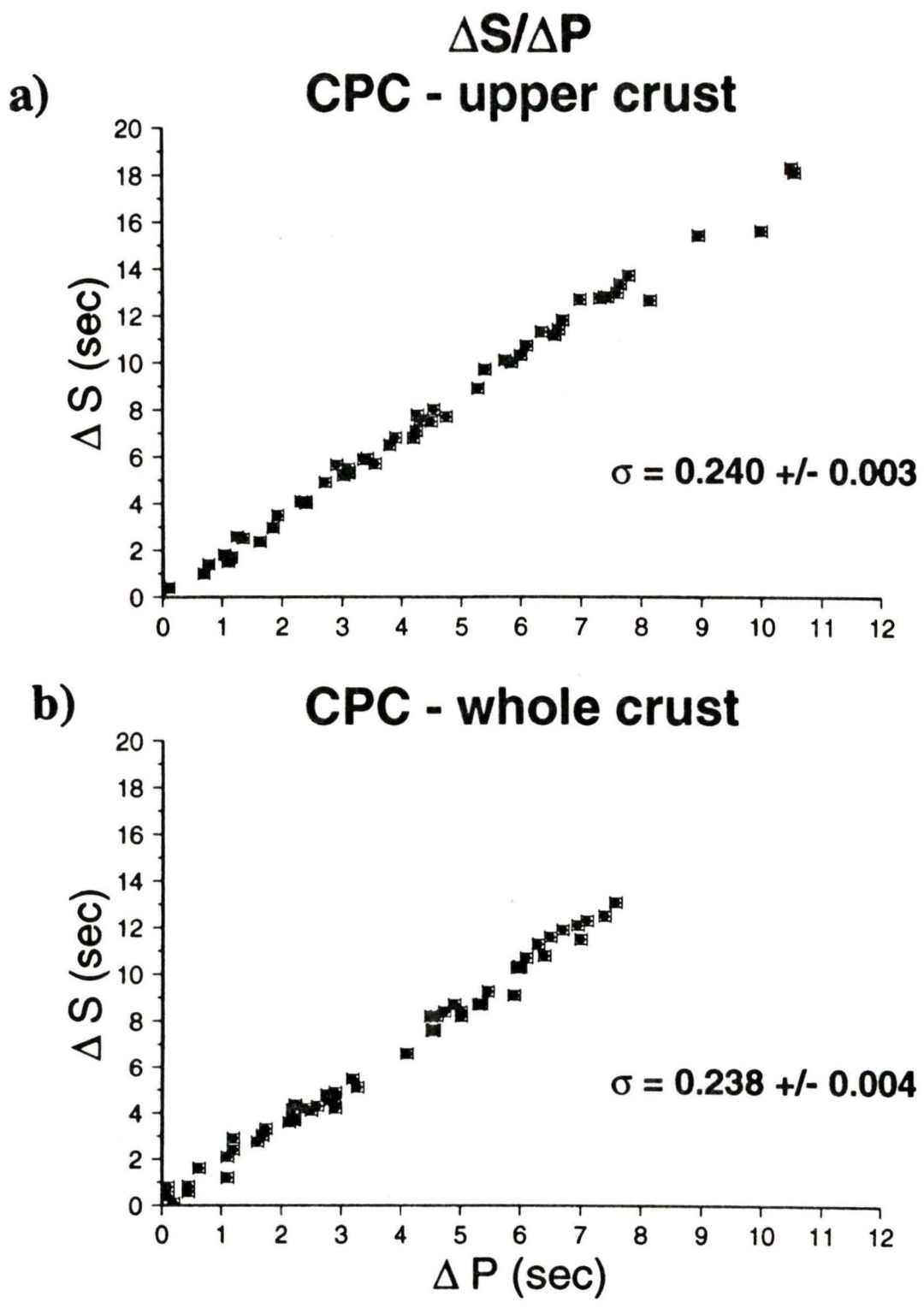

Figure 7.3 Plot of ΔS *vs* ΔP (in seconds) for the Coast Plutonic Complex (CPC). The slope gives the average $\Delta S/\Delta P$ for the portion of the crust the raypaths sample for a) the upper 15 km of the crust and b) the upper 30 km of the crust (or entire crust).

The sources of error divide themselves into man-made and natural errors. On the man-made side there are errors in observation - inexact readings of phase arrivals due to low signal-to-noise ratios. Natural sources of error arise from shear wave splitting which can give apparent differences in S wave travel times depending on station azimuth, lateral heterogeneity, travel time delays over faults, and hydrous zones in the crust. The error given for Poisson's Ratio for the results in this chapter is statistically correct, but may be a low estimate of the real error since natural sources of error were not measurable and therefore not taken into account in the numerical error determination.

7.3 VANCOUVER ISLAND

Vancouver Island lies within the Insular Belt with the exception of the very southwestern tip of the Island which forms part of the Cascadia Belt [*Varsek et al.*, 1993]. For the most part, Vancouver Island consists of Upper Devonian to Recent rocks; Devonian island arc volcanics (Sicker Group), Upper Triassic basalts (Karmutsen), Middle Jurassic granodiorites, granites, quartz monzonite, and quartz diorite (Island Intrusions), Lower Jurassic andesite, dacite, and rhyolite (Bonanza group), Upper Cretaceous sandstone, shale, conglomerates (Nanaimo Group), and Permian limestone (Buttle Lake) [*Douglas*, 1979]. With depth, Vancouver Island is very structurally complicated as it has been created by accretion at a subduction margin. It consists of an interfingering of layers, comprised of ancient terrane assemblages, underplated wedge sediments from the subduction zone, and igneous intrusions. From the gravity and magnetic model of Dehler and Clowes' [1992], the upper crust (Wrangellia) extends to approximately 14 km depth on the western side of the Island to approximately 20 km depth on the eastern side,

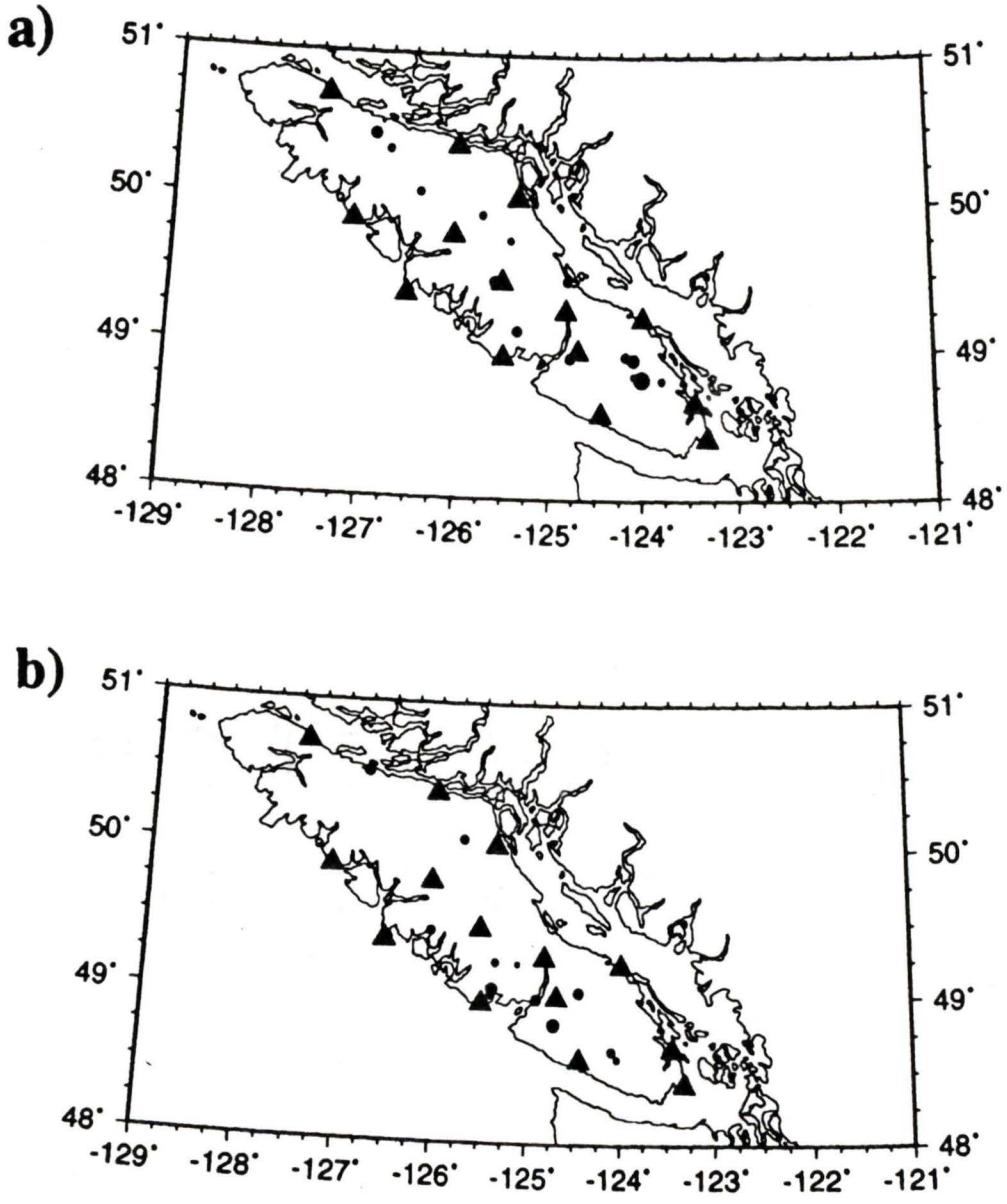

Figure 7.4 Location of stations (triangles) and events (circles) used to determine V_p/V_s (and hence σ) for Vancouver Island (Wrangellia portion) for a) the upper 15 km of crust and b) the upper 30 km (or entire crust)

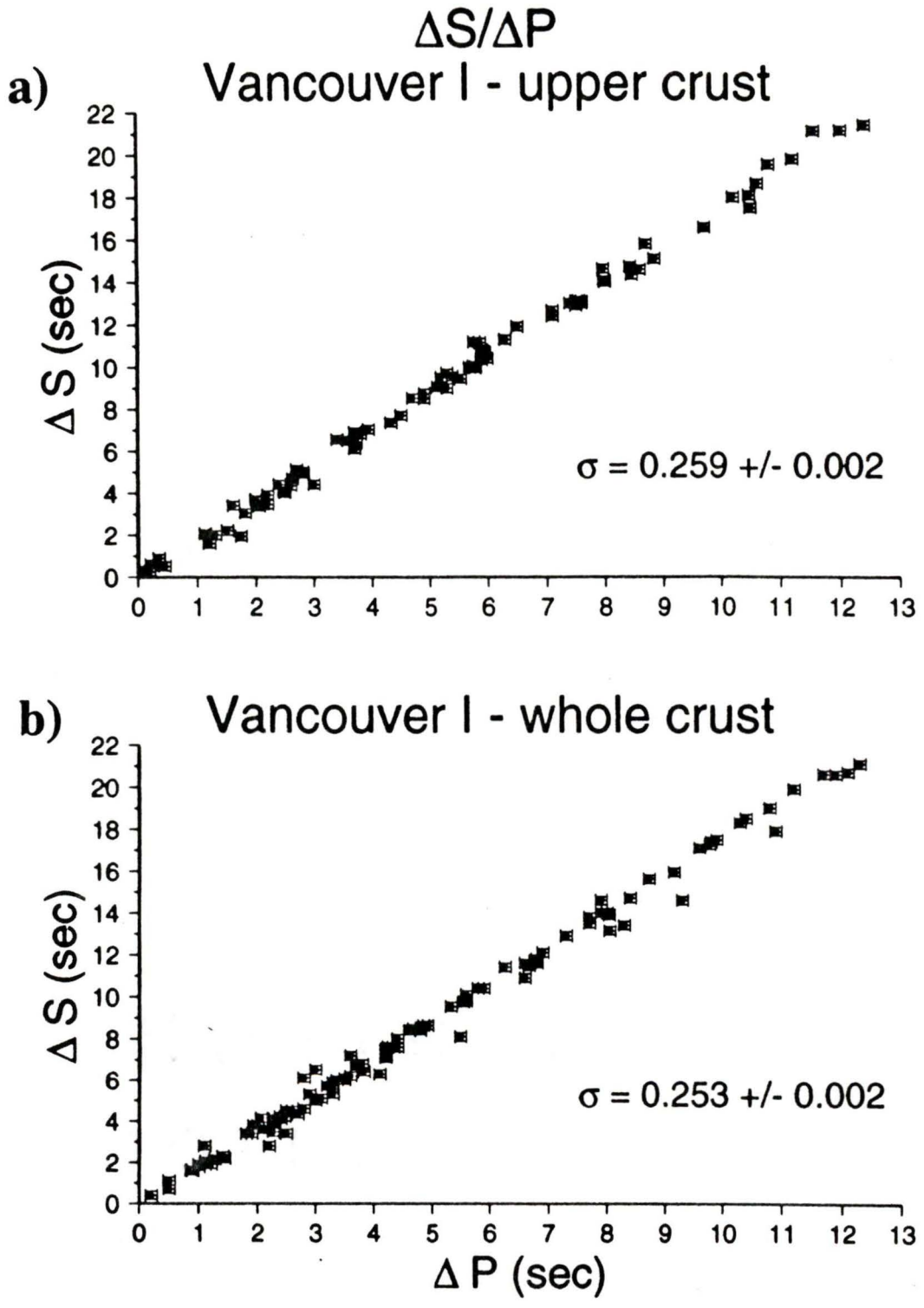

Figure 7.5 Plot of ΔS *vs* ΔP (in seconds) for Vancouver Island (Wrangellia portion). The slope gives the average ΔS/ΔP for the portion of the crust the ray paths sample for a) the upper 15 km of the crust and b) the upper 30 km of the crust (or entire crust).

while the lower crust extends down to approximately 25 km on the western side of Vancouver Island where it abuts against the downgoing Juan de Fuca oceanic plate to approximately 36 km on the eastern side where the Moho is encountered.

V_P/V_S ratios were again calculated from differences in arrival times between pairs of stations. Care was again taken to ensure that all ray paths lay within the Insular belt section of Vancouver Island. Figure 7.4 shows the location of stations and events used for the upper and lower sections of Vancouver Island. For the upper section, earthquake depths were less than 15 km; for the lower section, depths were between 20 and 25 km for the western side of Vancouver Island and between 20 and 36 km for the eastern side of Vancouver Island. For the lower section no earthquake depths were shallower than 20 km to ensure that all the lower hypocentres originated in the lower crust. All depths were chosen based on Dehler and Clowes' gravity and magnetic model as described above. Plots of ΔS versus ΔP data for both the shallow and deep region of Vancouver Island are shown in Figure 7.5. For the upper 15 km of Vancouver Island a total of 87 station pairs were used and a weighted mean of 1.7544 ± 0.0047 was obtained, with a Poisson's ratio of 0.2594 ± 0.0019. For the lower region of Vancouver Island a total of 108 station pairs were used and a weighted mean of 1.7384 ± 0.0044 was obtained with a Poisson's ratio of 0.2527 ± 0.0019. Again these values represent an integrated or averaged value of Poisson's ratio down to the depth range specified.

7.4 CONCLUSION

Poisson's ratio of 0.240 ± 0.003 for the upper Coast Plutonic Complex is lower than the value of 0.259 ± 0.002 for upper Vancouver Island, likely due to the higher quartz content of

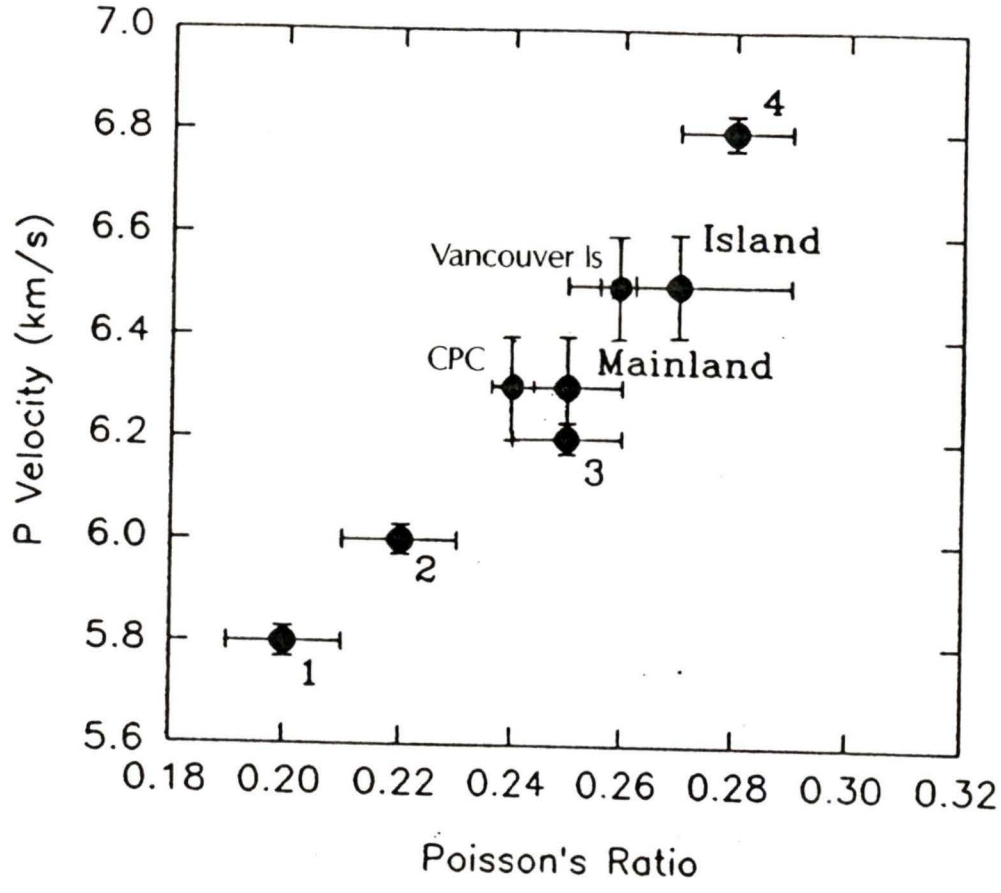

Figure 7.6 Comparison of Poisson's ratio results with Fallows' [1994] results (Island, Mainland), and other results for rocks of felsic to mafic composition [*Hall and Ali* , 1985]; 1 being most felsic, 4 being most mafic.

	σ	V_P/V_S
CPC < 15 km	0.240 ± 0.003	1.710 ± 0.007
CPC - whole crust	0.238 ± 0.004	1.706 ± 0.008
V.I. < 15 km	0.259 ± 0.002	1.754 ± 0.005
V.I. - whole crust	0.253 ± 0.002	1.738 ± 0.004
Fallows [1994]		
CPC ≤ 10 km	0.23 ± 0.02	
V.I. ≤ 10 km	0.27 ± 0.02	

Table 7.1 Poisson's Ratio results: CPC - Coast Plutonic Complex, V.I. - Vancouver Island. Results from this study compared with those of Fallows [1994].

the Coast Plutonic Complex. These values also agree (within the errors) with those of Fallows [1994] who obtained an average Poisson's ratio of $\sigma=0.23 \pm 0.02$ for the Coast Plutonic Complex and $\sigma=0.27 \pm 0.02$ for Vancouver Island. The bulk values of 0.240 for the Coast Plutonic Complex and 0.253 for Vancouver Island are not sufficiently different from $\sigma=0.25$, the value used for earthquake locations, and this calculated difference would result in an error of less than 1 km in epicentral location for most earthquakes. Figure 7.6 compares these two sets of results and shows that rocks with a high mafic content have higher P-velocities and Poisson's ratios than more felsic rocks.

CHAPTER 8

VICTORIA REGION

8.1 INTRODUCTION

The Victoria area on southern Vancouver Island is a highly populated region with three terrane bounding faults exposed at the surface, running through the populated area. A fourth major, northeast dipping fault, which has a surface exposure in the Olympic peninsula of Washington state, also underlies the Victoria region. Although they appear not to have been active in the recent geologic past, reactivation of any of these terrane bounding faults would present a seismic hazard to the region.

The southern end of Vancouver Island differs from the rest of the island both seismologically and geologically. It is located in the corner of the subduction zone and is far more seismically active than regions north of it. Geologically, southern Vancouver Island consists of two separate tectonic belts, the Cascadia belt (composed of Pacific Rim and Crescent

terranes) which extends south into Washington state, and the Insular belt (composed of Wrangellia terrane) which extends north to include the rest of Vancouver Island and the Queen Charlotte Islands (see figure 1.1). The area is intersected by three major terrane bounding faults, the Leech River Fault, the Survey Mountain Fault, and the San Juan Fault (figure 8.1). The Survey Mountain and San Juan Faults separate Wrangellia terrane from the Leech River schists to the south, and the Leech River Fault separates the Leech River schist from the Eocene Metchosin basalts. LITHOPROBE seismic reflection Line 2, also shown in figure 8.1, images the subsurface extension of the Leech River and Survey Mountain faults. The Line 2 interpretation also includes the subsurface extension of the Hurricane Ridge fault which outcrops in the Olympic Peninsula of Washington State and extends northwest, offshore of Vancouver Island [*Clowes et al.*, 1987]. From figures 4.2 and 4.3, it appears that the earthquakes formed linear trends that might correlate with the surface mapped faults through the Victoria area. The following study was carried out to see if this was so.

8.2 METHOD

Earthquakes which occurred in the Victoria region are plotted in figure 8.1. For comparison purposes events in this region were projected onto a line (figure 8.2) nearly coincident with the Lithoprobe Line 2 survey for which structural and geological interpretations exist [*Clowes et al.*, 1987]. Events north and south of Line 2 were not considered here. This plot also includes events with arrivals at only three stations which were not included in the North America plate data set (figure 2.3) because they did not meet the depth resolution of the rest of the data, but it was considered important to show all possible seismicity in the Victoria area for this study. To

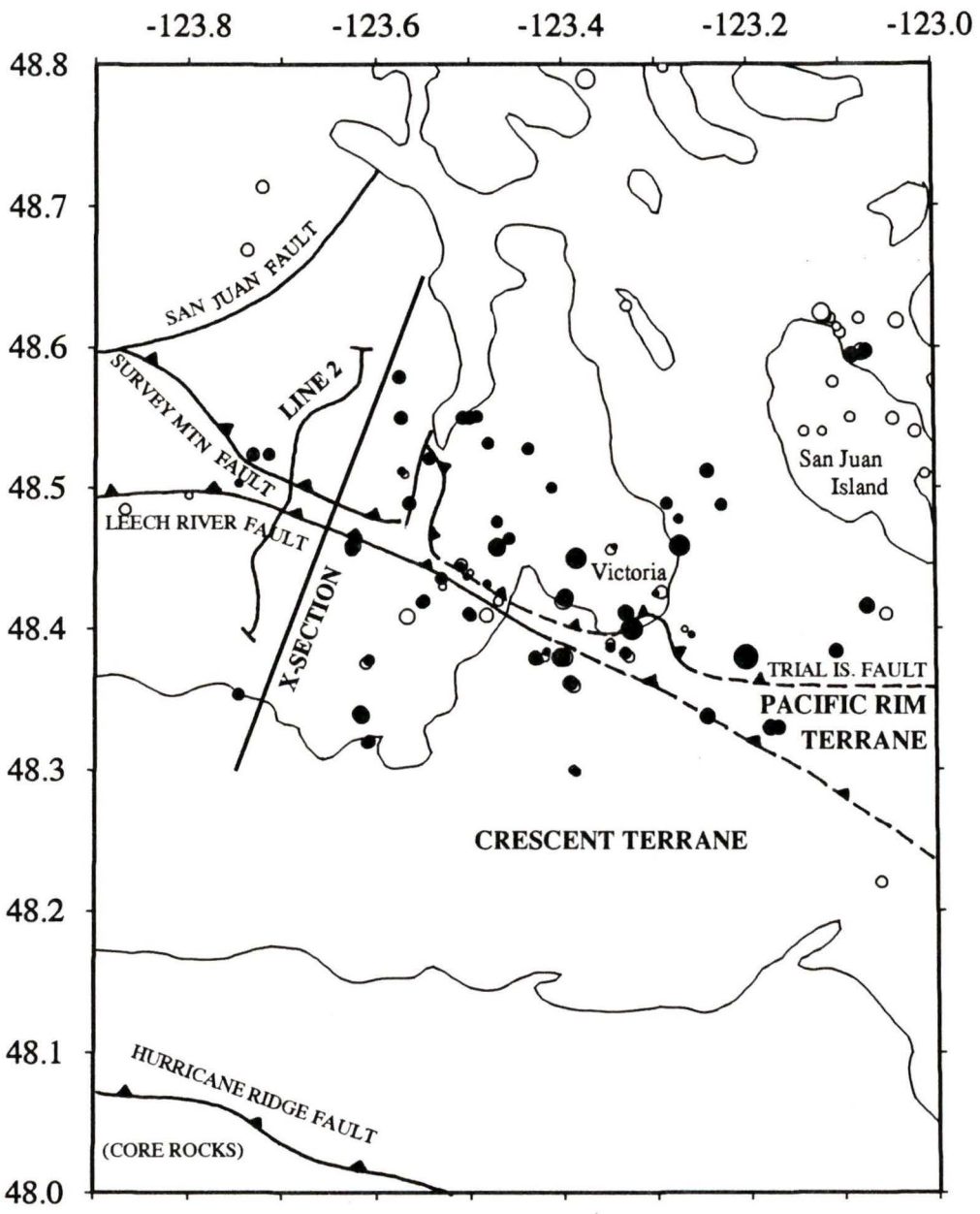

Figure 8.1 Earthquakes in the Victoria region (the open circles and most of the solid circles are $\leq$ 10 km in depth since that is the depth to which the surface exposed faults extend. A few larger, deeper earthquakes are also included in this data set). Closed circles are earthquakes used for this analysis which may be associated with pre-existing faults. The three major terrane bounding faults (which extend to depth), San Juan and Survey Mountain faults which separate Wrangellia from Pacific Rim terranes, and the Leech River fault which separates Pacific Rim and Crescent terranes, are shown here. The LITHOPROBE reflection Line 2 is shown here as well as the line of cross-section which the earthquakes were projected onto to compare with the subsurface geology.

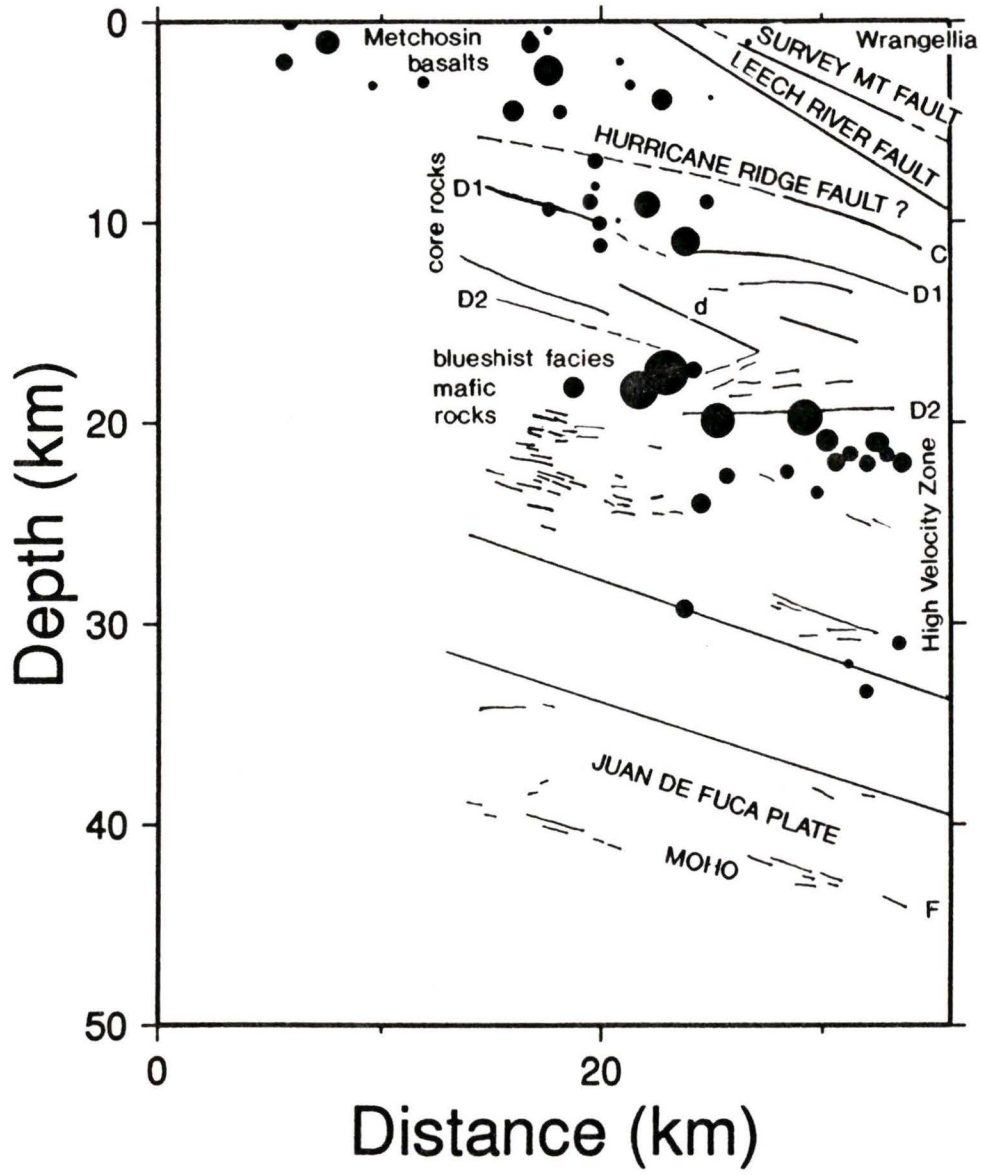

Figure 8.2 Earthquakes plotted with depth in the Victoria area. Geology and fault locations are from Lithoprobe Line 2 reflection survey (after *Clowes et al.*, 1986) and the Victoria area earthquakes were projected onto the cross-section shown in figure 8.1.

test the accuracy of the locations, all events were relocated with a common subset of seismic stations to stabilize their relative hypocentral locations. The stations chosen are shown in figure 8.3. This distribution of stations was chosen to be as equally distributed in azimuth as possible and to all lie roughly equidistant from the Victoria area. Stations VGZ and PGC, directly above the region of interest, were chosen to provide depth control for the location of these events. Unfortunately, not all events had arrivals at all these stations, so one event with good arrivals at all the stations was picked as the "key" event. This key event was located with the chosen subset of stations and traveltime residuals between this location and the original location were noted. The travel time residuals were then used as time corrections to all the other events in the subset and the other events were relocated. This moved all the subset events into a relative position with respect to the key event. Because of the balanced azimuthal distribution of stations and the small event-to receiver distances, bias due to lopsided station distribution should be reduced by this technique.

This relocation process did not appreciably change the hypocentral locations of this Victoria group of earthquakes. The majority of events shifted by approximately 1 km relative to that determined by routine processing, with the largest change in hypocentre location being 2.8 km. All changes in location were within the original errors in hypocentre location. The depth uncertainties in the original event locations were within 5 km. Figure 8.2 shows a cross-sectional view of the Victoria earthquakes superimposed on the geological interpretation of Lithoprobe Line 2 [*Clowes et al.*, 1987].

Focal mechanism solutions for this region are presented in figure 8.4, along with a composite solution with a P-axis oriented north-northwest.

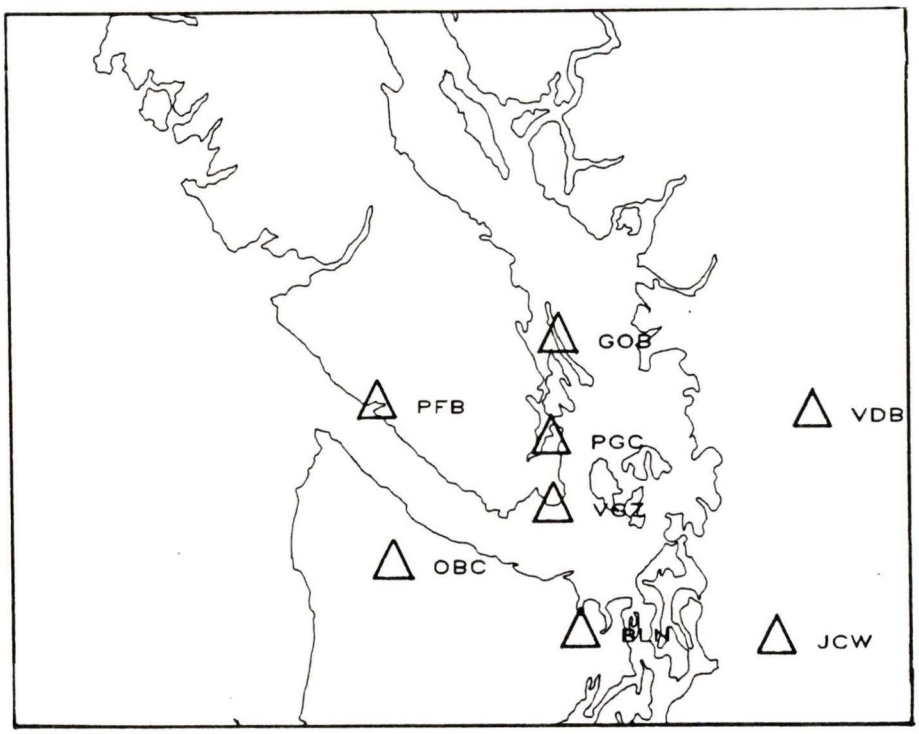

Figure 8.3 Distribution of seismic stations used to relocate events in the Victoria region. Stations were chosen so that there was an equal azimuth distribution of stations around the Victoria area and so that there was adequate depth control (stations PGC and VGZ which were directly above the region of interest) of the relocated events which were to be compared with subsurface extension of major faults.

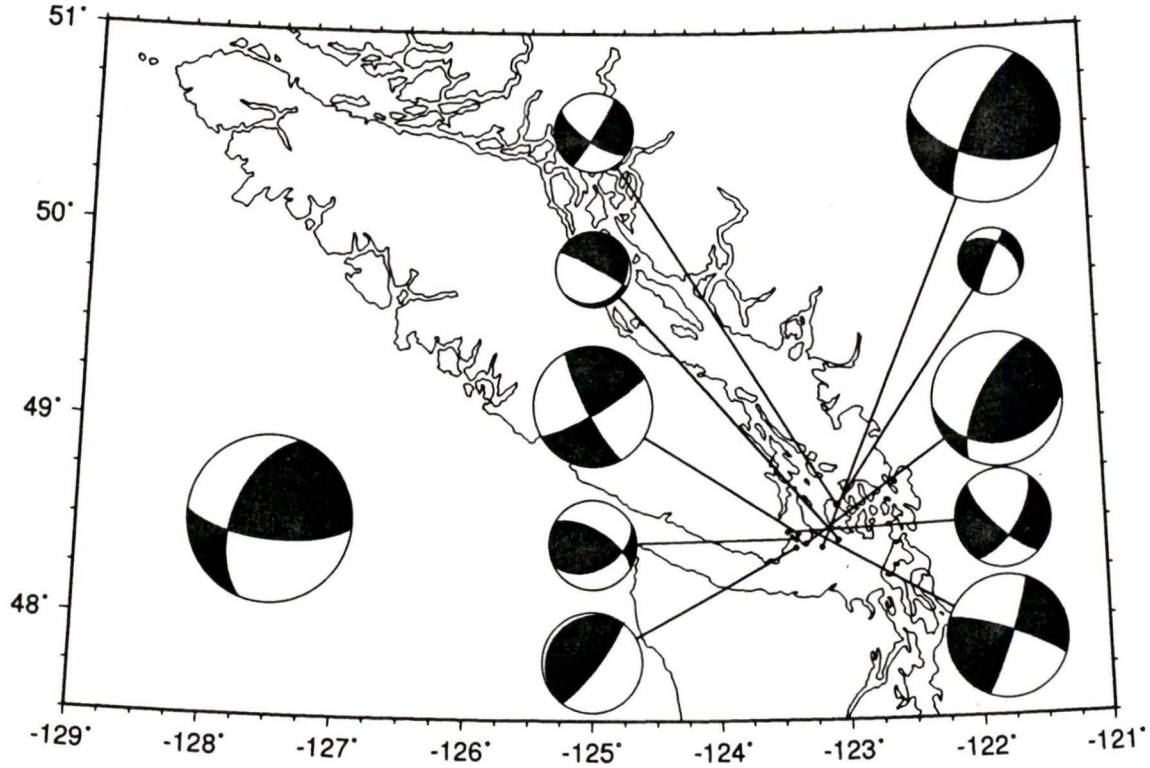

Figure 8.4 Focal mechanism solutions for Victoria area earthquakes. The composite solution has P and T-axes which agree with the regional distribution of P and T-axes for the southwestern British Columbia region.

8.3 DISCUSSION

When the earthquake hypocentres were projected onto the geologic interpretation of Lithoprobe Line 2 (figure 8.2), none of the earthquakes were seen to be associated with the subsurface extension of any of the three major faults shown in the cross-section. Even allowing for a change in depth within the relocation errors these events do not positively correlate with any of the major faults. The majority of the shallow event suite ($\leq$ 10 km) lie below the Leech River fault within the Metchosin basalts and the core rocks, a Cenozoic subduction complex mostly composed of deformed but well-layered turbidites [*Clowes et al.*, 1987]. The Hurricane Ridge fault separates these two rock packages. It is a terrane bounding fault which truncates the base of the Crescent terrane [*Clowes et al.*, 1987]. The deeper suite ($>$ 10 km) of events lies within the package of reflections which was interpreted by Clowes et al. (1987) as blueschist-facies/mafic rocks. The deeper suite of events also does not correlate with any interpreted fault. However the D1 to D2 zone is a highly reflective zone [*Clowes et al.*, 1987] and it appears as if the deeper suite of earthquakes is concentrated at the base of this zone (figure 8.3).

The composite focal mechanism solution obtained from the events which had first motion readings is shown in figure 8.4. It implies the faulting regime in this area to be oblique slip with a predominantly strike-slip component combined with a large thrust component. The majority of the shallow suite of earthquakes in figure 8.2 lies in the accretionary complex for which there is evidence of thrust faulting [*Clowes et al.*, 1987]. The composite focal plane solution indicates thrust faulting; however, the likely slip plane dips to the south whereas the subsurface faults in figure 8.3 dip to the northeast. The seismic reflection data indicate a small number of reflectors which clearly dip to the southwest, but these mostly lie to the northwest of Line 2 beneath Line 4 [*Clowes et al.*, 1987]. The P-axis is oriented in a north-northwest manner which agrees with the

maximum direction of compression for the regional stress tensor determined from other events. The fact that the earthquakes do not lie on any pre-existing faults supports the validity of the regional stress as determined from earthquake focal mechanism solutions. McKenzie [1969] suggested that shallow earthquakes occur by failure along weak planes and that deeper earthquakes, such as those within the subducted plate, are explained by fracture of a homogeneous material. From the plot of relocated earthquakes it is evident that they do not appear to occur by failure on major pre-existing weak planes, but from fracture within what appears to be a homogeneous material. This implies that the fracture direction is a result of the direction of maximum compressive stress and has not been further offset from that direction by slip on a pre-existing fault. But does an overall structural grain as detected by Lithoprobe line 2 survey affect faulting directions? Clowes *et al.* [1987] showed that the reflective layers D1-D2 and E1-E2 show a structural grain with a strike of 110° and a dip of 18°N which does not line up with either P or T-axes directions.

Consequently earthquakes are not associated with pre-existing faults or with the observed structural grain. Since the Victoria focal mechanism orientations are similar to the overall regional focal mechanism orientations, it is reasonable to conclude that faulting is a result of the regional tectonic stress. This means that the orientations of the P and T-axes determined in this thesis are a reasonable approximation to the orientation of σ_1, σ_2, and σ_3, the regional tectonic stress directions.

CHAPTER 9

CONCLUSIONS

The earthquakes considered in this thesis are in southwest British Columbia within the North America plate. The data set is comprised of digital data from 1975 (the inception of the WCTN digital seismic network) until 1991, with the majority of the data from 1981 (when the expansion of the seismic network started to take place) until 1991. Determinations of b-values and Poisson's ratio (σ) have been made for discrete portions of the North America plate in southwestern British Columbia and focal mechanism have been computed for 111 of the above mentioned earthquakes. Composite plots of the P and T-axes (determined from the focal mechanism solutions) were made from which the directions of the regional maximum (σ_1) and minimum (σ_2) compressive stresses were determined. This analysis provides important constraints on the current tectonic regime. The following paragraphs summarize the main conclusions of this study:

1. a) All earthquakes in the North American plate during this time period (1975-1991) were less than magnitude 4. When plotted against depth the earthquakes show a bimodal distribution with

minimum near 10 km. The shallow group (0-10 km) contains 40% of the events, most of which are less than 6 km deep. The majority of the events within the Coast Plutonic Complex belong to the shallow suite of earthquakes. The deeper group (10-30 km) has the greatest concentration, peaking at 20 km depth. The majority of events beneath Vancouver Island belong to this deeper suite of earthquakes. There is no preferential magnitude distribution with depth.

b) The highest concentration of earthquakes is located near the bend in the subduction margin where the coastline changes from north-south in Washington state to northwest-southeast in British Columbia.

2. Most of the seismicity occurs beneath the lowlands of the Strait of Georgia (Georgia basin) and Puget Sound and appears to be correlated with this topographic low.

3. Seismicity shows no definitive correlation with gravity or magnetic signature of the crust, either at a shallow or a deep level.

4. B-values were determined for shallow and deep portions of southwestern B.C. (0.89, 0.99), Vancouver Island (1.22, 0.85), the Coast Plutonic Complex (0.75, 0.85), and the mainland portion of the coastline bend in the North America plate (0.61, 0.97).

5. Rheological profiles must reflect the observed bimodal seismic distribution and this indicates that a three-layer crustal model is needed. From rheological modelling of the crust, beneath the Strait of Georgia, it is possible that the region from 8-14 km depth is a fluid rich layer.

6. From a focal mechanism analysis of earthquakes in southwestern British Columbia the P-axes dominate the stress solution, are oriented mainly north-northwest and lie horizontal. The average orientations of the P-axes are taken as an indicator of the maximum regional compressive stress. The T-axes lie perpendicular to the subduction zone and are oriented in a girdle in a west-southwest direction. This implies right-lateral shear or north-northwest compression in this region.

7. Poisson's ratio in the coast Plutonic Complex is $\sigma=0.24$ and on Vancouver Island $\sigma=0.26$. This probably reflects the quartz content of the crust. The Coast Plutonic Complex is composed of quartz-rich granodiorites and diorites which have a high quartz content whereas Vancouver Island is composed of more mafic igneous rock, interlayered with sedimentary sequences which have a lower quartz content.

8. In the Victoria area, earthquakes can be associated with a three-dimensional geological interpretation deetermined from Lithoprobe and related studies. In the region from the surface down to 11 km, earthquakes occur in the brittle Metchosin basalts (Crescent terrane), between the Leech River and Hurricane Ridge faults, and the deformed layered turbidites of the core rocks (accretionary wedge). In the 18 to 25 km region the earthquakes appear to lie directly underneath the Lithoprobe D2 layer and may be correlated with this.

9. In the Victoria area, it can be said with confidence that seismicity is not correlated with subsurface extensions of major faults exposed at the surface. This supports the conclusion that P and T-axes determined from focal mechanisms represent the current regional stress directions, as opposed to aligning with pre-existing faults that resulted from past regional stress regimes

which may have been oriented in different directions from today's regional stress regime.

REFERENCES

Aki, K., and P.G. Richards, 1980. *Quantitative Seismology*, W. H. Freeman and Company, San Francisco.

Anderson, D.L., 1989. *Theory of the Earth*, Blackwell Scientific Publications, Boston.

Atwater, T., 1970. Implications of plate tectonics for the Cenozoic tectonic evolution of western North America, *Geological Society of America Bulletin*, **81**: 3513-3536.

Bates, R.L., and J.A. Jackson (eds.), 1984. *Dictionary of Geological Terms*, 3rd ed., American Geological Institute, Doubleday, New York.

Clowes, R.M., M.T. Brandon, A.G. Green, C.J. Yorath, A. Sutherland Brown, E.R. Kanasewich, and C. Spencer, 1987. LITHOPROBE-southern Vancouver Island: Cenozoic subduction complex imaged by deep seismic reflections, *Canadian Journal of Earth Sciences*, **24**: 31-51.

Coles, R.L., and R.G. Currie, 1977. Magnetic anomalies and rock magnetizations in the southern Coast Mountains, British Columbia: possible relation to subduction, *Canadian Journal of Earth Sciences*, **14**: 1753-1770.

Crosson, R.S., 1972. Small earthquakes, structure, and tectonics of the Puget Sound area, *Bulletin of the Seismological Society of America*, **62**: 1133-1171.

Crosson, R.S., 1981. Review of seismicity in the Puget Sound region from 1970 through 1978: A brief summary in: J.C. Yount, (ed.) *Earthquake Hazards of the Puget Sound Region, Washington State*, USGS Open File Report, Menlo Park, California.

Crosson, R.S., 1983. Review of seismicity in the Puget Sound region from 1970 through 1978 in: J.C. Yount and R.S. Crosson, (eds.) *Proceedings of Workshop 14, Earthquake Hazards of the Puget Sound Region, Washington*, US Geological Survey Open-File Report 83-19,, p. 6-18.

Davis, E.E., and R.D. Hyndman, 1989. Accretion and recent deformation of sediments along the northern Cascadia subduction zone, *Geological Society of America Bulletin*, **101**: 1465-1480.

Davis, E.E., and R.P. Riddihough, 1982. The Winona Basin: Structure and tectonics, *Canadian Journal of Earth Sciences*, **19**: 767-788.

Dehler, S.A., and R.M. Clowes, 1992. Integrated geophysical modelling of terranes and other structural features along the western Canadian margin, *Canadian Journal of Earth Sciences*, **29**: 1492-1508.

Dehler, S.A., and R.M. Clowes, 1995. Structure of the northern Cascadia subduction zone derived from integrated geophysical modelling, **manuscript in preparation.**

Douglas, R.J.W., 1979. *Fraser River, British Columbia-Washington*, Geological Survey of Canada, Geological Atlas: 1386A.

Dragert, H., and R.D. Hyndman, 1995. Continuous GPS monitoring of elastic strain in the northern Cascadia subduction zone, *Geophysical Research Letters*, **22**: 755-758.

Dragert, H., and M. Lisowski, 1990. Crustal deformation measurements on Vancouver Island, British Columbia: 1976 to 1988 in: P. Vyskocil, C. Reigber, and P.A. Cross, (eds.) *Global and Regional Geodynamics*, Springer-Verlag, New York, p. 241-250.

Dragert, H., R.D. Hyndman, G.C. Rogers, and K. Wang, 1994. Current deformation and the width of the seismogenic zone of the northern Cascadia subduction thrust, *Journal of Geophysical Research*, **99**: 653-668.

Enkin, R.J., 1990. *Formation et deformation de l'asie depuis la fiu de l'ere primaire*, Ph.D. Dissertation, L'university Paris.

Fallows, S.J., 1994. *Upper crustal velocity structure of the southwestern Canadian Cordillera from explosion recordings on the WCTN earthquake seismic net*, MSc Thesis, University of Victoria,Victoria,BC, p.

Fitch, T.J., 1972. Plate convergence, transcurrent faults, and internal deformation adjacent to southeast Asia and the western Pacific, *Journal of Geophysical Research*, **77**: 4432-4460.

GEOSOFT Inc., 1992. *GEOSOFT - Potential Field Interpretation and Modelling Package*, GEOSOFT Inc., Toronto.

Gephart, J.W., 1985. Principal stress directions and the ambiguity in fault plane identification from focal mechanisms, *Bulletin of the Seismological Society of America*, **75**: 621-625.

Gephart, J.W., 1990a. FMSI: A FORTRAN program for inverting fault/slickenside and earthquake focal mechanism data to obtain the regional stress tensor, *Computers and Geosciences*, **16**: 953-989.

Gephart, J.W., 1990b. Stress and the direction of slip on fault planes, *Tectonics*, **9**: 845-858.

Gephart, J.W., and D.W. Forsyth, 1984. An improved method for determining the regional stress tensor using earthquake focal mechanism data: application to the San Fernando earthquake sequence, *Journal of Geophysical Research*, **89**: 9305-9320.

Gutenberg, B., and C.F. Richter (eds.), 1954. *Seismicity of the Earth and Associated phenomena*, Princeton University Press, Princeton, New Jersey.

Hall, J., and M. Ali, 1985. Shear waves in a seismic survey of Lewisian basement: an extra control on Lithological variation and porosity, *Quarterly Journal of the Geological Society of London*, **142**: 677-688.

Holbrook, W.S., W.D. Mooney, and N.I. Christensen, 1992. The seismic velocity structure of deep continental crust in: dm Fountain, R.J. Arculus, and R.W. Kay, (eds.) *Continental Lower Crust*, Elsevier, Amsterdam.

Irving, E., and P.J. Wynne, 1991. Paleomagnetic evidence for motions of parts of the Canadian Cordillera, *Tectonophysics*, **187**: 259-275.

Isacks, B.L., J. Oliver, and L.R. Sykes, 1968. Seismology and the new global tectonics, *Journal of Geophysical Research*, **73**: 5855-5900.

Jones, A.G., D.I. Gough, R.D. Kurtz, J.M. DeLaurier, D.E. Boerner, J.A. Craven, R.G. Ellis, and G.W. McNeice, 1992. Electromagnetic images of regional structure in the southern Canadian Cordillera, *Geophysical Research Letters*, **12**: 2373-2376.

Kirby, S.H., 1983. Rheology of the lithosphere, *Reviews of geophysics and space physics*, **21**(6): 1458-1487.

Kisslinger, C., 1980. Evaluation of *S* to *P* amplitude ratios for determining focal mechanisms from regional network observations, *Bulletin of the Seismological Society of America*, **70**: 999-1014.

Lewis, T., 1991. Heat flux in the Canadian Cordillera in: D.B. Slemmons, E.R. Engdahl, M.D. Zoback, and D.D. Blackwell, (eds.) *Neotectonics of North America*, Geological Society of America, Decade Map Volume 1, Boulder, Colorado, p. 445-456.

Lewis, T.J., W.H. Bentkowski, E.E. Davis, R.D. Hyndman, J.G. Souther, and J.A. Wright, 1988. Subduction of the Juan de Fuca plate: Thermal consequences, *Journal of Geophysical Research*, **93**: 15207-15225.

Lewis, T.J., W.H. Bentkowski, and R.D. Hyndman, 1992. Crustal temperatures near the Lithoprobe Southern Canadian Cordillera Transect, *Canadian Journal of Earth Sciences*, **29**: 1197-1214.

Lowe, C., and G. Ranalli, 1993. Density, temperature, and rheological models for the southeastern Canadian Cordillera: implications for its geodynamic evolution, *Canadian Journal of Earth Sciences*, **30**: 77-93.

Ma, L., R. Crosson, and R. Ludwin, 1990. Focal Mechanisms of western Washington earthquakes and their relationship to regional tectonic stress.

Malone, S.D., G.H. Rothe, and S.W. Smith, 1975. Details of microearthquake swarms in the Columbia Basin, Washington, *Bulletin of the Seismological Society of America*, **65**: 855-864.

Massey, N.W.D., 1986. Metchosin Igneous Complex, southern Vancouver Island: Ophiolite stratigraphy developed in an emergent island setting, *Geology*, **14**: 602-605.

McKenzie, D.P., 1969. The relation between fault plane solutions for earthquakes and the directions of the principal stresses, *Bulletin of the Seismological Society of America*, **59**: 591-601.

McKenzie, D.P., and W.J. Morgan, 1969. The evolution of triple junctions, *Nature*, **224**: 125-133.

Mogi, K., 1962. Magnitude-frequency relation for elastic shocks accompanying fractures of various materials and some related problems in earthquakes, *Bulletin of the Earthquake Research Institute*, **40**: 831-853.

Mogi, K., 1967. Earthquakes and fractures, *Tectonophysics*, **5**: 35-55.

Monger, J.W.H., R.A. Price, and D.J. Tempelman-Kluit, 1982. Tectonic accretion and the origin of the two major metamorphic and plutonic welts in the Canadian Cordillera, *Geology*, **10**: 70-75.

Morgan, W.J., 1968. Rises, trenches, great faults, and crustal blocks, *Journal of Geophysical Research*, **73**: 1959-1982.

Muller, J.E., 1977. Evolution of the Pacific margin, Vancouver Island and adjacent regions, *Canadian Journal of Earth Sciences*, **14**: 384-396.

Quamar, T, 1992. *Stress directions inferred from earthquake focal mechanisms in Washington and Northern Oregon*, Seismological Society of America Annual Meeting - abstract.

Ranalli, G., and D.C. Murphy, 1987. Rheological stratification of the lithosphere, *Tectonophysics*, **132**: 281-295.

Reasenberg, P.A., and D. Oppenheimer, 1985. FPFIT, PFPLOT and FPPAGE: Fortran computer programs for calulating and displaying earthquake fault-plane solutions. USGS open-file report 85-739.

Riddihough, R.P., 1977. A model for recent plate interactions off Canada's west coast, *Canadian Journal of Earth Sciences*, **14**: 384-396.

Riddihough, R., 1984. Recent movements of the Juan de Fuca plate system, *Journal of Geophysical Research*, **89**: 6980-6994.

Rogers, G.C., 1979. Earthquake fault plane solutions near Vancouver Island, *Canadian Journal of Earth Sciences*, **16**: 523-531.

Rogers, G.C., 1983. *Seismotectonics of British Columbia*, Ph.D. Dissertation, University of British Columbia, Vancouver, B.C., 247p.

Rogers, G.C., 1994. Earthquakes in the Vancouver area in: J.W.H. Monger, (ed.) *Geology and Geological Hazards of the Vancouver Region, Southwestern British Columbia*, Geological Survey of Canada, Bulletin 481,, p. 221-229.

Scholz, C.H., 1968. The frequency-magnitude relation of microfracturing in rock and its relation to earthquakes, *Bulletin of the Seismological Society of America*, **58**: 399-415.

Sibson, R.H., 1974. Frictional constraints on thrust, wrench and normal faults, *Nature*, **249**: 542-544.

Snoke, J.A., J.W. Munsey, A.G. Teague, and G.A. Bollinger, 1984. A program for focal mechanism determination by combined use of polarity and SV-P amplitude ratio data, *Earthquake Notes*, **55**: 15.

Stacey, R.A., 1973. Gravity anomalies, crustal structure, and plate tectonics, *Canadian Journal of Earth Sciences*, **10**: 615-628.

Telford, W.M., L.P. Geldart, R.E. Sheriff, and D.A. Keys, 1976. *Applied Geophysics*, Cambridge University Press, New York.

Tiffin, and D. Seeman, 1985. *Juan de Fuca Plate Map: Relief*, Pacific Geoscience Centre, .

Varsek, J.L., R.A. Cook, R.M. Clowes, J.M. Journeay, J.W.H. Monger, R.R. Parrish, E.R. Kanasewich, and C.S. Spencer, 1993. Lithoprobe crustal reflection structure of the southern Canadian Cordillera 2: Coast Mountains transect, *Tectonics*, **12**: 334-360.

Vine, F.J., 1966. Spreading of the ocean floor-New evidence, *Science*, **154**: 1405-1415.

Weichert, D.H., 1980. Estimation of the earthquake recurrence parameters for unequal observation periods for different magnitudes, *Bulletin of the Seismological Society of America*, **70**: 1337-1346.

Wessel, P., and W.H.F. Smith, 1993. Free software helps map and display data, *EOS Transactions, American Geophysical Union*, **72**: 441,445-446.

Wheeler, J.O., and P. McFeely, 1991. *Tectonic Assemblage Map of the Canadian Cordillera and adjacent parts of the United States of America*, Geological Survey of Canada, 1712A.

Wyss, M., 1973. Towards a physical understanding of the earthquake frequency distribution, *Geophysical Journal of the Royal Astronomical Society*, **31**: 341-359.

Yelin, T.S., and R.S. Crosson, 1982. A note on the south Puget Sound basin magnitude 4.6 earthquake of 11 March 1978 and its aftershocks, *Bulletin of the Seismological Society of America*, **72**: 1033-1038.

Yorath, C.J., 1990. *Where Terranes Collide*, Orca, Victoria, 31p.

Zelt, B.C., R.M. Ellis, and R.M. Clowes, 1993. Crustal velocity structure in the eastern Insular and southernmost Coast belts, Canadian Cordillera, *Canadian Journal of Earth Sciences*, **30**: 1014-1027.

VITA

Surname: Mulder Given Names: Taimi Lynn

Place of Birth: Edmonton, Alberta, Canada

Educational Institutions Attended:

University of Victoria	1992 to 1995
University of British Columbia	1981 to 1987

Degrees Awarded:

B.Sc.	University of British Columbia	1987

Publications:

Lowe, C., D.A. Seemann, T. Mulder. 1991. Geophysical constraints on geometry and tectonics of the Bowser Basin, northern British Columbia, Canada - preliminary interpretation, *EOS*, **72**, p. 503.

Mulder, T. and M. Lamontagne. 1990. *Analysis of CLTN Traces from Events in the Saguenay Region*, Internal paper, Geophysics Division, GSC, Ottawa, 14 pp.

Mulder, T. and G.C. Rogers. 1992. Preliminary analysis of focal mechanisms of small crustal earthquakes in southwest British Columbia, *PNAGU abstract*.

Mulder, T. and G.C. Rogers. 1993. Small crustal earthquakes in southwest British Columbia, (abstract), *1993 Spring Meeting abstract volume*, Canadian Geophysical Union.

Mulder, T. and G.C. Rogers. 1993. Crustal earthquakes in southwestern British Columbia, (abstract), *1993 Fall Meeting abstract volume, supplement to Eos, Transactions*, American Geophysical Union, p. 201.

Mulder, T. and G.C. Rogers. 1994. North American plate earthquakes in southwest British Columbia, Canada, (abstract), *1994 Spring Meeting abstract volume*, Canadian Geophysical Union.

Wang, K., T. Mulder, G.C. Rogers, R.D. Hyndman. 1995. Case for very low coupling stress on the Cascadia subduction fault, *Journal of Geophysical Research*, **100**, p.12907-12918.

PARTIAL COPYRIGHT LICENSE

I hereby grant the right to lend my thesis to users of the University of Victoria Library, and to make single copies only for such users or in response to a request from the Library of any other university, or similar institution, on its behalf or for one of its users. I further agree that permission for extensive copying of this thesis for scholarly purposes may be granted by me or a member of the University designated by me. It is understood that copying or publication of this thesis for financial gain shall not be allowed without my written permission.

Title of Thesis: Small Earthquakes in Southwestern British Columbia (1975-1991)

Author [redacted]
Taimi Lynn Mulder
September 29, 1995